Chapter 8

Human-structure interaction

8.1 Introduction

In section 2.6.6, a discussion was presented on the forces exerted by people on a floor and the research conducted on the human-structure interaction. It was observed that most design codes treat the occupants of a floor as extra load, uniformly distributed across the slab, while bio-mechanical studies suggest that the human body has significant energy absorption capabilities and is best modelled as a spring-mass-damper system. Since people not only impose dynamic loads but also interact with the structure, an awareness of this interaction is required to understand firstly, how the structure will respond, and secondly, how people may perceive the vibrations.

Ellis et al. (1994) found that when the mass of the people is reasonably large in comparison with the mass of the structure, such as in sports grandstands, the natural frequency of the system changes to reflect the crowd fundamental frequency, and a significant amount of energy absorption takes place. Similarly, some work has also been conducted on the best model to represent a single person [Ji and Ellis (1994b), Foschi et al. (1995), Folz and Foschi (1991)]. These studies all concluded that a SDOF mass-spring-damper is sufficient in representing a human body. Other representations have also been proposed, such as modelling the body as a continuous system [Ji (1995)], as two SDOF systems [ISO2631/1 (1985)], or as a 15DOF system [Nigam and Malik (1987)].

In general, the subject of human-structure interaction is poorly covered in literature and only a few notable findings can be recorded. Indeed, none of the perceptibility design guidelines, presented in section 2.2.2, takes the occupants of the structure into account in any way. It is likely, however, that an individual's annoyance due to floor vibrations is a function of the amount of energy being transmitted to the body, which must be dependent on the interaction between the body and the vibrating structure. This chapter presents the results of experiments on the human-structure interaction, which give a natural frequency for the human body of 10.43Hz and a damping capacity

of 50% critical. An analytical model is presented, which assumes the human body as a SDOF system, and the results are compared with the existing design codes, which assume the occupants as extra mass. The models are seen to be in good agreement with the experimental results.

8.2 Description of experiments

The main purpose of these experiments was to assess the effect of a human on the vertical vibration behaviour of the slab. Therefore, the majority of the tests were conducted with a single person (or two people) standing on the floor. Crowd effects and the significance of the occupants' position and posture were not part of this investigation.

Tests with the human body were conducted on the following slab configurations:

- Bare slab (fully tensioned)
- Slab with one standing man
- Slab with dead weight equivalent to mass of the man placed at same position as the man (hereafter referred to as ***equivalent weight***)
- Slab with two standing men
- Slab with *equivalent weight* of the two men

Figure 3.18 (page 64) shows the position of the standing man on the model slab. In tests where two men were used, they were symmetrically positioned on the slab. In each case, a sine-sweep test was carried out to obtain the FRF and also a shaker cut-off test was conducted to obtain time-domain decay response. The majority of the analysis is focused on the fundamental frequency of the model floor, as it is in the range of possible annoyance to occupants. However, some analysis is also presented on the effect of a human on the higher harmonics of floor vibration.

8.3 Experimental results

Having obtained FRF and time-domain data for the various configurations described above, the results were analysed to derive natural frequency and damping values of the slab in each case. Detailed results of these tests are included in appendix A. Table 8.1 gives selected relevant readings at some slab configurations. These are discussed in the following sections. In each plot, the response of the bare slab is also illustrated for comparison purposes.

Table 8.1: Selected human-structure interaction results (taken from appendix A)

Test configuration	Average fund. frequency (Hz)	Average damping (% of critical)
bare slab (fully tensioned)	8.02	1.10
bare slab + one man	7.76	3.84
bare slab + equiv. mass of one man	7.68	1.45
slab + both screed layers	10.15	1.25
slab + screed layers + one man	9.96	3.11
slab + screed layers + equiv. mass of one man	9.93	1.28
slab + screed layers + two men	9.96	3.46
slab + screed layers + equiv. mass of two men	9.81	1.28

8.3.1 Effects on natural frequency

From table 8.1, it can be seen that the fundamental frequency of the slab reduced with the presence of a standing man, and with his equivalent weight. The latter result would be expected, as an increase in the mass of a system would lead to a decrease in its natural frequency. The reduction in frequency with the standing man, however, is in contrast with the results obtained by Ellis and Ji (1997). They conducted similar tests on a laboratory beam of fundamental frequency 18.68Hz, and found this to increase when a person stood on the slab. The reasons for the discrepencies between the two findings are explained later in section 8.4.1, and are basically due to the difference in the fundamental frequencies of the two slabs.

8.3.2 Damping effects

Effect of one man on bare slab

Figure 8.1 shows FRF magnitude plots of the bare slab with the standing man and with his equivalent weight. It can be seen that by considering the human as extra mass, the transfer function amplitude is only marginally reduced, whereas this decrease is around 75% when considering the actual person. The width of the fundamental peak is also much broader with the man, indicating a substantial increase in damping. From the damping measurements, this increase is seen to be over three-fold, as compared to 32% when considering the man as a mass (table 8.1). The time-domain plots of figure 8.2 substantiate these results and it can clearly be seen that the standing man absorbs a significant amount of the slab vibration energy.

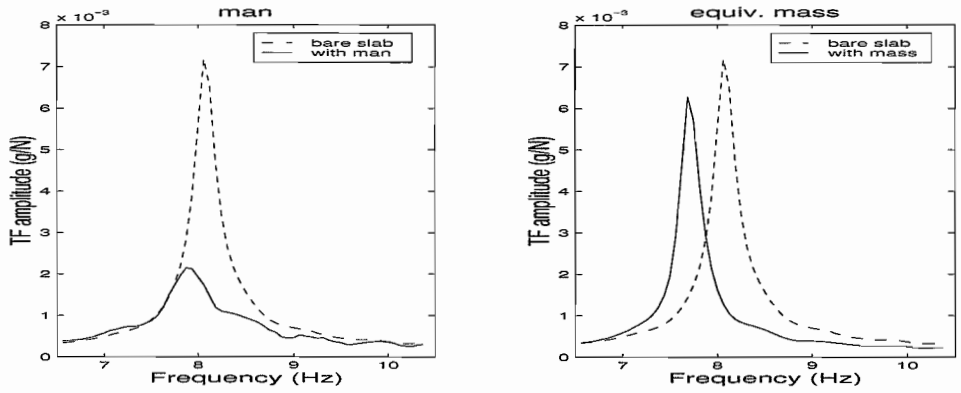


Figure 8.1: FRF plots of slab with standing man and equivalent weight of man

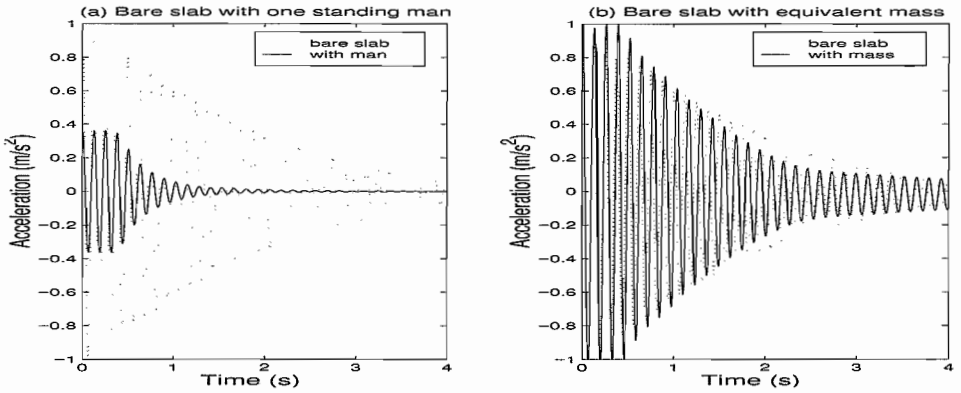


Figure 8.2: Time-domain graphs of slab with standing man and his equivalent weight

Effect of two men on the slab

Figures 8.3 and 8.4 show frequency and time-domain results when two men were standing on the slab. From table 8.1, it is seen that with two men, the increase in damping is of the same order as with one standing man, leading to the observation that the effect of the extra person is marginal. A comparison between one and two people standing on the slab is shown in figure 8.5, from which it can be reasonably assumed that in laboratory experiments, one person is sufficient in representing the increase in damping due to the occupants. This assumption will become incorrect when considering a crowd, as the mass of the people is significantly increased. In such cases, consideration must also be given to the percentage of the crowd that is stationary. A person who is not stationary has minimal energy absorption capabilities [Ji and Ellis (1993)].

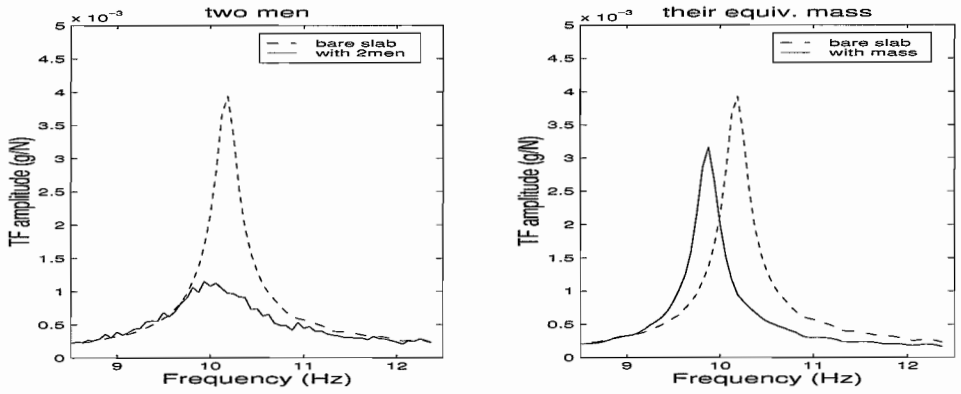


Figure 8.3: FRF plots of two standing men and their equivalent weight

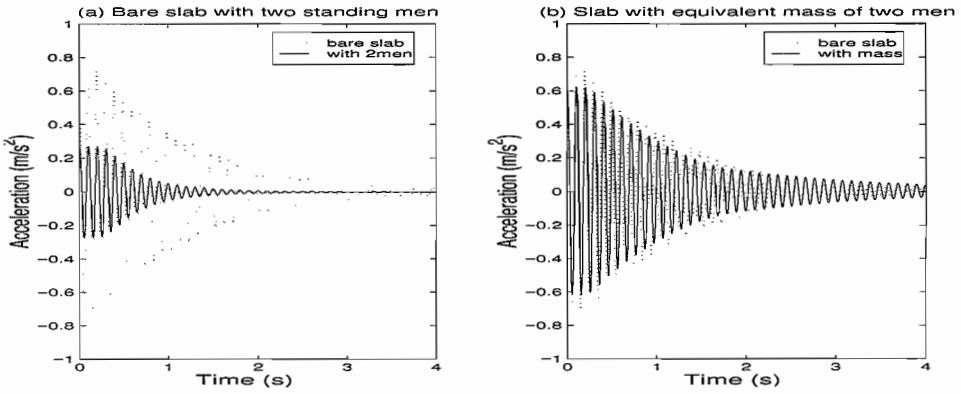


Figure 8.4: Time-domain graphs for two standing men and their equivalent weight

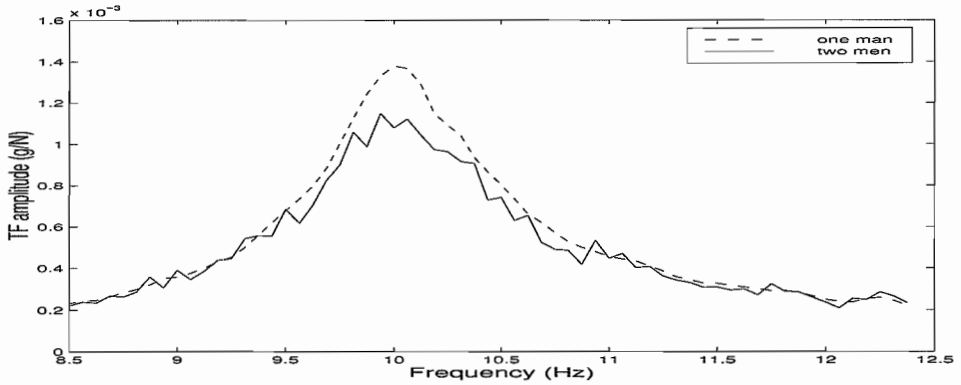


Figure 8.5: Comparison of the effects of one man and two men

8.3.3 Effect of man at higher frequencies

Figure 8.6 illustrates FRF plots of the effect of the standing man and his equivalent mass on the amplitude of the second natural frequency of the slab. Similarly, Figure 8.7 shows this effect at the third natural frequency. It can clearly be seen that at higher frequencies, the energy absorption

effect of the body is completely lost. It is evident that at these frequencies resonance of the body does not occur, and it becomes feasible to assume the body as a mass. Hence, the energy absorption effect of the body must be confined to its range of fundamental frequency, which is reported to be between 4-16Hz when standing [Herterich and Schnauber (1992)].

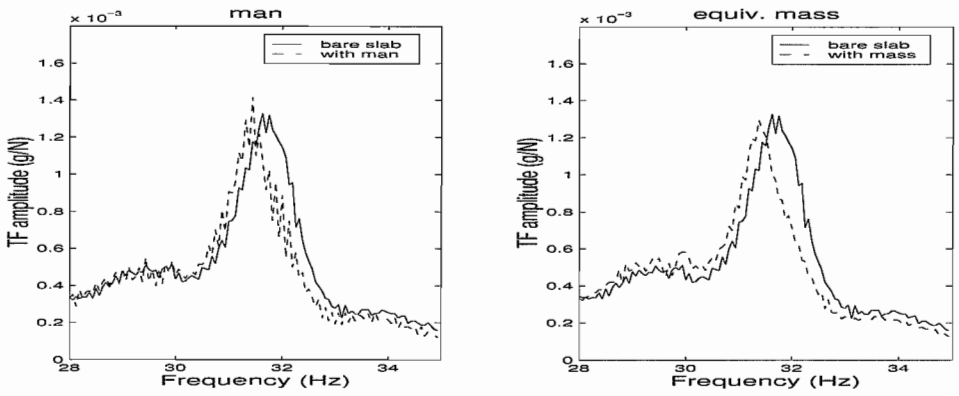


Figure 8.6: FRF plots of man and equivalent weight at second slab frequency

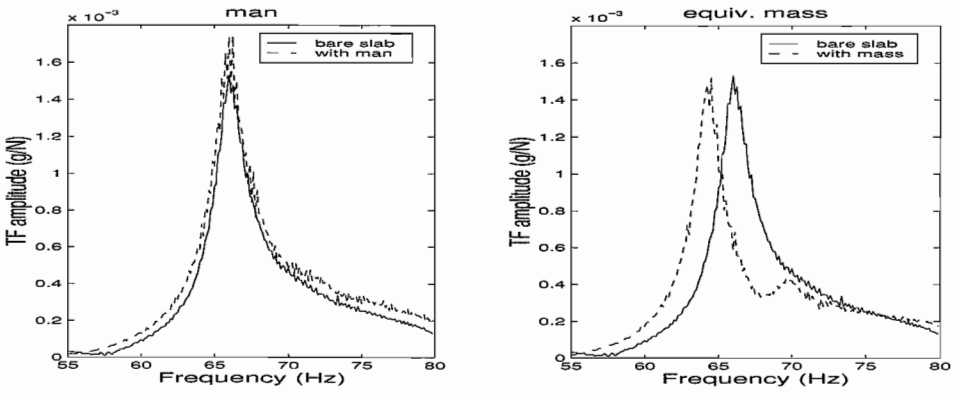


Figure 8.7: FRF plots of man and equivalent weight at third slab frequency

8.3.4 Summary of experimental results

- The fundamental frequency of the model slab decreased with the addition of a stationary standing man, and also with his equivalent weight.
- A stationary man significantly increased the model slab damping ratio by as much as 250%, compared to 32% when considering the man as a mass.
- Two men stationary on the slab lead to an increase in damping which was only marginally more than one man stationary on the slab.
- The energy absorption capacity of the body was confined within a fixed frequency range and was lost at higher frequencies.

8.4 Human-structure models

In this section, a numerical model is devised, which assumes the body and the slab as two separate SDOF systems. First, the undamped response of the 2DOF system is analysed, with respect to the experimental results, to derive values for the fundamental frequency and stiffness of the human body. These are then used in a time-stepping damped 2DOF model to derive a value for the damping inherent in the body. It is shown that a SDOF model is adequate in representing the stationary body, and that its interaction with a floor is best represented by a 2DOF model.

8.4.1 Undamped 2DOF model

Consider the undamped 2DOF system of figure 8.8, with M_1^* and K_1^* representing the generalised slab mass and stiffness (see appendix B), and M_2^*, K_2^* being the generalised body mass and stiffness respectively. Of the above parameters, the only unknown is K_2^*, which can be derived using the experimentally measured natural frequencies of table 8.1, when considering the combined 2DOF human-structure system.

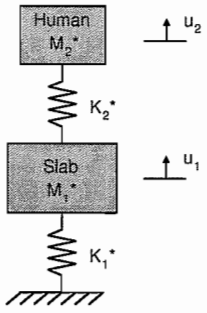


Figure 8.8: 2DOF undamped lumped mass-spring model of slab-human system

For the system of figure 8.8, the equation of motion is given by:

$$\begin{bmatrix} M_1^* & 0 \\ 0 & M_2^* \end{bmatrix} \begin{bmatrix} \ddot{u}_1 \\ \ddot{u}_2 \end{bmatrix} + \begin{bmatrix} K_1^* + K_2^* & -K_2^* \\ -K_2^* & K_2^* \end{bmatrix} \begin{bmatrix} u_1 \\ u_2 \end{bmatrix} = \begin{bmatrix} 0 \\ 0 \end{bmatrix} \tag{8.1}$$

Assuming harmonic motion of the system with frequency, ω, the determinant of the co-efficients in equation 8.1 must be equal to zero, leading to:

$$M_1^* M_2^* \omega^4 - \left[K_2^* M_1^* + M_2^* \left(K_1^* + K_2^*\right)\right] \omega^2 + K_1^* K_2^* = 0 \tag{8.2}$$

This equation can be used to analyse the effect of the body when considered as a mass only, and also when considering its interaction with the supporting structure. These cases are dealt with separately below.

Consideration of equivalent mass

Assuming the human body to be represented only as a mass, the value of K_2^* in figure 8.8 will tend to ∞. Rearranging equation 8.2, given $\omega_1 = \sqrt{\frac{K_1^*}{M_1^*}}$ and $\omega_2 = \sqrt{\frac{K_2^*}{M_2^*}}$, leads to:

$$K_2^* = \frac{\omega^2 M_1^* M_2^* \left(\omega_1^2 - \omega^2\right)}{M_1^* \left(\omega_1^2 - \omega^2\right) - M_2^* \omega^2} \tag{8.3}$$

If K_2^* tends to ∞, the denominator of equation 8.3 must tend to zero, so that the natural frequency of the combined system will be:

$$\omega^2 = \omega_1^2 \cdot \frac{M_1^*}{M_1^* + M_2^*} \tag{8.4}$$

This means that, as expected, the addition of extra mass leads to a reduction in the fundamental frequency of the primary system, depending on M_2^*. In the case of the experimental results, table 8.1 gives ω_1=($2\pi \times 8.02$)rads/s, and appendix B gives M_1^*=806kg. Also, as the focus is on addition of mass only, M_2^* is taken to be the total mass of the body (i.e. 75kg). By substituting the values into equation 8.4, the natural frequency of the system is obtained as 7.65Hz. This compares with the experimentally derived value of 7.68Hz (table 8.1), which shows good agreement.

Consideration of human-structure interaction

With K_2^* in figure 8.8 being positive and finite, the interaction between the two masses, M_1^* and M_2^*, must be considered. By expressing $\mu = \frac{M_2^*}{M_1^*}$, equation 8.2 can be written as:

$$\omega^4 - \left[\omega_1^2 + \omega_2^2 \left(1 + \mu\right)\right] \omega^2 + \omega_1^2 \omega_2^2 = 0 \tag{8.5}$$

for which the solution is:

$$\omega^2 = \frac{1}{2}\left[\omega_1^2 + \omega_2^2 \left(1 + \mu\right) \mp \sqrt{\left[\omega_1^2 + \omega_2^2 \left(1 + \mu\right)\right]^2 - 4\omega_1^2 \omega_2^2}\right] \tag{8.6}$$

Introducing a new parameter, $\Omega = \frac{\omega_2}{\omega_1}$, and substituting into equation 8.6, gives:

$$\left(\frac{\omega}{\omega_1}\right)^2 = \frac{1}{2}\left[1 + \Omega^2 \left(1 + \mu\right) \mp \sqrt{\left[1 + \Omega^2 \left(1 + \mu\right)\right]^2 - 4\Omega^2}\right] \tag{8.7}$$

Figure 8.9 shows a plot of equations 8.7 for different values of mass ratio, μ. The following observations can be gathered from the figure:

i) At any value of μ, the fundamental frequency of the slab is inbetween the two natural frequencies of the combined 2DOF system.

ii) As the number of people increases (i.e. larger μ), the difference between the two natural frequencies of the combined 2DOF system increases.

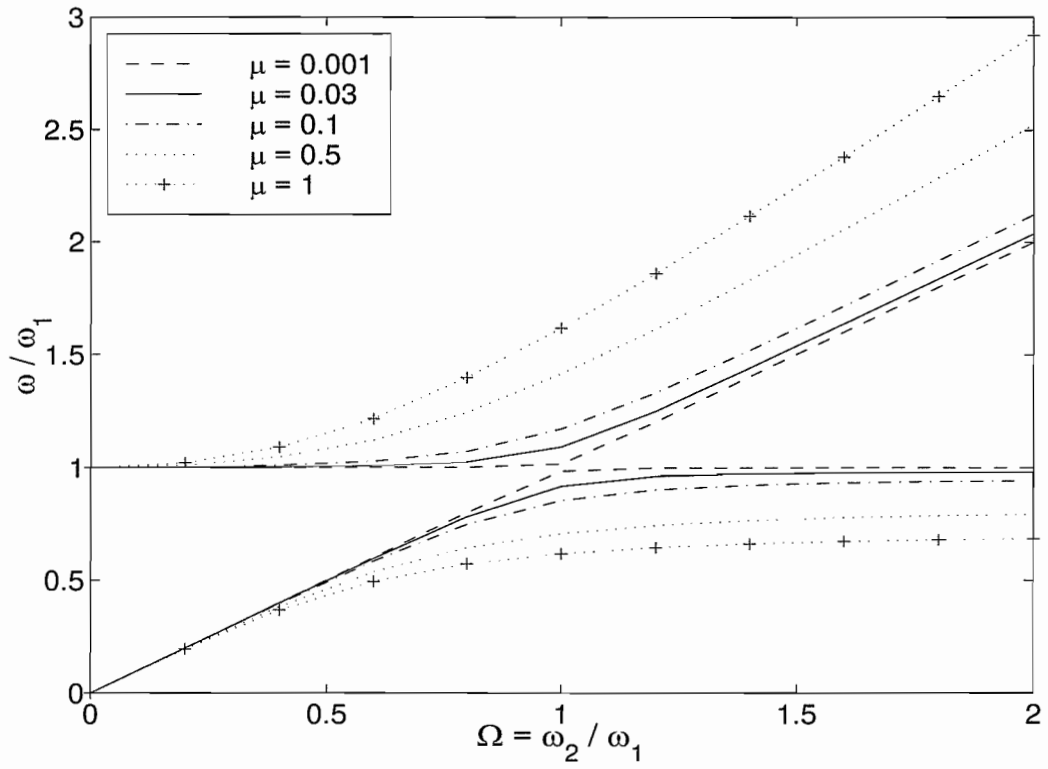


Figure 8.9: Plot of equations 8.7 for different mass ratios

iii) A clear dividing line can be seen at the point where Ω=1.0. For Ω >1.0 (i.e. structure frequency is lower than body frequency), the fundamental frequency will gradually reduce as μ increases, and a higher frequency mode appears. For Ω <1.0 (i.e. high frequency structure), the original frequency will increase as μ increases, with a new lower frequency mode appearing. This explains the difference between the results described here and those found by Ellis and Ji (1997) (see section 8.3.1). In these tests, the slab frequency was lower than the body frequency, hence a reduction in fundamental frequency was observed. The beam tested by Ellis & Ji had a fundamental frequency higher than the body frequency, which increased with the standing man. Ellis & Ji also noted that the 'new' modes, as a result of the occupants, will be mainly due to the occupants vibrating and will not necessarily be seen from the structural response. This was found to be true for the case of the experimental slab.

iv) Figure 8.9 can also be used for structure-TMD systems where for maximum effect Ω=1.0, and for a given μ, the natural frequencies of the system can be obtained. However, for a structure-TMD system, the mass ratio is generally very small and $\omega \approx \omega_1$.

v) From the results of the experimental slab, it is possible to derive a value for ω_2, given all other parameters in equation 8.7, as described below.

Derivation of the generalised mass of the body

The derivation of an accurate value for M_2^* is at present not fully understood and very few findings are reported. The most notable investigation was perhaps by Ji (1995) who represented the body as a continuous system and derived its modal masses. For the purpose of this discussion, a simple method is used to derive M_2^* by assuming the body as a rod undergoing axial vibrations (figure 8.10), and considering the energies involved.

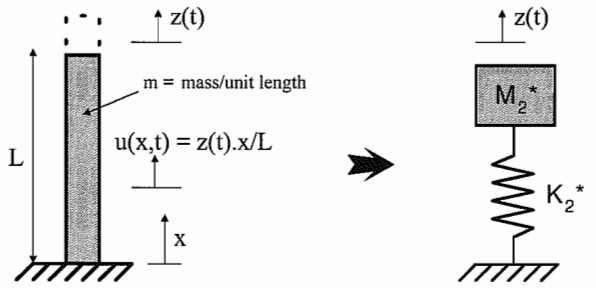


Figure 8.10: Simplification of the body as an axially vibrating rod

Equating kinetic energies of the rod and its generalised SDOF representation, leads to:

$$\int_0^L \frac{1}{2} m\dot{u}^2 dx = \frac{1}{2} M_2^* \dot{z}^2 \qquad \text{which gives} \qquad M_2^* = \int_0^L m\frac{x^2}{L^2} dx = \frac{mL}{3} \tag{8.8}$$

In the case of the experimental slab, the standing man had a mass of 75kg, giving M_2^*=25kg.

Derivation of body natural frequency and stiffness

Refering to equation 8.7 and figure 8.9, a value for the fundamental frequency of the human body is derived. Taking M_2^*=25kg and M_1^*=806kg (appendix B), gives a value for μ=$\frac{M_2^*}{M_1^*}$=0.03. Similarly, from the experiments, table 8.1 gives a combined frequency of 7.76Hz, which with a slab frequency of 8.02Hz, gives $\frac{\omega}{\omega_1}$=0.968. By substituting these into equation 8.7, a value of $\Omega = \frac{\omega_2}{\omega_1}$=1.30 is obtained. Hence, these tests give a fundamental frequency for the body of f_2=10.43Hz. This corresponds well with 9.96Hz given in [Ellis and Ji (1997)] and is within the 2DOF values of ISO2631/1 (1985), being 5.03 and 12.49Hz [Folz and Foschi (1991)]. It is also within the range of values given by Ji (1995), for different modal masses, which are between 9.96 and 11.87Hz. When considering a group of people, the frequency differences between individuals can be neglected and the frequency of the human bodies are treated as a constant coefficient [Ji and Ellis (1994b)]. Furthermore, equation 8.7 also suggests a new mode to appear at 10.77Hz. This would be mainly due to the person vibrating and was not observed in the measured results, which were taken on

the slab. Note that both the individual body and slab fundamental frequencies are inbetween the frequencies of the combined human-structure system.

Using the fundamental frequency of the body, its stiffness is found from $\omega_2 = \sqrt{\frac{K_2^*}{M_2^*}}$, which is K_2^*=1.07×10^{5}N/m. This is greater than the 2DOF values of ISO2631/1 (1985), being 6.2×10^4 and 8.0×10^{4}N/m, but is smaller than the derived values by Ji (1995) for a continuous system, being in the range 1.86×10^5 to 8.55×10^{5}N/m for different modal masses.

8.4.2 Damped 2DOF and SDOF models

In this section, the derived values of the body frequency and stiffness are used in a damped 2DOF model, (figure 8.11), and a typical value for the damping of the human body is obtained. The approach is very similar to the time-stepping model presented for the structure-TMD system, explained in section 7.4.2. The main difference between the human and TMD models is the value of mass ratio, μ, and the damping inherent in the secondary mass, ζ_2. The human body is heavier than a TMD system, particularly if a crowd is involved, hence increasing μ. Similarly, the damping of a human body can be as high as 47.5% critical [Ji and Ellis (1994b)]. This significant increase in damping of the secondary mass leads to much faster decay of slab vibration, as shown by the experimental results. The variables in the model are updated to best represent the experimental data and comparisons are made. Also, a SDOF damped model is presented for the slab without the standing man. These models are described in more detail below.

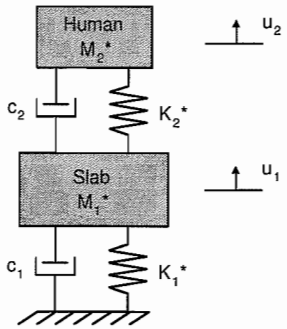


Figure 8.11: 2DOF lumped mass-spring-damper model of slab-human system

Description of the models

The 2DOF model is a time-stepping solution of a lumped mass-spring-damper system, as described in section 7.4.2. The generalised values of mass and stiffness, for the slab and the body, are taken

as those given in the previous section. The initial conditions are taken as zero displacement for both man and slab but an initial velocity, V, is assumed applied to the slab (as in equation 7.16, page 152). The subsequent slab response decay is then analysed. Figure 8.12 is a plot of this model for an arbitrary V and ζ_2, using the experimental values for all other slab variables.

In addition to the 2DOF model, a SDOF model was also devised, which would represent the slab without the standing man. This model is used to investigate the possibility of assuming the man as an extra mass on the slab, without any inherent damping and stiffness. Figure 8.13 shows a typical plot of the model using the experimental slab properties.

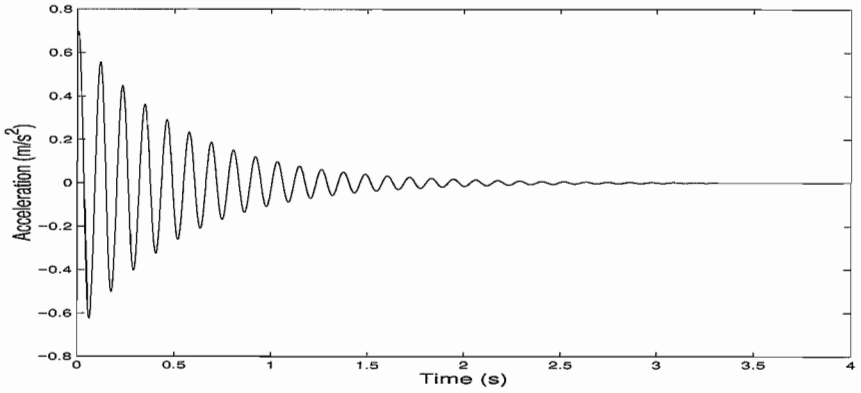


Figure 8.12: Typical plot of 2DOF slab response model with standing man

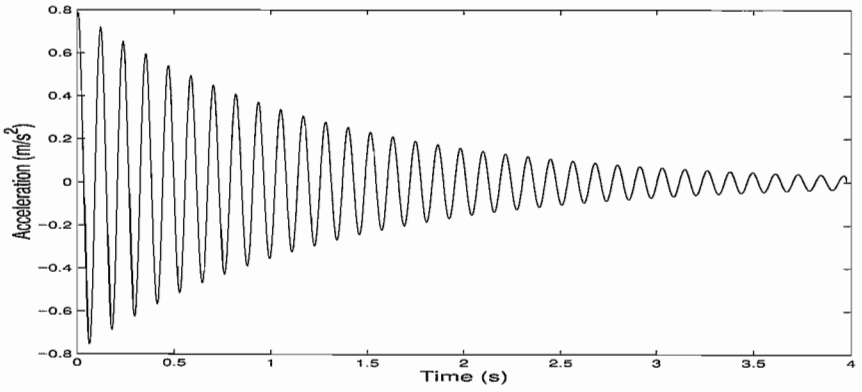


Figure 8.13: Typical plot of SDOF slab response model with equivalent mass of man

Derivation of model human damping

Having arrived at the SDOF and 2DOF models and updated V to best fit the experimental results, it was possible to compare the experimental and model plots and hence arrive at a value for human body damping (ζ_2 in model). An extensive MATLAB programme was written which would iterate for ζ_2 through a range of values. This iteration routine is similar to that described in section 7.4.2.

After carrying out the operation for all experimental plots, the value of body damping was derived to be mostly within the range 45% to 55% critical. Factors such as posture, tensioning of the muscles, or bending of the knees would contribute to the observed variability in ζ_2. The derived range, however, is in good agreement with Griffin (1990), [as reported by Ji and Ellis (1994b)], who gives a value of 47.5% at a sitting position. For the remainder of this report, an average value of 50% critical is taken to represent the damping ratio for the human body.

Useability of the models

Figure 8.14 shows a typical plot of the 2DOF model compared with the experimental response of the slab with a standing man. It can be seen that the model satisfactorily represents the experimental data. This fit was also observed in all other cases of the slab with the standing man, including the case of two standing men. Similarly, figure 8.15 shows a typical plot of the SDOF model with mass of slab adjusted up to account for the increase of mass due to the standing man. In both cases, good agreement is achieved. However, when model results of slab response with man and his equivalent weight are plotted, figure 8.16, a large difference is observed, which illustrates that the standing man has very high energy absorption capabilities and should not be regarded as extra mass.

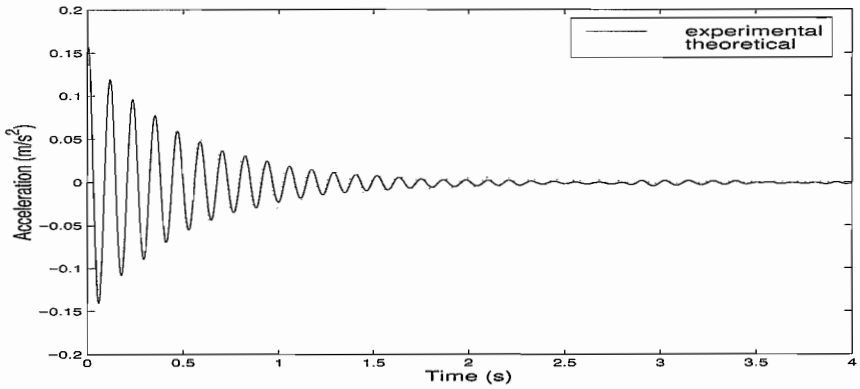


Figure 8.14: Typical plot of final model for slab response with standing man

8.4.3 Sensitivity analyses

Having derived suitable models for the interaction of the human body with the structure, here a sensitivity analysis is carried out to investigate the effect of changes in body mass and stiffness. Figure 8.17 shows plots of slab response with a stationary person of average weight, as compared with 40% heavier and lighter occupants. It can be seen that the rate of decay of slab vibrations is

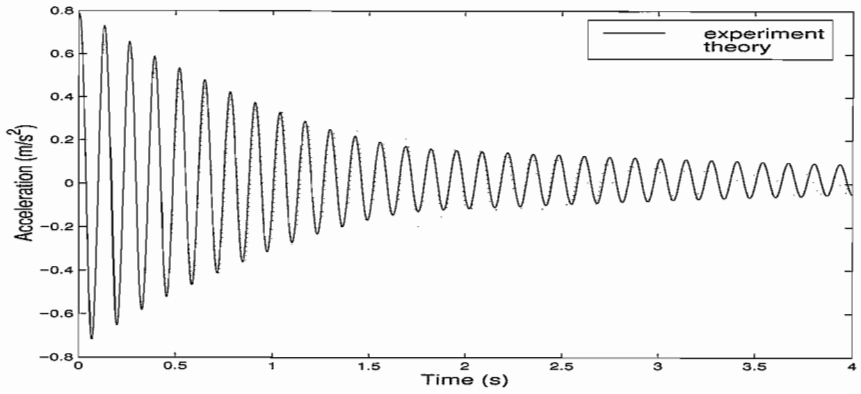


Figure 8.15: Typical plot of final model for slab response with mass equivalent to man

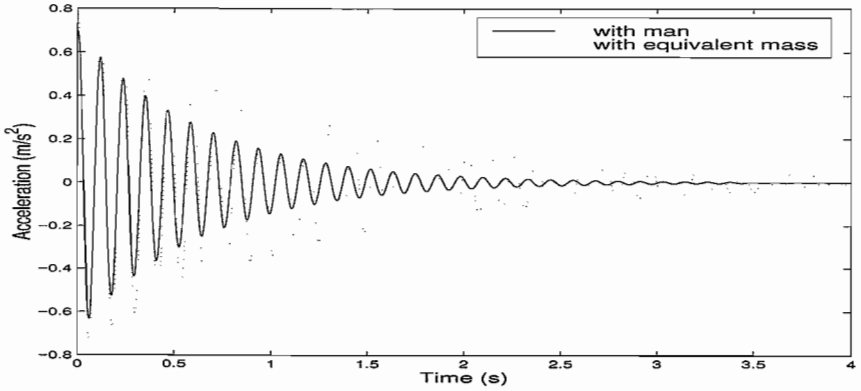


Figure 8.16: Comparison of SDOF and 2DOF damped models with same initial velocity

marginally faster with the heavier occupant. This is to be expected, as the heavier the occupant, the greater the effect of the secondary dashpot in the model (figure 8.11). However, the model is not very sensitive to a change in occupant mass. Here, an increase in body mass of 40% leads to an increase in damping of the slab of approximately 10%, and also to a reduction of slab natural frequency of nearly 1%.

Perhaps a better indication of the sensitivity of the model is when changes to the fundamental frequency of the body are considered (i.e. variations in body stiffness). As described previously, these experiments yielded a natural frequency for the body of 10.43Hz, which lies within the suggested range of 4-16Hz. Figure 8.18 illustrates the model slab response with the body frequency at 10.43Hz, and also at the upper and lower boundaries of the recommended range. It can be seen that the fastest decay of vibrations occurs at the calculated frequency of 10.43Hz. Damping of the slab decreases at other values of body frequency.

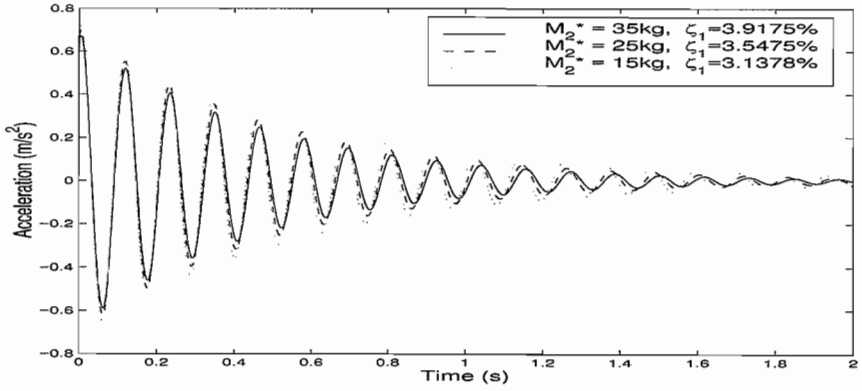


Figure 8.17: Sensitivity of model to variations in body mass

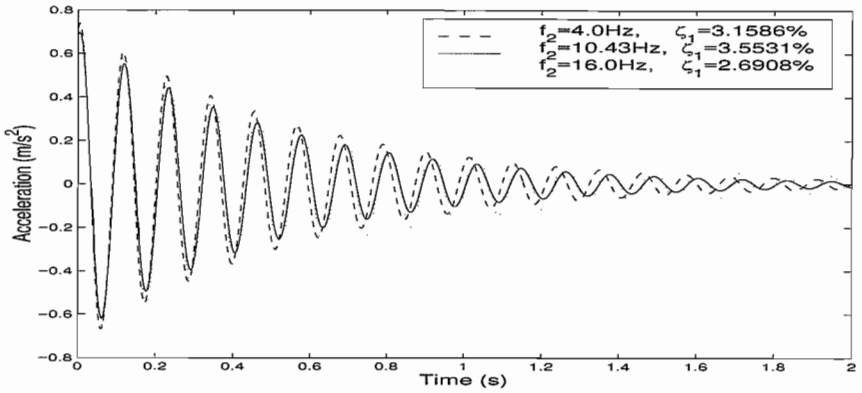


Figure 8.18: Sensitivity of model to variations in body fundamental frequency

8.5 Derivation of human body response

Having shown that the human body has a significant energy absorption capacity, in this section the body response to a given floor vibration is evaluated. Figure 8.19 shows the model response ratio of the secondary mass (human body) to the primary mass (floor slab), with damping of the body taken as 50% critical. It is observed that at resonance, the response of the body is 46% higher than the acceleration of the floor. Hence, the aviodance of such a case can be regarded as a design target for the human perception of vibration. The implications in design of this difference in the responses are discussed in the next section.

To investigate the response of the human body to a given vibratory motion of the floor, consider the primary structure of figure 8.11, M_1^*, subjected to a harmonic excitation, $Pe^{i\omega t}$. The motion of such a system will take the form of equation 8.1, with damping and force incorporated: (also see equation 7.5, page 150)

$$\begin{bmatrix} M_1^* & 0 \\ 0 & M_2^* \end{bmatrix} \begin{bmatrix} \ddot{u}_1 \\ \ddot{u}_2 \end{bmatrix} + \begin{bmatrix} c_1 + c_2 & -c_2 \\ -c_2 & c_2 \end{bmatrix} \begin{bmatrix} \dot{u}_1 \\ \dot{u}_2 \end{bmatrix} + \begin{bmatrix} K_1^* + K_2^* & -K_2^* \\ -K_2^* & K_2^* \end{bmatrix} \begin{bmatrix} u_1 \\ u_2 \end{bmatrix} = \begin{bmatrix} P \\ 0 \end{bmatrix} e^{i\omega t} \qquad (8.9)$$

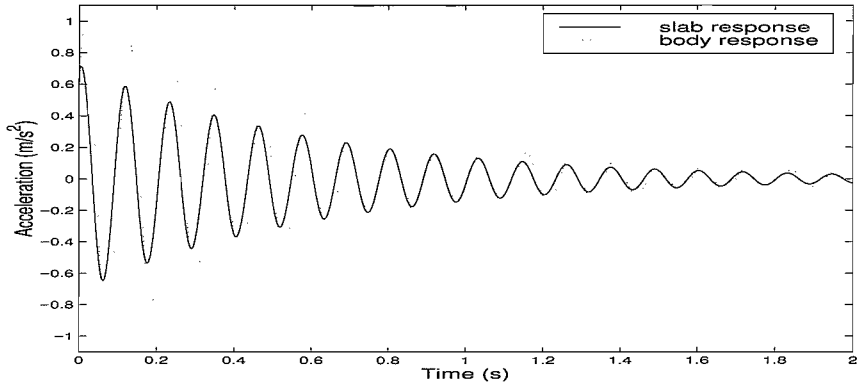


Figure 8.19: Comparison of model slab response with that of human body

Assume the solution to be in the form:

$$\begin{bmatrix} u_1 \\ u_2 \end{bmatrix} = \begin{bmatrix} X_1 \\ X_2 \end{bmatrix} e^{i\omega t} \tag{8.10}$$

and for simplicity write:

$$\begin{bmatrix} K_1^* + K_2^* & -K_2^* \\ -K_2^* & K_2^* \end{bmatrix} = \begin{bmatrix} K_{11} & K_{12} \\ K_{21} & K_{22} \end{bmatrix} = \mathbf{K} \qquad \begin{bmatrix} c_1 + c_2 & -c_2 \\ -c_2 & c_2 \end{bmatrix} = \begin{bmatrix} C_{11} & C_{12} \\ C_{21} & C_{22} \end{bmatrix} = \mathbf{C}$$
$$\begin{bmatrix} M_1^* & 0 \\ 0 & M_2^* \end{bmatrix} = \begin{bmatrix} M_{11} & M_{12} \\ M_{21} & M_{22} \end{bmatrix} = \mathbf{M} \qquad \begin{bmatrix} P \\ 0 \end{bmatrix} = \mathbf{P} \qquad \begin{bmatrix} X_1 \\ X_2 \end{bmatrix} = \mathbf{X} \qquad \begin{bmatrix} u_1 \\ u_2 \end{bmatrix} = \mathbf{U} \tag{8.11}$$

Substitution of equations 8.10 and 8.11 into 8.9 gives:

$$\left[\mathbf{K} - \omega^2\mathbf{M} + i\omega\mathbf{C}\right]\mathbf{X} = \mathbf{P} \tag{8.12}$$

for which the total response is derived using equation 8.10 and is given by:

$$\mathbf{U} = \mathbf{B}\mathbf{P}e^{i\omega t} \qquad \text{where} \qquad \mathbf{B} = \left[\mathbf{K} - \omega^2\mathbf{M} + i\omega\mathbf{C}\right]^{-1} \tag{8.13}$$

Hence:

$$\mathbf{B} = \begin{bmatrix} B_{11} & B_{12} \\ B_{21} & B_{22} \end{bmatrix} = \frac{1}{D}\begin{bmatrix} K_{22} - \omega^2 M_{22} + i\omega C_{22} & -K_{12} - i\omega C_{12} \\ -K_{21} - i\omega C_{21} & K_{11} - \omega^2 M_{11} + i\omega C_{11} \end{bmatrix} \tag{8.14}$$

where D is the determinant of $[\mathbf{K} - \omega^2\mathbf{M} - i\omega\mathbf{C}]$ given by:

$$D = \left(K_{11} - \omega^2 M_{11} + i\omega C_{11}\right)\left(K_{22} - \omega^2 M_{22} + i\omega C_{22}\right) - \left(K_{12} + i\omega C_{12}\right)^2 \tag{8.15}$$

Using standard relationships for complex numbers, the coefficients in $\mathbf{B}$ can be expressed in terms of real amplitudes, giving:

$$\mathbf{B} = \begin{bmatrix} \frac{\sqrt{a^2+b^2}}{\sqrt{g^2+h^2}} & \frac{\sqrt{c^2+d^2}}{\sqrt{g^2+h^2}} \\ \frac{\sqrt{c^2+d^2}}{\sqrt{g^2+h^2}} & \frac{\sqrt{e^2+f^2}}{\sqrt{g^2+h^2}} \end{bmatrix} \tag{8.16}$$

where

$$a = K_{22} - \omega^2 M_{22} \qquad b = \omega C_{22} \qquad c = K_{12}$$
$$d = \omega C_{12} \qquad e = K_{11} - \omega^2 M_{11} \qquad f = \omega C_{11}$$
$$g = \left(K_{11} - \omega^2 M_{11}\right)\left(K_{22} - \omega^2 M_{22}\right) - K_{12}^2 - \omega^2\left(C_{11}C_{22} - C_{12}^2\right)$$
$$h = \omega\left[C_{11}\left(K_{22} - \omega^2 M_{22}\right) + C_{22}\left(K_{11} - \omega^2 M_{11}\right) - 2C_{12}K_{12}\right] \tag{8.17}$$

Substitution of equation 8.16 into equation 8.13, gives the overall response of the two masses as:

$$u_1 = \frac{\sqrt{a^2+b^2}}{\sqrt{g^2+h^2}} P e^{i\omega t} \qquad \text{and} \qquad u_2 = \frac{\sqrt{c^2+d^2}}{\sqrt{g^2+h^2}} P e^{i\omega t} \tag{8.18}$$

Hence, the response ratio of the secondary mass (human body) to the primary mass (floor slab) is given by:

$$\left(\frac{u_2}{u_1}\right)^2 = \frac{c^2+d^2}{a^2+b^2} = \frac{K_{12}^2 + \omega^2 C_{12}^2}{\left(K_{22} - \omega^2 M_{22}\right)^2 + \omega^2 C_{22}^2} \tag{8.19}$$

In terms of the floor and body properties, equations 8.11 can be used to express the above as:

$$\left(\frac{u_2}{u_1}\right)^2 = \frac{K_2^{*2} + \omega^2 c_2^2}{\left(K_2^{*2} - \omega^2 M_2^*\right)^2 + \omega^2 c_2^2} \tag{8.20}$$

Writing $(K_2^* = M_2^* \omega_2^2)$ and $(c_2 = 2\zeta_2 M_2^* \omega_2)$, reduces equation 8.20 to:

$$\frac{u_2}{u_1} = \sqrt{\frac{\omega_2^2\left(\omega_2^2 + 4\omega^2\zeta_2^2\right)}{\left(\omega_2^2 - \omega^2\right)^2 + 4\omega^2\omega_2^2\zeta_2^2}} = \sqrt{\frac{1 + 4\left(\frac{\omega}{\omega_2}\right)^2\zeta_2^2}{\left[1 - \left(\frac{\omega}{\omega_2}\right)^2\right]^2 + 4\left(\frac{\omega}{\omega_2}\right)^2\zeta_2^2}} \tag{8.21}$$

Figure 8.20 is a plot of equation 8.21 for different values of ζ_2. It can be seen that for each ζ_2, the response ratio reaches a maximum at the condition of resonance, when the body frequency equals the loading frequency. For avoidance of human annoyance to vibration, the response ratio should be small. As expected, figure 8.20 shows that notable reductions in the ratio are achieved with higher values of human body damping. In each case, the maximum response ratio can be derived by substituting $\omega = \omega_2$ in equation 8.21 to get:

$$\left(\frac{u_2}{u_1}\right)_{max} = \sqrt{\frac{1 + 4\zeta_2^2}{4\zeta_2^2}} \tag{8.22}$$

From the experimental results, putting the derived value of ζ_2=50% critical into equation 8.22, gives a response ratio of 1.41 between the body and the floor. This means that the body response is 41% larger than the structural response. It compares with 46% obtained from figure 8.19, hence good agreement is observed. Using the response ratio of 1.46 from figure 8.19, equation 8.22 gives an optimal human damping ratio of 47% critical, which is within the range obtained from the experiments (i.e. 45-55% critical) given in section 8.4.2.

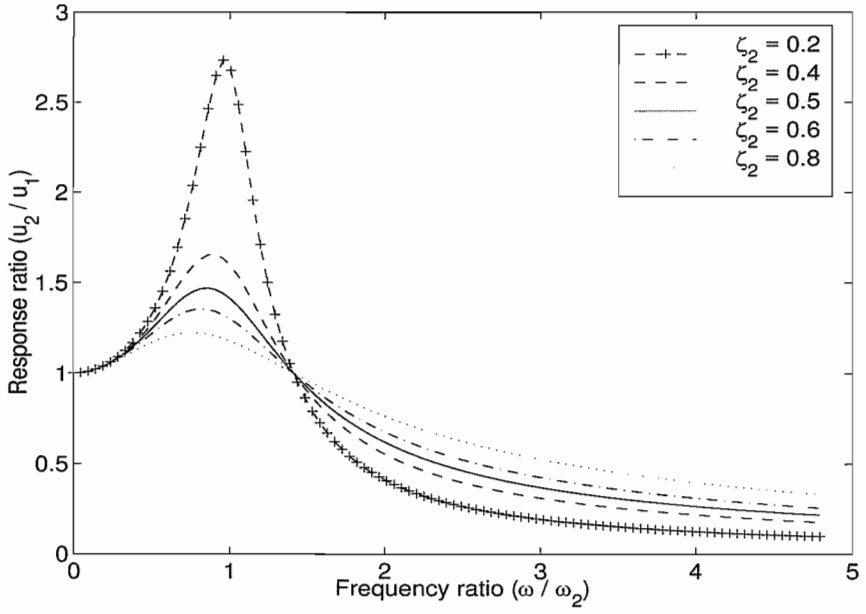


Figure 8.20: Variation of response ratio with loading frequency and human damping

8.6 Design implications

In order to understand how structures respond to dynamic loads generated by people, it is necessary to understand how people and structures interact. It has been shown that the human-structure interaction is similar in nature to a structure-TMD system, with the difference that the ratio of critical damping of the body has been measured as 50%, as compared to generally below 10% for a TMD. This suggests that the human body is a very good energy absorber. However, a TMD is usually a specially designed device, fixed onto a structure, and is always available to perform its function. The downside with people is that although the human body is a natural mass-spring-damper system, it will not always be present on a structure. In addition, when a human body changes from its stationary state to a moving state, its effect as an energy absorber is totally lost, because the body does not vibrate with the slab and acts solely as a load [Ellis and Ji (1997)]. This limits the use of people as energy absorbers.

The experiments have shown that at frequencies low enough to cause annoyance to occupants, the human body absorbs much of the floor energy. This effect is lost at higher frequencies. Therefore, with its significant energy absorption capacity and usable range of natural frequencies, the human body is very effective in reducing floor vibrations. In cases where a crowd is present, it is unlikely that all the occupants are not stationary, hence the stationary people will absorb the energy imposed by the moving ones. As the number of occupants and their movements change, so will the nature of the 2DOF system representing their interaction with the structure. It follows that this possible

source of energy dissipation should be accounted for in design codes, rather than assuming the occupants as extra mass. This leads to two implications: (1) evaluating structural response where people are involved, and (2) evaluating human response to vibration.

It has been shown in section 8.5 that the response ratio of the secondary mass (human body) to the primary mass (model slab) is of the order of 1.5, with damping of the body at 50%. In other words, when the integer multiple of the load frequency equals the fundamental frequency of the human body, the body experiences accelerations up to 50% higher than the measured floor accelerations. The avoidance of such a case can be regarded as a design target, which leads to perhaps the most important difference between the 2DOF models of TMD-structure and human-structure systems. In the design of a TMD, the frequency of the TMD should be close to the frequency of the structure for maximum response reduction, and thus maximum response in the TMD. The design for reducing human sensitivity, however, should focus on avoiding resonance with the structure frequency, hence aiming for a low response of the secondary mass (i.e. the body). So the TMD is designed on the basis of the slab but the slab should be designed on the basis of the human body.

The importance of considering the response of the human body is explained by a simple example. For vibrational serviceability problems, such as people walking across a floor, there must always be someone in a stationary position to feel the vibration. This person will therefore absorb energy and reduce the vibrations. If the stationary person were to be replaced by a transducer, it would monitor a larger vibration from the same source (i.e. there is no added energy absorption). Also, if people's perception of vibration were to be investigated, a transducer on the floor would only measure floor motion, which would be different to a person's motion, as proved in section 8.5.

It can therefore be argued that the accelerations quoted in subjective ratings of some criteria are that of the structure, and the accelerations within the human body are up to 50% higher than the measured floor accelerations. This is implicitly taken into account in the perceptibility criteria, by the subjective ratings of occupants, but not explicitly noted in any of the guidelines. It is hence important that an appropriate model of human-structure interaction is adopted in the guidelines for different situations and activities, and that the effect of the occupants be considered in the design of the structure. Furthermore, in the design codes where minimum frequency limits are quoted, the presence of a crowd will lead to interactions with the supporting structure, affecting its fundamental frequency, which also needs to be considered in the design.

Chapter 9

Field test results

9.1 Introduction

This chapter presents the results of vibration tests performed on a full-scale floor in order to obtain its dynamic properties. There are many reported floor vibration tests in the literature [Pernica and Allen (1982), Rainer and Swallow (1986), Maguire and Severn (1987), Osborne and Ellis (1990), Caverson (1992), Pavic et al. (1994), Zaman (1996)]. These all give fundamental parameters of natural frequency and damping, but less evidence exists of tests conducted to investigate the acceleration response of floors in detail. In the tests described here, the usual dynamic parameters were first measured and then the floor was excited at its fundamental frequency, as well as controlled walking tests, to derive its acceleration response. These were used in different acceptibility guides to classify the slab dynamic behaviour. This was part of a series of tests commissioned by the Steel Construction Institute (SCI) in order to establish a database of floor acceleration measurements due to human activities.

The tested slab was the first floor of the SCI headquarters in Silwood Park, Ascot. The test was of a commercial nature and was conducted on 24th October 1998, when the building was unoccupied. A plan of the floor area was provided, from which locations of expected high response were deduced. Impact tests were conducted on these points to find the most critical, but representative, location for more comprehensive tests. Forced vibration experiments were then carried out on the chosen location to measure more accurately the floor natural frequencies, damping, stiffness, and mode shapes. Based on the derived fundamental frequencies, walking tests were conducted across the floor with eleven different paces and walking styles, and the responses measured accordingly. Where possible, the results are compared with those of the model slab tests and differences are discussed. A detailed description of test procedures and results can be found in Williams and Falati (1998).

9.2 Description of the floor

The first floor of the SCI headquarters building is currently being used as an open-plan office area, divided by both full-height and cantilever partitions. Other non-structural components include false flooring, false ceiling, mechanical ductwork, and a significant amount of office furniture. Figure 9.1 gives an indication of the layout of the floor, and its non-structural components. Figure 9.2 shows a detailed plan as supplied by the SCI. The dotted lines indicate the approximate positions of the false flooring panels. The floor itself consists of a 130mm deep concrete slab cast on top of a 1.2mm gauge Holorib deck, supported by the main and intermediate beams. Above the slab, the 20mm false flooring panels provide 150mm of void for electrical cables and mechanical ductwork. The panels merely rest on their pedestals in a similar formation as layout 2 of the model slab tests (see section 3.6.4), and are covered by a layer of carpet tiles. The full-height partitions are made of glass and span from top of floor panels to the underside of the false ceiling, a height of 2600mm.

The vibration tests were conducted on the floor panels (after lifting carpet tiles) and on the bare concrete slab in a selected grid, as shown in figure 9.3. At time of testing, the floor was free of personnel, other than those performing the tests. The following sections give a detailed account of these tests.



Figure 9.1: A view of the first floor in the SCI building

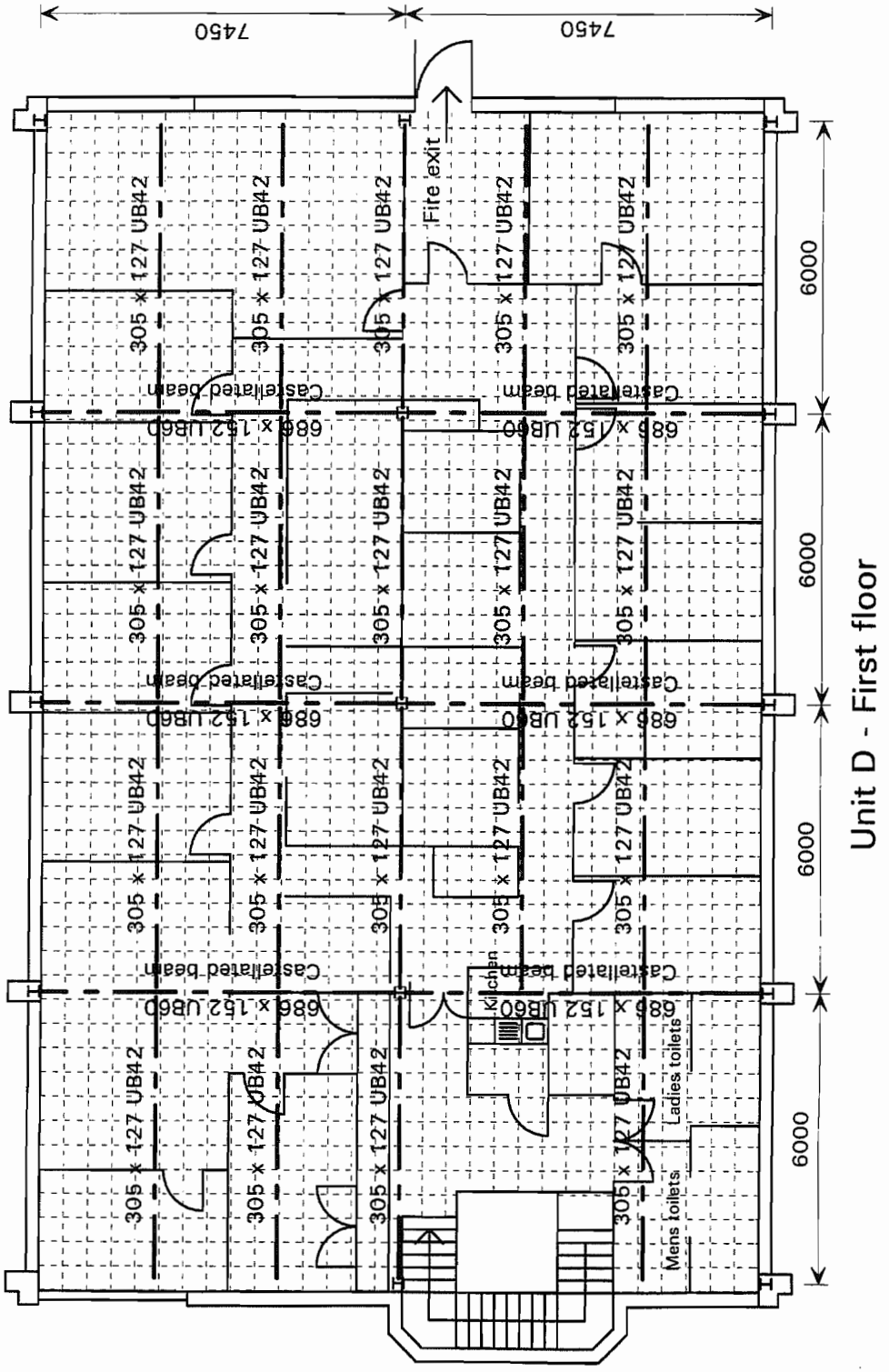


Figure 9.2: Detailed plan of the floor showing main and intermediate beams

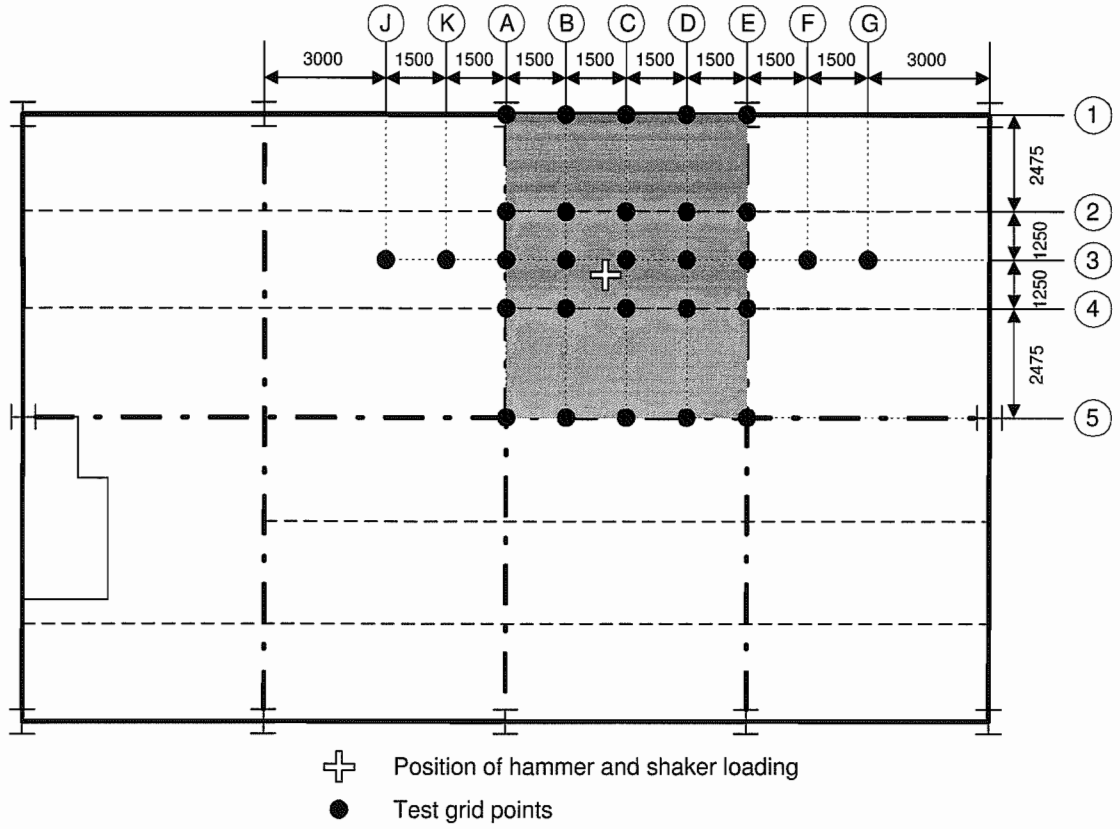


Figure 9.3: Plan of floor showing test grid locations

9.3 Impact tests

Two types of impact test were undertaken on the floor to find the critical location. These were instrumented hammer and heeldrop tests. The hammer test is deemed to be a more accurate measurement technique, as the force exerted on the floor is known.

9.3.1 Instrumented hammer excitation

These tests were conducted on seven locations across the floor area to find the panel with the lowest fundamental frequency and highest response. The points tested were $B2$, $B4$, $C3$, $D2$, $D4$, $G3$ and $J3$ (figure 9.3). The equipment used is explained in section 3.3.1 and the test procedure is described in section 4.5.1. Following initial trials, the position of hammer impacts was chosen to be stationary on the bare concrete, near the centre of a selected panel, as shown in figure 9.3. The response was measured by placing the accelerometer at each point and applying ten hammer blows to obtain an accurate average reading for that point. During each test, the coherence function was constantly monitored for effects of external excitations and the tests were repeated if the coherence at the modes fell below 80%. A typical transfer function and its coherence is shown in figure 9.4.

Note that the coherence for this slab is less than the model floor tests. This is because the hammer excitation does not always input a large enough force to excite a real size floor adequately.

The frequencies obtained at all seven points are given in table 9.1 in increasing order. The lowest frequency mode appeared at around 8.4Hz for many of the tested points, and was hence deemed to be the fundamental natural frequency of the particular floor area. Tests at the centres of adjacent panels gave equal or higher values of fundamental frequency. This could have been anticipated from examination of figure 9.3, as position $C3$ is the centre of one of the largest spanning sections of the floor area. It was this position, and the entire floor panel in which it lies, which was selected for subsequent detailed tests. The heeldrop tests confirmed this choice as described below.

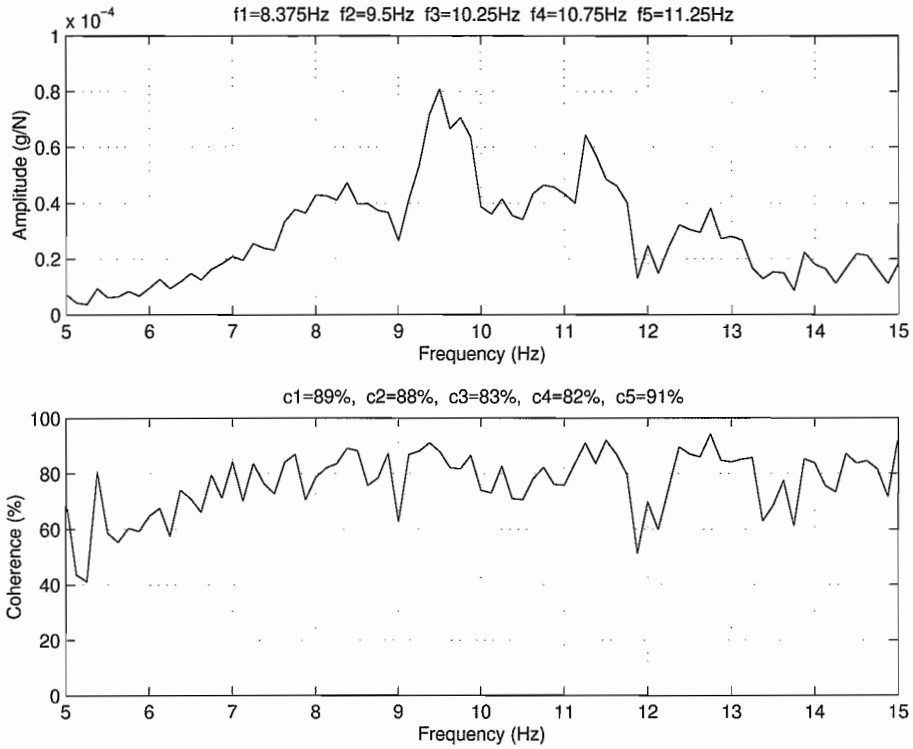


Figure 9.4: Hammer test transfer function and coherence at $C3$

Table 9.1: Instrumented hammer test principal frequencies

Test position	**Transfer function peak frequencies (Hz)**				
$B2$	8.63	9.63	11.0	11.38	
$B4$	8.44	9.25	9.88	11.25	12.0
$C3$	8.38	9.50	10.25	10.75	11.25
$D2$	8.38	9.63	10.25	11.0	11.88
$D4$	8.38	9.0	9.75	10.38	11.38
$G3$	8.38	9.25	10.13	11.50	
$J3$	8.50	9.25	10.75	11.50	11.88

9.3.2 Heeldrop excitation

These tests were conducted at grid points $A3, B2, B3, C3, D2$ and $G3$ as shown in figure 9.3. At each point, a minimum of three heeldrops was undertaken to give an average of response readings. It was found that the position of application of a heeldrop, in respect to the accelerometer, affected the readings. Similar readings were obtained when: (i) the heeldrop and accelerometer were on the concrete slab, (ii) heeldrop on bare false floor panel with accelerometer on adjacent panel, and (iii) heeldrop on carpeted false floor panel with accelerometer on adjacent panel. However, when the heeldrop and accelerometer were on the same false floor panel, much higher readings were recorded, presumably due to localised high-frequency "rattling" of the panel on its supports. These tests were therefore discounted. All results reported here are for a heeldrop on a bare panel with the accelerometer on the adjacent panel.

After recording, the response data in the time-domain were converted to the frequency domain in the form of a power spectrum. For clarity, all frequencies above 25Hz were filtered out. The response and corresponding power spectrum for position $C3$ is shown in figure 9.5. The frequencies obtained from the spectra of all tested points are given in table 9.2 in increasing order. These can be compared with values of table 9.1, which show good agreement.

Table 9.2 also shows the values of peak acceleration response obtained at each point. These are averages of all the tests at a particular point, which sometimes exhibited a substantial range. Note that as expected, the peak accelerations for this floor are significantly lower than those for the model slab tests (table 5.7, page 97). This was due to the heavy mass of the field floor compared to the amplitude of applied load (i.e. lower mass ratio between applier and floor). For this floor, the largest responses were measured at points $C3$ and $G3$, which are centres of adjacent panels. Having a smaller fundamental frequency, the panel containing $C3$ was considered the more critical panel and was tested further, as described below.

Table 9.2: Heeldrop peak acceleration and principal frequencies

Test position	**Peak accel. (m/s^2)**	**Power spectra peak frequencies (Hz)**		
$A3$	0.17	8.44	10.10	
$B2$	0.27	8.23	9.61	10.47
$B3$	0.28	8.23	9.64	
$C3$	0.31	8.28	9.53	10.51
$D2$	0.25	8.22	9.55	10.55
$G3$	0.35	9.82		

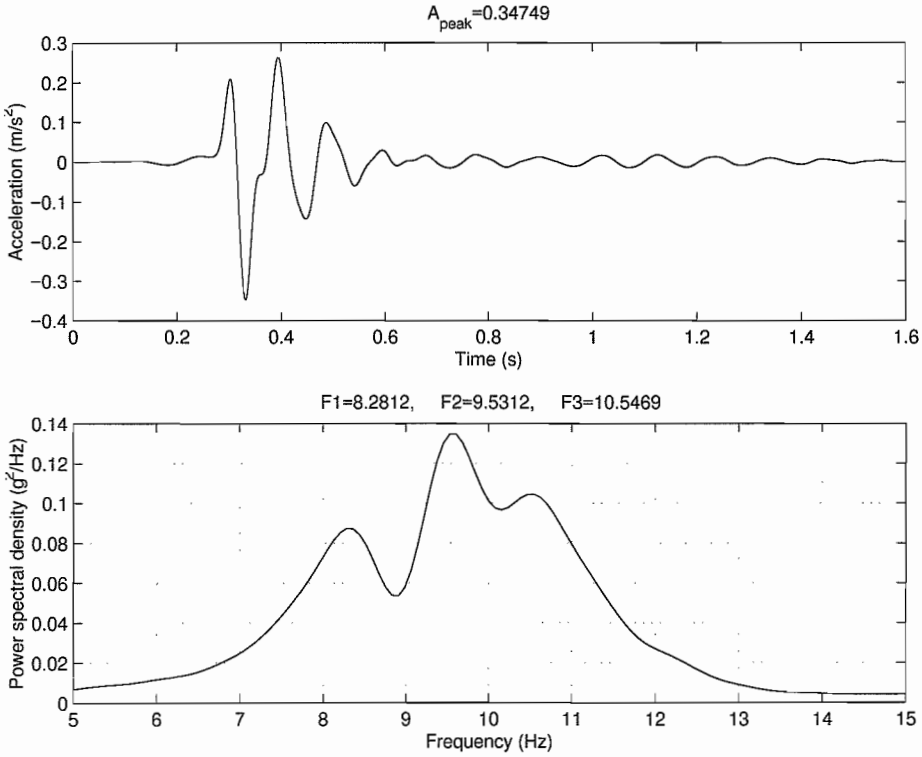


Figure 9.5: Time and frequency representations of response due to heeldrop at $C3$

9.4 Forced vibration tests

Following initial impact tests, which identified the shaded panel in figure 9.3 as a critical area, a comprehensive shaker test setup was used to measure the dynamic characteristics of the floor at the critical modes of vibration. The equipment used is described in section 3.3.2 and the test procedure is explained in section 4.5.2. The shaker was positioned on the bare concrete 0.5m from $C3$, near the centre of the test area. The floor panel was then divided into a 5×5 grid as shown in figure 9.3. Sine-sweep and single sine-wave loading tests were undertaken, as described below.

9.4.1 Sine-sweep loading

Figure 9.6 shows a typical transfer function following a sine-sweep loading, and figure 9.7 shows SDOF curves fitted at the first two modes. The values of frequency, damping, and stiffness are the parameters which define these curves and hence provide the best estimate of the equivalent parameters defining the modes of the structure (see section 4.6.4). From these tests, at the fundamental mode, the average damping ratio was 5.4% at a frequency of 8.3Hz, with the stiffness at $C3$ being 8.9×10^6N/m. At the second mode, damping was 4.2% with 9.7Hz and stiffness of 1.4×10^7N/m at $C3$. These values of damping are around a factor of four greater than the model slab readings.

Apart from obvious structural differences, the higher damping values are due to the presence of furniture, false flooring, partitions and mechanical ductwork. The derived values are also in good agreement with the ratios suggested by Murray (1981) and particularly with those mentioned in AISC (1997) (see section 2.6.4). For higher modes, the closeness of the peaks made the SDOF curve fitting less accurate. The peak frequencies (from the transfer function) for modes 3 and 4 were 10.6Hz and 11.4Hz respectively.

The mode shapes for the chosen panel were derived, and the continuity of the floor slab was assessed by taking measurements of response at adjacent panels. These measurements were taken along the centreline of the panels (gridline 3 in figure 9.3). The first four perceived modes of vibration for the tested floor panel and cross-sections of the mode shapes are shown in figures 9.8-9.11.

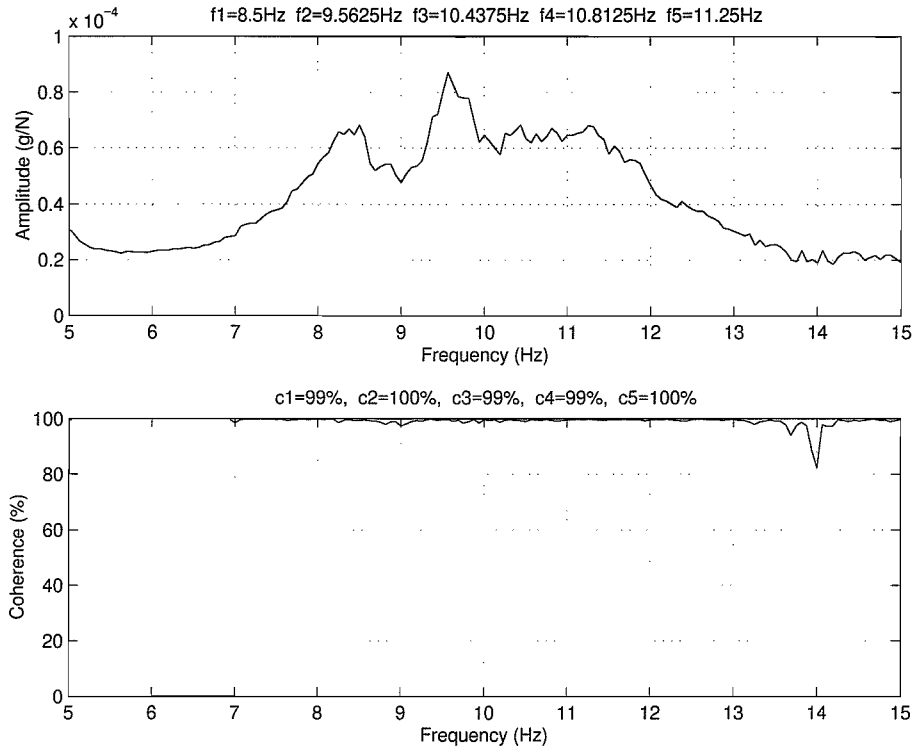


Figure 9.6: Transfer function and coherence of sine-sweep test at $C3$

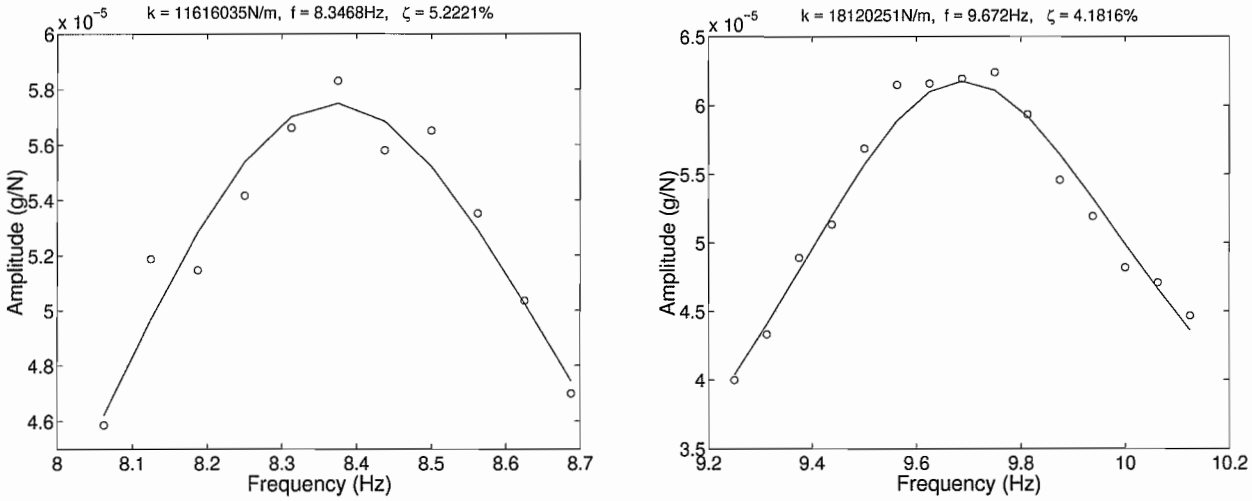


Figure 9.7: SDOF model fitted to modes 1 and 2 at $B4$

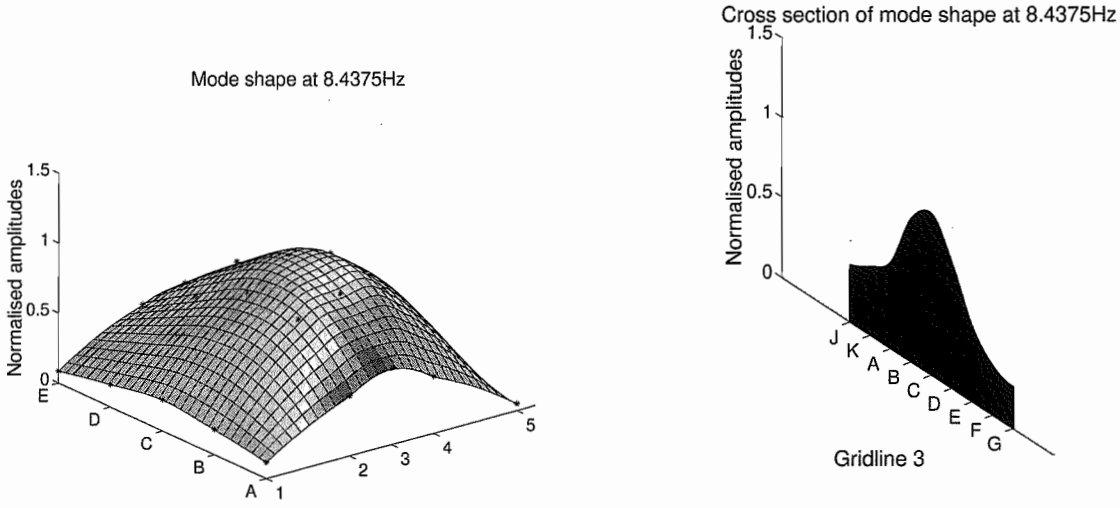


Figure 9.8: Mode 1 modeshape and cross-section at gridline 3

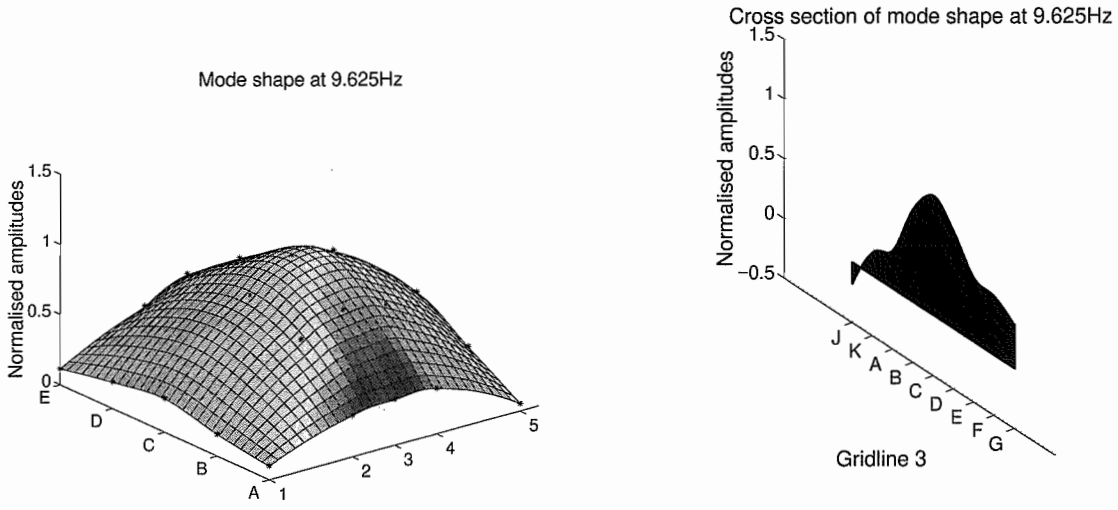


Figure 9.9: Mode 2 modeshape and cross-section at gridline 3

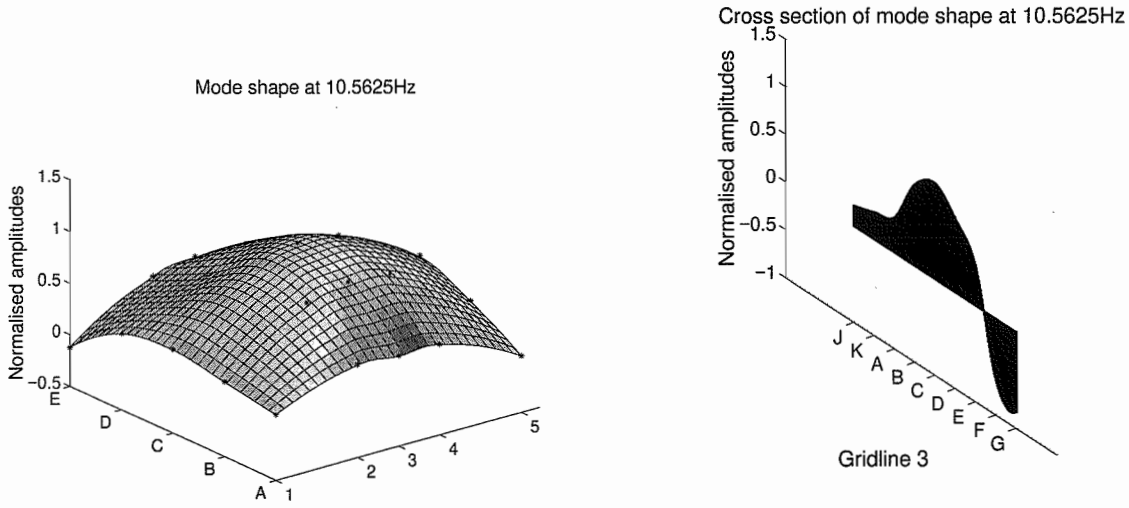


Figure 9.10: Mode 3 modeshape and cross-section at gridline 3

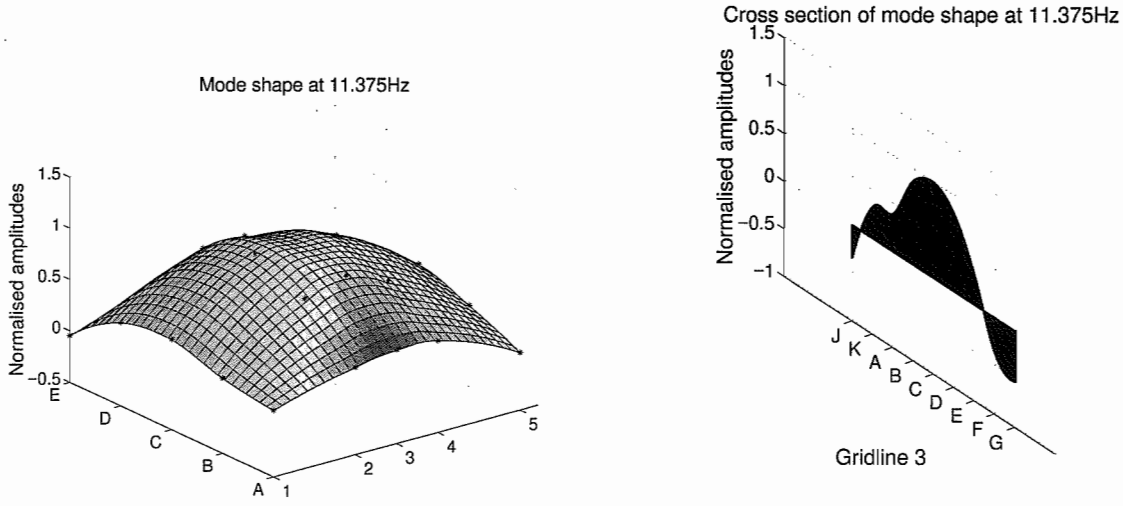


Figure 9.11: Mode 4 modeshape and cross-section at gridline 3

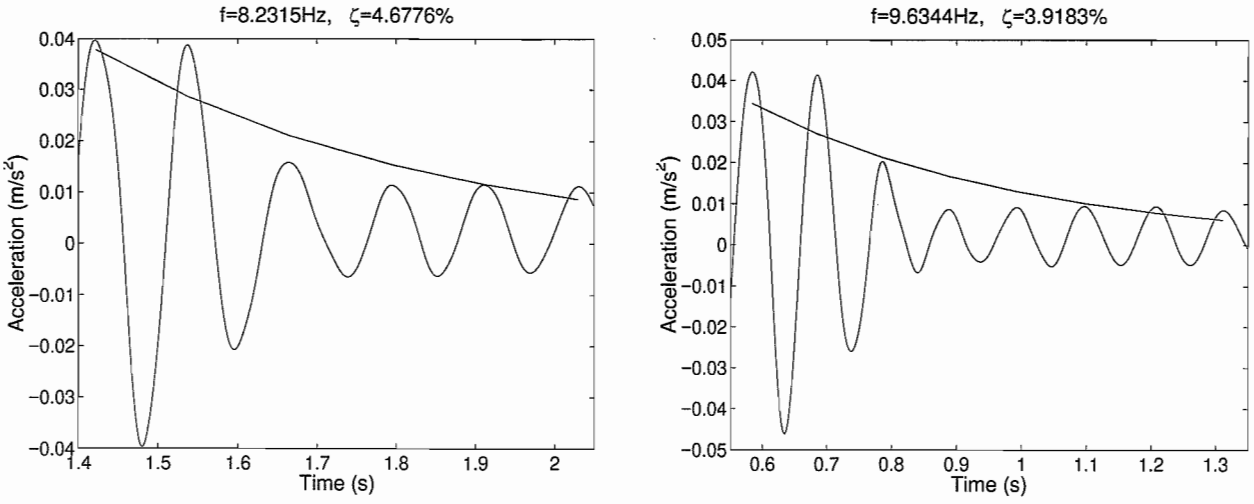


Figure 9.12: Measured and best fit decay model for modes 1 and 2 at $C3$

9.4.2 Single sine-wave loading

A total of thirteen single sine-wave tests were carried out with 8.5Hz and 9.6Hz loadings at points $A4, C2, C3$ and $D2$ in figure 9.3. The shaker was suddenly stopped and the resulting decay of oscillation was measured, which would give a further independent assessment of damping for the particular mode. Figure 9.12 shows typical decay responses at the first two frequencies, with the damping calculated by fitting a SDOF curve on a specified section of the decay. The best fit curve, based on a linear system, is defined by the parameters of damping and frequency (see section 4.6.4). With these tests, average damping was 4.7% at 8.3Hz and 4.1% at 9.5Hz. Note that the decay of vibrations is not a pure exponential, as the damping will not be purely viscous (see section 2.6.2). In comparison with a typical model slab decay response (figure 4.15, page 86), more non-linearity exists in the field slab. Although the curve fitting is not perfect, the overall derived values for damping and natural frequency agree satisfactorily with the results of the previous section.

Tests with standing man

Single sine-wave tests were also conducted at points $C2, C3$ and $D2$ with three people standing by the accelerometer during the tests. Figure 9.13 shows a comparison of the response decays, with and without the men, at the second mode. The presence of the men has little effect on the overall response measured by the accelerometer. However, the average readings of all tests showed that at the first mode, the damping increased to 5.7% with a frequency of 8.1Hz, and at the second mode, damping became 4.8% with a frequency of 9.5Hz. Hence, the presence of the men had the effect of marginally increasing damping at the region where they were standing.

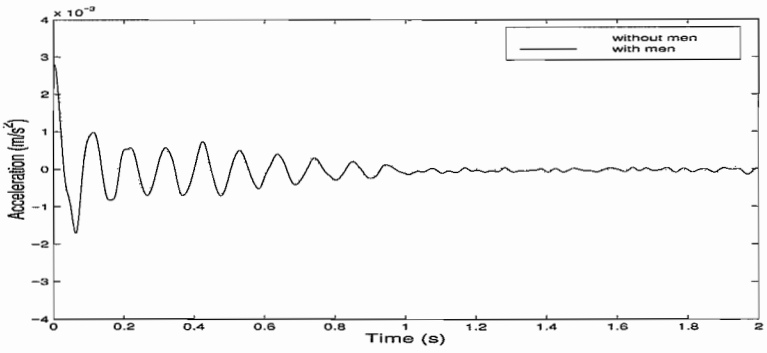


Figure 9.13: Comparison between experimental results of bare slab and with three men standing by the sensor at $D2$ (sine-wave loading of 9.5Hz)

To investigate this effect further, the 2DOF and SDOF models of chapter 8 were implemented on the field results with ζ_2 taken as 50% (as for one man). Figure 9.14 shows that the models represent

the presence of the men satisfactorily. In this case, the mass of the men compared to the mass of the slab is very small and hence the effect is not as significant as for the model slab tests. This is observed in figure 9.15, which shows a comparison between the 2DOF and SDOF models. When compared to figure 8.16 (page 181), these results show that the mass ratio is a critical factor in the structure-human interaction and if the mass of the people is small compared to the mass of the slab, a SDOF model would suffice. However, if the mass ratio is large, the representation is best shown by a 2DOF model (as in chapter 8).

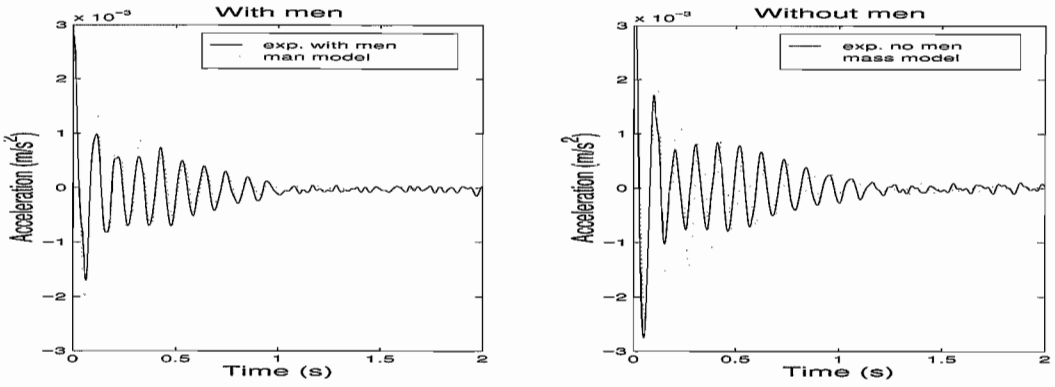


Figure 9.14: Comparison between model and experimental results

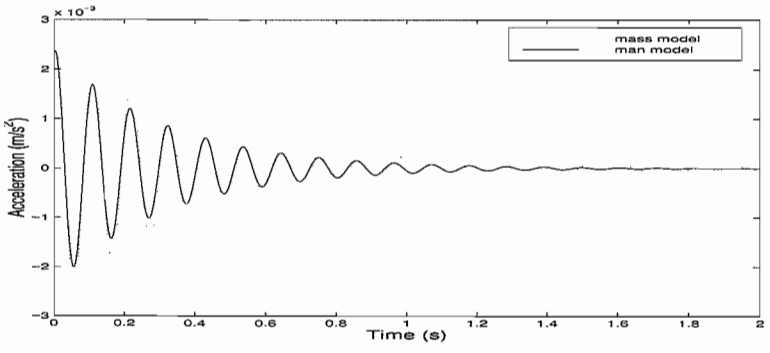


Figure 9.15: Comparison between 2DOF human-structure model and SDOF slab model

9.5 Walking tests

With the accelerometer positioned at $C3$, walking tests were undertaken to monitor the vibration levels generated on the floor when in normal use. A portable computer was used to generate a beat at a pre-selected frequency, so that the pace of the walker could be controlled. The direction of walking was in a straight line across the panel from position $A3 \rightarrow E3$ and was started at an adjacent panel so that the walker had already established his forward momentum on approaching

$A3$. Only the lower modes of vibration are likely to be excited and pacing at an integer fraction of these frequencies can cause resonance, representing the worst loading cases.

The types of test were: normal walking, running, walking on the spot, and jumping on the spot. Each test was repeated with a different walker to account for variability of loading. Table 9.3 gives the type of test, along with walking frequency, response frequency, root mean square acceleration, and peak acceleration (both averaged over tests with different walkers). When compared with the results of the model slab (section 5.7.2, page 98), the induced acceleration responses for the field slab are significantly lower, due to differences in boundary conditions and mass ratios. Below, each test is examined in more detail.

Table 9.3: Results of walking measurements at position $C3$

Test No.	Description of walk	Typical pace frequency (Hz)	Typical response freq. (Hz)	Average peak accel. (m/s^2)	Average RMS accel. (m/s^2)
1	2Hz (controlled)	2.03	8.03, 10.06	0.071	0.014
2	2.5Hz (controlled)	2.25	8.47, 9.09, 10.75, 11.31	0.094	0.015
3	3Hz (controlled)	3.16	9.56	0.126	0.021
4	normal (uncontrolled)	2.16	8.63, 10.88	0.066	0.012
5	Two men at 2Hz (controlled)	2.06	8.13, 9.44, 10.25, 10.84, 11.41	0.108	0.022
6	Two men at 2.5Hz (controlled)	2.41	8.09, 9.53, 10.28, 11.56, 12.16	0.124	0.020
7	Running at 3Hz (controlled)	3.28	9.69	0.115	0.022
8	normal running (uncontrolled)	2.63	8.0, 9.69	0.127	0.020
9	Walking on the spot at 2Hz (controlled)	1.97	8.0, 9.97	0.097	0.021
10	Jumping on the spot at 2Hz (controlled)	2.0	8.06	0.215	0.043
11	Jumping on the spot at 2.5Hz (controlled)	2.5	7.53, 10.03	0.339	0.087

Test 1 was conducted at a pacing rate of approximately $\frac{1}{4}$ of the fundamental frequency of the floor. Thus, the fourth harmonic of the walking pace would be in resonance with the floor. A typical acceleration time-history and power spectrum are shown in figure 9.16. Note the build up of vibrations as the walker approaches and passes the centre of the floor. The footfalls can also be noticed from the increasing peak at every fourth cycle. The relatively high damping of the floor eliminates the possibility of a build-up of floor vibration due to successive footfalls. The spectrum shows that this pace of walking excites the first and third modes of the floor.

Test 2 was an attempt to excite the second floor frequency with the fourth harmonic of walking, hence the walker traversed at a faster pace. From table 9.3, it is observed that as well as first and second modes, some higher modes were also excited at this pace.

Test 3 was an even faster walk, which verged on the border with running, in an attempt to excite the second and third modes with the third harmonic of walking force. Table 9.3 shows that the response was dominated by the second mode at 9.56Hz. In this instance, the pace of walking was so high that the damping between footfalls was less than previous cases, leading to accumulation of vibration response and higher acceleration readings.

Test 4 originated after testing all obvious possible controlled walking paces. The walker was now asked to traverse across the panel at a normal pace without the use of the timing signal. This test was repeated with three different walkers and a typical result is shown in figure 9.17, for time and frequency domains. The walking frequencies and induced accelerations varied in a wide range from 0.007m/s^2 to 0.017m/s^2 RMS. The mode of vibration being excited in this case depended strongly on the pace of walking of each individual involved.

Tests 5 and 6 were similar to tests 1 and 2 but two walkers were used in each case. A timing signal was used and the walkers attempted to co-ordinate their walking pace. The results of figure 9.18 indicate that at the same walking frequency, the same modes are excited as with one walker (figure 9.16), but the accelerations are increased by a sizeable margin.

Test 7 involved a person running across the panel at 3Hz and **test 8** was running without the use of the timing signal. Results of figure 9.19, for uncontrolled running, show that consecutive footsteps are fast enough not to allow damping of the vibrations between footfalls. In this case, first and second modes were excited and in comparison to uncontrolled walking (figure 9.17), much higher acceleration readings were measured.

Test 9 was performed by a person walking on the spot, adjacent to the accelerometer, at $\frac{1}{4}$ of floor fundamental frequency. The essential difference between this test and normal walking is that the walker does not have a forward momentum and hence the energy is concentrated only in the vertical direction. Therefore, a relatively large acceleration response can be observed in figure 9.20, as compared with the similar case of normal walking (figure 9.16). Notice however, that roughly the same modes of vibration were excited in both cases.

Tests 10 and 11 were performed in an attempt to produce the worst possible loading case, by which the person was jumping on the spot adjacent to $C3$ at a controlled frequency of $\frac{1}{3}$ and $\frac{1}{4}$ of floor fundamental frequency. As expected, these cases produced the highest responses. This type of activity can be regarded as a gymnasium or dance floor loading and from figure 9.21, it has significantly high harmonic component amplitudes and can excite one or more of the lower modes of the floor. For these cases, also note the substantial peaks at the lower harmonics of the loading. Similar results were also found in BRE 426 (1997).

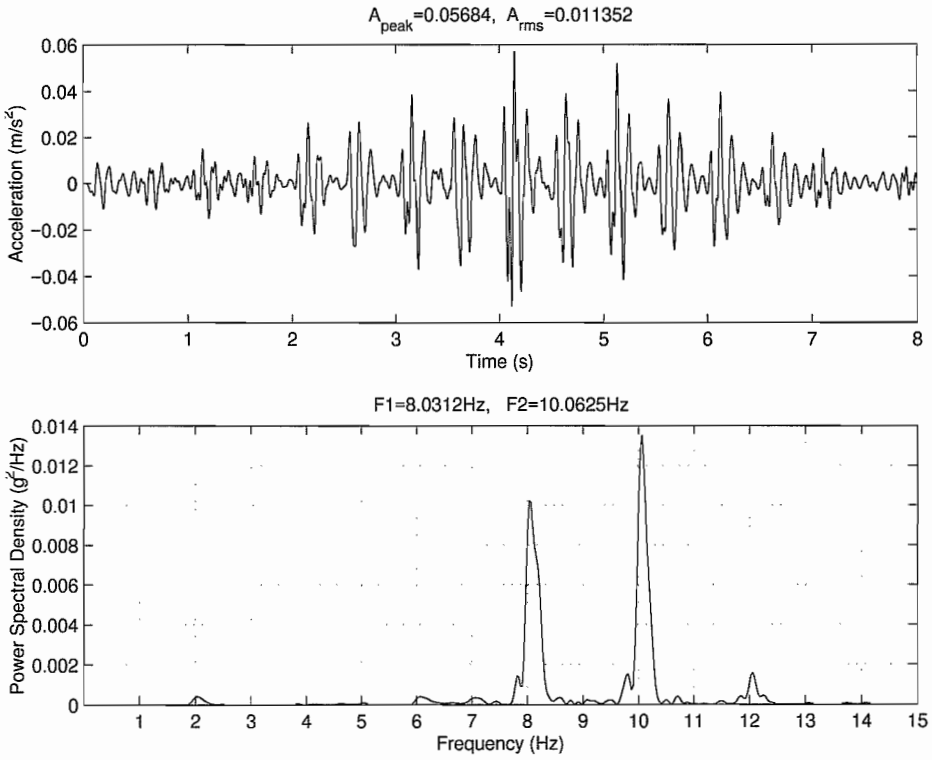


Figure 9.16: Typical response to controlled walking at 2Hz measured at $C3$ (Test 1)

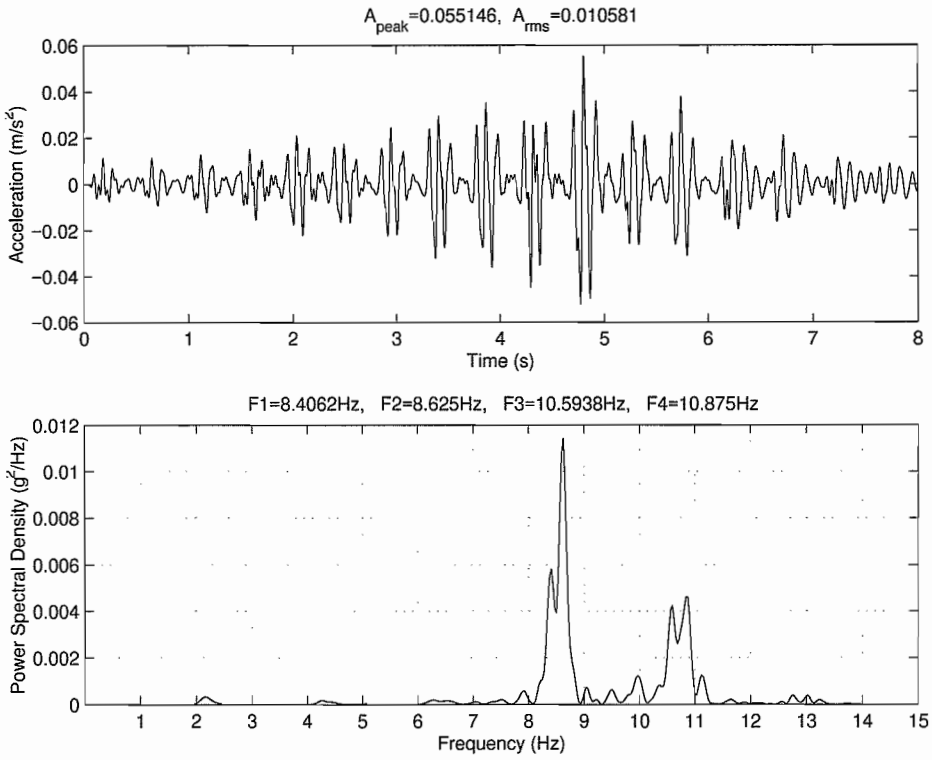


Figure 9.17: Typical response to uncontrolled walking measured at $C3$ (Test 4)

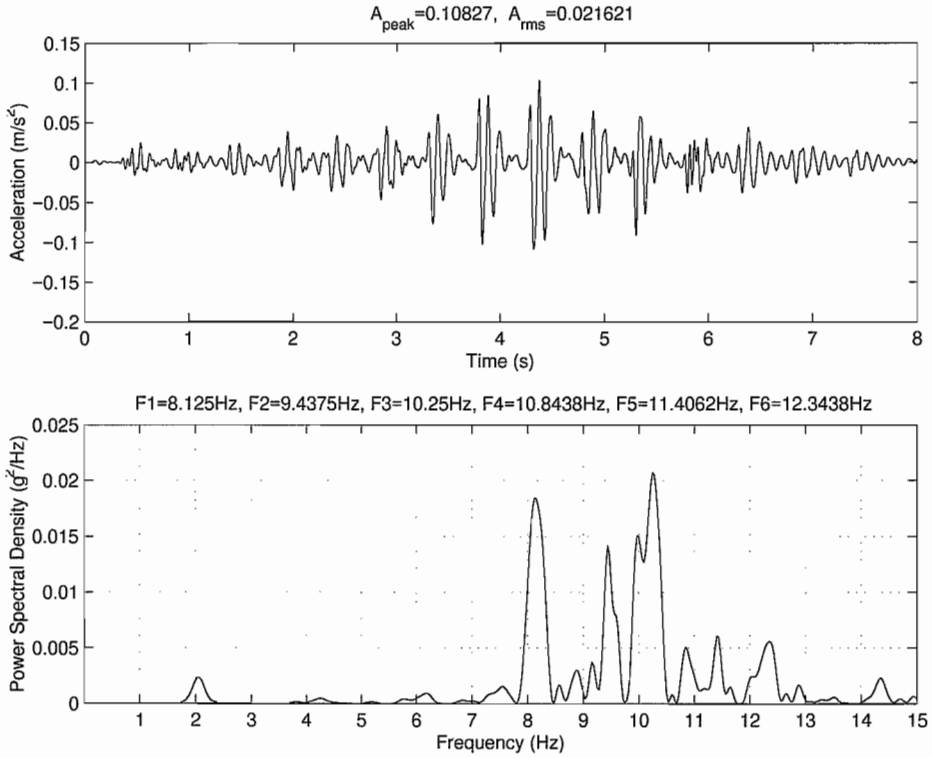


Figure 9.18: Typical response to controlled walking of two men at 2Hz measured at $C3$ (Test 5)

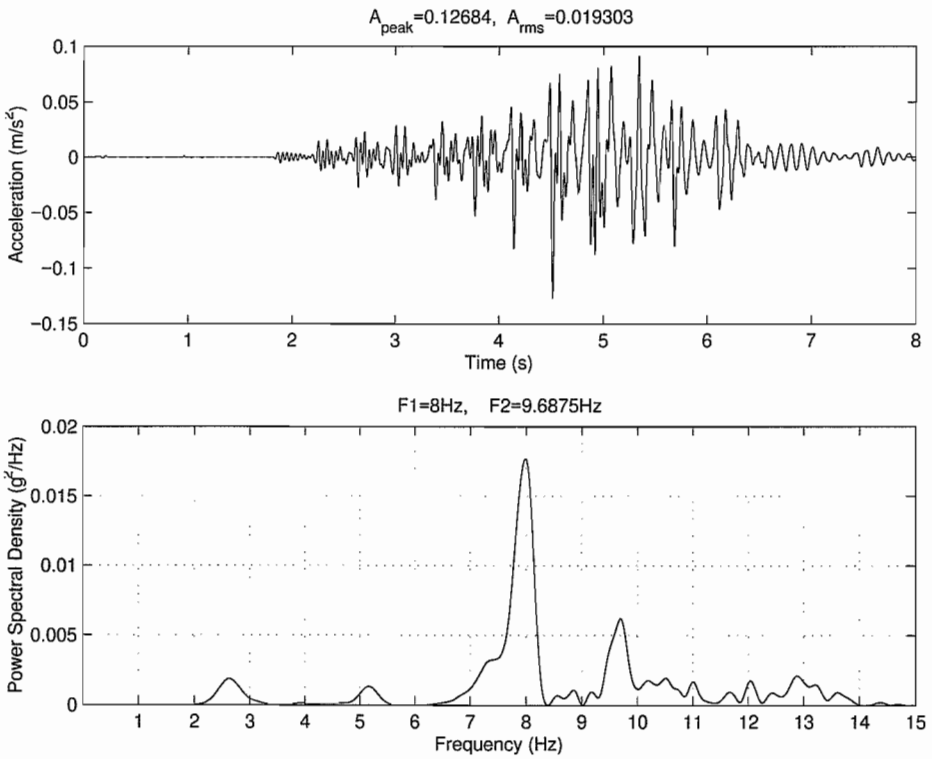


Figure 9.19: Typical response to uncontrolled running measured at $C3$ (Test 8)

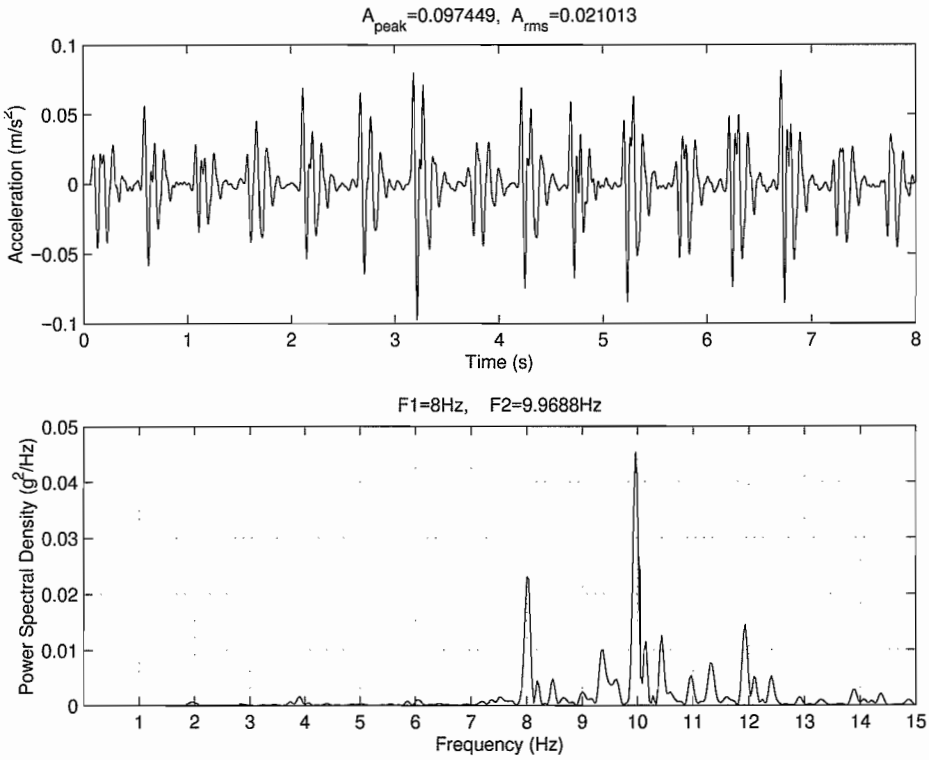


Figure 9.20: Typical response to walking on the spot at 2Hz measured at $C3$ (Test 9)

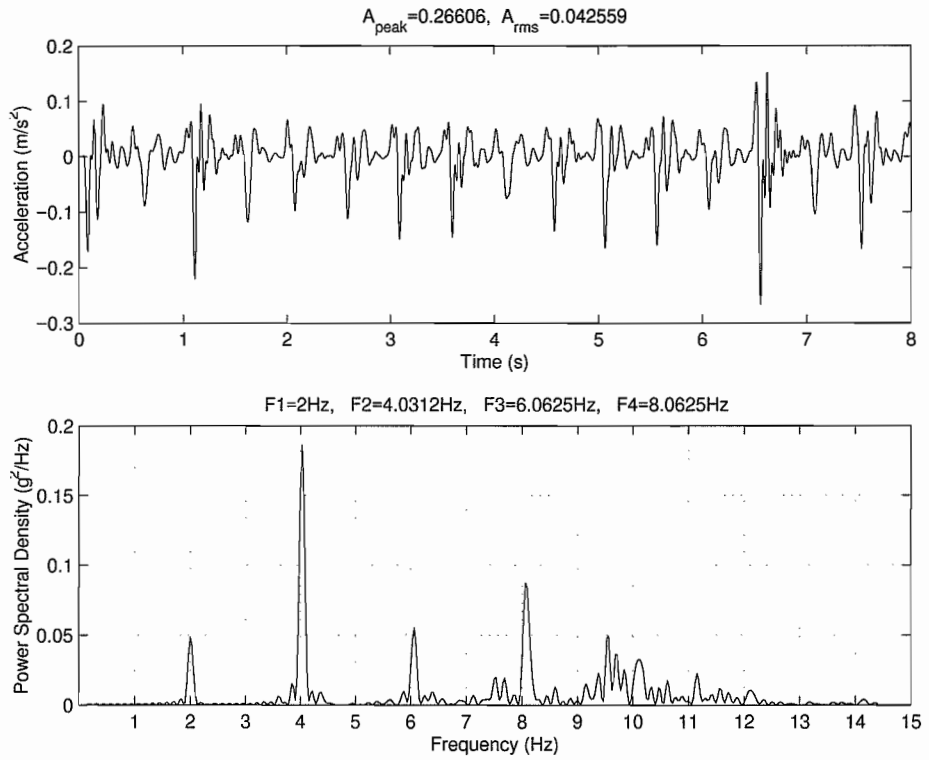


Figure 9.21: Typical response to jumping on the spot at 2Hz measured at $C3$ (Test 10)

9.6 Classification of the floor

In this section, the walking and heeldrop response readings are used and the floor is assessed for vibration acceptibility, using the CSA and ISO/BSI/ANSI perceptibility guidelines of section 2.2.2.

Figures 9.22-9.26 show the obtained acceleration responses plotted in the two scales. For forces imposed due to walking, both guidelines classify the floor as acceptable in office or residential environments (figure 9.22). When walking was controlled to create the worst case loading, (test 3), the ensuing accelerations are seen to be at the limit of acceptibility of the ISO/BSI/ANSI scales for offices, when the load was regarded as intermittent (i.e. 4×base curve, see table 2.3, page 15). In comparison with equivalent model slab results, (figure 6.30, page 136), smaller responses are observed with the field slab. The effect of more than one person walking is shown in figure 9.23, where an increase in acceleration is observed to levels which are on, or slightly above, ISO/BSI/ANSI scales. These vibrations are below the acceptibility levels of CSA scales. The floor is still regarded as acceptable with two men walking in unison. For cases involving a group, the liklihood of walking-in-step is low, but in the event, higher accelerations would be expected.

The measurements for running at 3Hz and walking at 3Hz are similar (figure 9.24), since at this pace the walker is close to breaking into running. The accelerations are again higher than normal walking and on the limit of acceptibility of ISO/BSI/ANSI scales. For cases of jumping, much higher response readings were observed (figure 9.25), to an extent that the guidelines classify the ensuing vibrations as unacceptable. If the jumps are of transient nature, the responses fall within the acceptibility limits of both guidelines. Hence, the use of this floor for sports activities (such as gymnasium, etc.) would need further investigation for serviceability vibrations.

Figure 9.26 shows the response of the floor due to heeldrop loading. As with the results of heeldrop tests on the model slab, (figure 6.32, page 137), the responses are much higher than the cases of walking or even jumping. Both scales classify the floor as on the border of acceptibility following heeldrop tests. Hence, the use of heeldrop as a simplified loading function for the classification of floors is questionable.

In summary, both scales regard this floor as acceptable for walking vibrations, although the acceptibility limits vary. Since the CSA scales are based on heeldrop loading results, the levels of acceptibility are seen to be higher than the ISO/BSI/ANSI scales. When subject to heeldrop loading, which is transient, the classification of the floor becomes very similar between the two guidelines. This pattern of results was also observed in the model slab tests (see section 6.6).

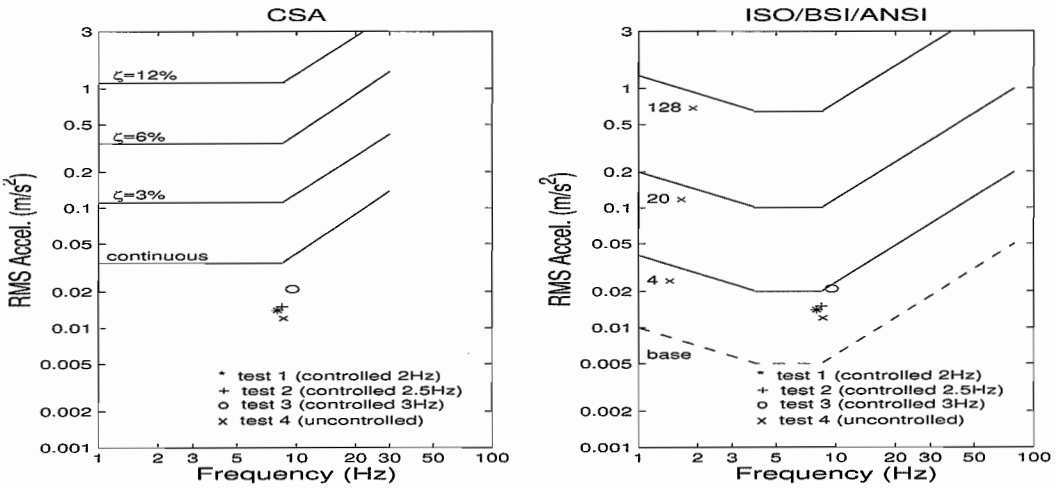


Figure 9.22: Vibration acceptibility due to walking

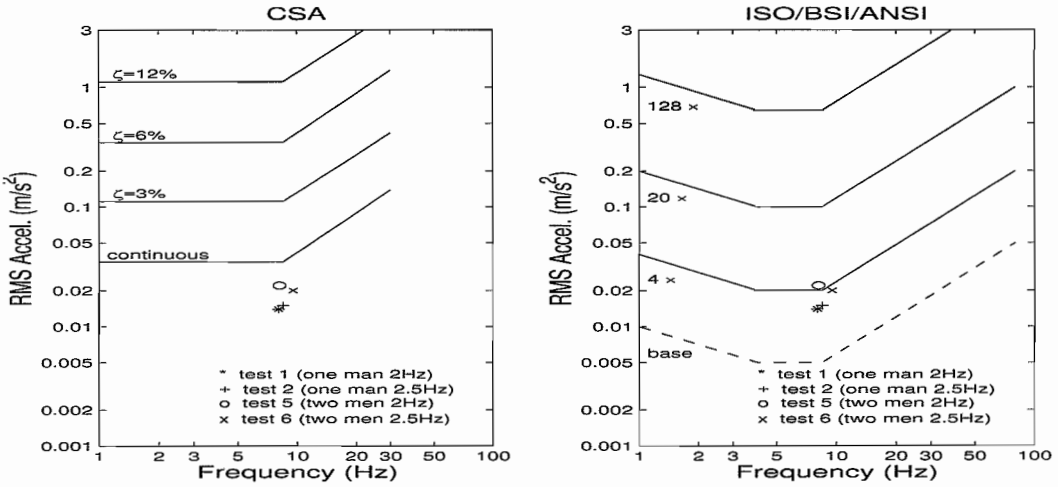


Figure 9.23: Vibration acceptibility due to more than one person walking

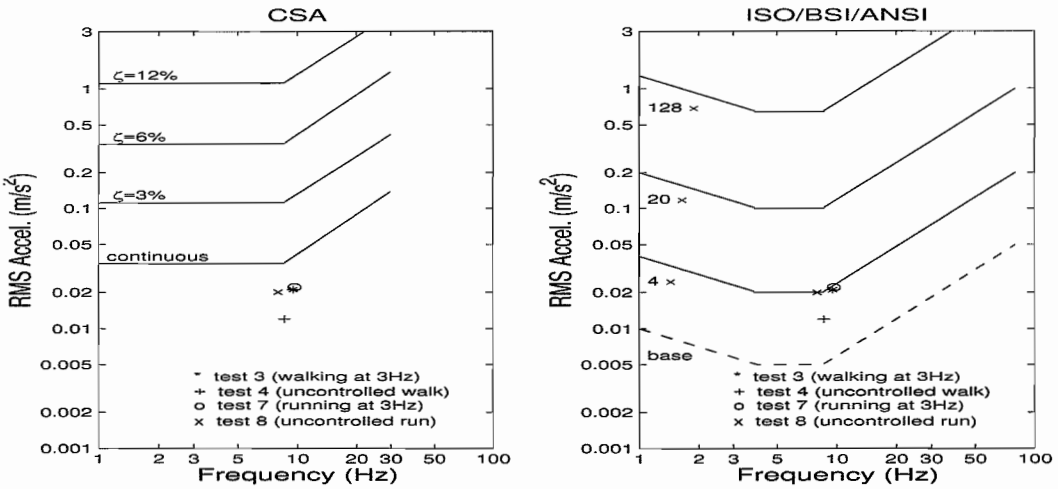


Figure 9.24: Vibration acceptibility due to running

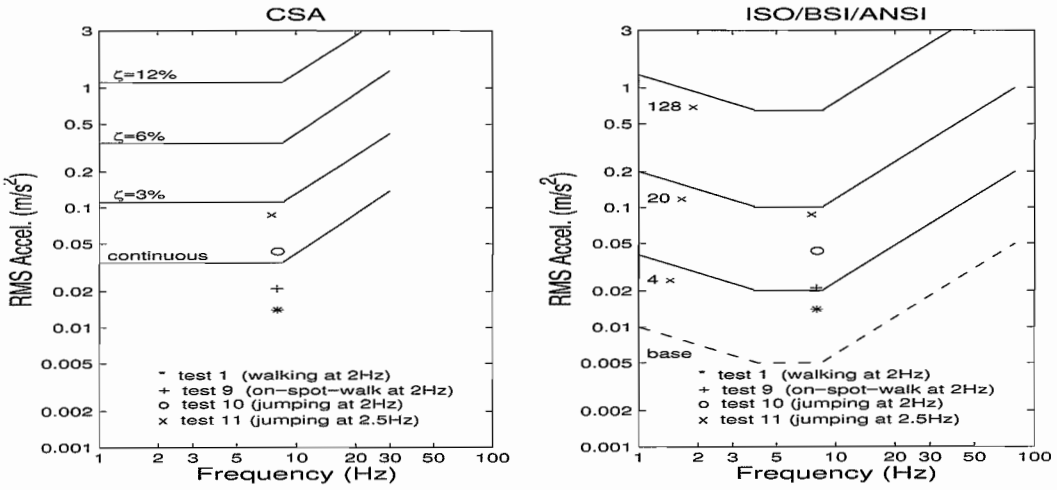


Figure 9.25: Vibration acceptibility due to jumping

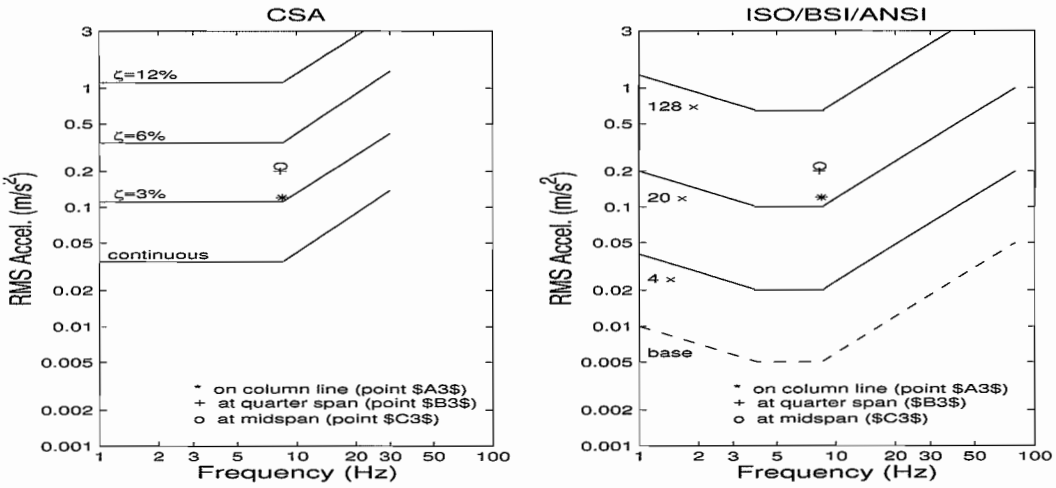


Figure 9.26: Vibration acceptibility due to heeldrop loading

Chapter 10

Conclusions

10.1 Introduction

This research programme has investigated the effects of various architectural and non-structural components on the overall dynamic behaviour of floor slabs. In particular, the research was focused on post-tensioned floors, with the effect due to: prestressing force, false flooring, full-height and cantilever partitions, viscoelastic screed layers, TMD systems, and human-structure interaction. Such additions on a floor have the effect of changing its dynamic behaviour, particularly the key parameters of natural frequency and damping. Although natural frequency can be estimated with varying accuracy, the damping mechanisms on a floor are generally less understood. The common approach in design is to pre-suppose a damping value based on past experience of similar structures. As it is widely believed that non-structural components on a floor make a significant contribution to its damping capacity, research into the effects of such components is merited.

This dissertation has described tests on a 50% scaled one-way spanning post-tensioned concrete slab, subjected to continuous and transient loading (as well as walking). The response and dynamic properties of the test floor were measured after each change to its configuration and the results were complemented by analytical modelling. The test procedure and laboratory results were investigated on a full-scale field slab and were seen to agree well with real floors. In this chapter, the findings are explained due to each non-structural component, and recommendations are given as to their use. Suggestions for further investigation are explained in section 10.4. First, some comments are made as to the best test procedure technique.

10.2 Experimental procedures

10.2.1 Loading apparatus

The impact hammer test equipment was supplied as a standard kit and did not require significant modification. The shaker equipment, however, was designed and built specifically for the research programme, as explained in section 3.3.2. The following list summarises the advantages and disadvantages of each method:

- In the hammer test, the frequency and amplitude of the forcing vibrations are inversely proportional such that for a larger frequency range, the tester must be content with a low forcing amplitude. Moreover, the actual range of applied frequencies is restricted, which is determined by different hammer tips (see figure 3.3, page 50). As a result, one cannot look at the behaviour of the floor in the proximity of its natural frequencies, but has to be content with a large range around one or more of the natural frequencies.
- In the shaker test, the frequency and amplitude of the imposed force are independent, so that one can be altered without affecting the other. In this way, by increasing the amplitude at a frequency range close to one of the floor natural frequencies, better resonance at that frequency can be achieved, with sharper and clearer peaks of the transfer function.
- In the shaker test, the input energy can be concentrated at the region of resonance, so that the response of the floor becomes large. This is a distinct advantage in the floor damping measurements, because once the shaker is switched off, a clear exponential decay of response is observed. In the hammer test, the applied impulse energy to the floor is not sufficient to give a very high response.
- For the same grid point on a floor, the shaker test gives better coherence values than the hammer test. This is illustrated for the field slab by comparing figures 9.4 (page 191) and 9.6 (page 194). The reasons for better shaker coherence are that more energy is concentrated in the required frequency range, and that the continuous forcing vibration can drown out the external noise. In the hammer test, the short transient vibration is prone to external noise, which may occur at the instant of impact.
- For field tests, the hammer apparatus is less bulky and involves fewer components, hence requires less time to be ready on site. The comparison between the two test setups can be seen in figure 4.4 (page 75).

A detailed study of the hammer and shaker apparatus was conducted by Falati (1996), who concluded that both methods were perfectly sound in the testing of floors for vibration. However, he suggested that if all aspects were considered, the advantages of the shaker test out-scored those of the hammer. With the research programme being focused on damping capacity measurements, the ability of the shaker to input extra energy at given frequencies was seen to be a major advantage. Hence, the shaker equipment was utilised in most of the tests.

10.2.2 Measurement apparatus

During the testing programme, measurements were made of the loading applied, and the acceleration response of the slab. The data were analysed and recorded by the spectrum analyser. Throughout the experiments, the loadcell and accelerometers were checked for errors and recalibrated, where possible. At all times, the QA procedures of section 5.8 were adhered to, which included: immediate repeatability checks, homogeneity checks, reciprocity checks, coherence function checks, and end of test repeatability checks. The use of these checks in any site investigation is strongly recommended.

10.3 Model slab vibration behaviour

10.3.1 Effect of prestressing force

The slab was tested in the states of: no prestress, 57% prestress, and full prestress. The following conclusions were derived from these tests and their analytical representation:

- Modelling prestressing as an external axial force is not a true representation of its effects. It can be shown by energy considerations that the line of action of the prestressing force moves integral with the bending of the slab and has no effect on the slab fundamental frequency (see section 6.2.1).
- Slab natural frequency is independent of prestressing force but indirectly affected by it, due to a change in section modulus and amount of cracking in the slab.
- The theoretical methods of natural frequency estimation, in their present form, can give inaccurate predictions for post-tensioned floors, partly because they do not take the level of prestress into account.

- It is possible to approximately predict the changes in natural frequency, due to a prestress force, by considering the changes in the effective second moment of area, I_e, of the slab. If these changes in I_e are included in the theoretical methods of frequency estimation, closer predictions to experimental results can be obtained.
- Damping of the slab greatly reduces with an increase in prestress due to closing up of microcracks and, hence, an increase in effective second moment of area, I_e. However, the relationship between ζ and I_e is not clear.
- The addition of live load decreases the natural frequencies and increases damping depending on the level of prestress.

10.3.2 Effect of false flooring

Tests to assess the contribution of flase floor panels to slab dynamic behaviour, gave the following conclusions and recommendations:

- False floor panels reduce the overall slab fundamental frequency due to the added mass. This reduction is dependent upon the number of false floor panels used.
- When rigidly attached to the pedestals, the floor panels simply added mass to the structure and did not introduce any significant additional damping. In these tests, the increase in slab damping was 6%.
- When some panel edges rested on the pedestals, there was a marked increase in damping. This was most likely caused by sliding and/or gapping between the panels and pedestals. Here, the increase in slab damping was 66%.

The results show that contrary to popular belief, merely the presence of false floors does not enhance the dynamic behaviour of the system. It depends on factors such as the type of flooring used and the nature of their installation. This raises the possibility that false floors could be designed to allow increased motion between panel and pedestal as a deliberate energy dissipation device. Of the false flooring systems available in market today, the results suggest that the use of panels which rest on the pedestals (e.g. heavy timber panels), may lead to an increased damping capacity of a floor, compared to panels which are rigidly fixed to the floor.

10.3.3 Effect of full-height partitions

The results of tests have shown that a significant effect on the slab vibration parameters is gained by the addition of full-height partitions. When rigidly attached between two floors, the partition effectively acts as a line support, resulting in a substantial increase in slab stiffness. In the model slab tests, addition of a single full-height partition at midspan, led to an increase in floor fundamental frequency from 8Hz to 20Hz (i.e.+154%). Also, an increase in fundamental mode damping of 77% was observed. By measuring the behaviour of the partition itself, it was found to undergo axial bending deformations at the same frequency as the slab vibration. Hence, the results illustrate that partitions, which are regarded as non-structural components, can in fact behave in a structural way and add extra stiffness to the main system. If well designed, this is a very inexpensive way of alleviating annoying vibrations on a problematic floor.

As described in section 6.4.1, an analytical model was established, which represented the full-height partition as an extra spring, acting on the underside of the slab and rigidly fixed at the bottom (see figure 6.8, page 113). From this model, a simple design proposal was derived for simply supported beams in the form:

$$f_{0_c}^2 = f_0^2 + \frac{k_p}{2\pi^2 \rho b h L} \sin^2\left(\frac{\pi a}{L}\right) \tag{10.1}$$

where k_p is the stiffness of the partition material, (a) is the distance of the partition from the nearest support, f_0 is the beam frequency before addition of the partition, and f_{0_c} is the frequency after the partition has been installed. This formula can be used in two ways. Either the effect on the fundamental frequency following the addition of pre-planned partitions can be derived, or a target frequency can be decided (see table 2.5, page 44), which would determine the type and stiffness of the partition walls needed. Typical stiffness values for gypsum plasterboard partitions are given in table 6.5, which were derived experimentally (see appendix E).

10.3.4 Effect of cantilever partitions

It has been found that cantilever partitions can be designed to have maximum beneficial effect on slab vibration properties. They were seen to be most effective when positioned perpendicular to the slab span and at a point where the fundamental mode shape of the slab has a high slope. This is because when the slab is undergoing vibration, a rotation is applied at the base of the partitions, leading to sway and hence dissipation of energy. The larger the rotation, the bigger the sway. Therefore, a partition at midspan will have less energy dissipated compared to one at quarter span (see section 6.4.2).

The experimental results were supported by an analytical model of a cantilever beam subjected to a sinusoidal base rotation (see figure 6.15, page 121), which was derived from the vertical vibration response of the slab. The model results show that the frequency of the base rotation has a governing influence on the natural modes of the partitions. The model and experimental results were seen to be in good agreement for the tested partitions (see figure 6.20, page 125).

Finally, experiments have shown that if the cantilever partitions are connected to each other, transfer of energy takes place from ones with higher response to ones with lower response, increasing the overall energy absorption of the whole partition system.

10.3.5 Effect of viscoelastic screed layers

As explained in section 6.5.1, problems were encountered in the mixing and casting stages of the screed layers. It was observed that using viscoelastic material, as an admixture to concrete, requires a certain amount of experience in order to obtain the correct mix. Hence, the problems encountered with casting of the screed layers were more likely due to the inexperience of the casting team. As a result, the cube strengths and Youngs moduli of the treated concrete were much lower than expected.

The effect of the screed layers on natural frequency of the slab was satisfactorily predicted by regarding the layers as structural, rather than non-structural, additions. The predictions were seen to be marginally higher than the experimental results and the differences were attributed to the bonding between the screed and the main slab. The damping capacity of the slab was also seen to increase with the addition of the layers. This increase was 5% with a layer of 50l/m^3 Concredamp concentration, and 14% with a screed of 85l/m^3 Concredamp concentration. These increases were less than expected and attributed to the casting problems explained above.

To show that using such treated screed layers is a viable option in reducing slab response, an analysis was presented of a two layered composite structure (see section 6.5.3). In the analysis, full bonding of the two layers was assumed and the overall damping of the composite structure was derived as the weighted average of the damping ratios of individual components such that:

$$\zeta = \frac{\sum \zeta_i S_i}{\sum S_i} \tag{10.2}$$

where S_i is the energy stored by the i^{th} component and ζ_i is its damping ratio. For a free viscoelastic layer, by considering the stored strain energy in each layer, a prediction of the overall slab damping due to the addition of the two screed layers could be achieved (equation 6.51, page 129).

Ideally, the damping of the viscoelastic layer would be expected to be much higher than the slab. Although this was not achieved in the experimental tests, the overall damping of the composite would be expected to increase with higher values of screed layer damping ratio.

10.3.6 Addition of tuned vibration absorbers

As explained in chapter 7, a simple tuned mass damper (TMD) system was proposed to reduce vibrations of long-span floor slabs. The system consisted of layers of plywood sheets, simply supported on angle sections at the underside of the slab. The tuning of the system was carried out by placing weights on the plywood. Different sizes and configurations of plywood were attempted and it was possible to reduce vibrations of the model experimental slab by as much as 80%. Of the eight different layouts attempted, the one with two layers of plywood and polythene in-between gave best results (see section 7.3.1). Some of the findings from the experiments were:

- two layers of plywood TMD gave faster slab vibration decay than one layer
- wider plywood sheets showed faster decay of slab as opposed to narrow plywood
- narrowply had twice the response at TMD level compared to wideply
- with polythene or rubber between two ply layers, slab decay was marginally faster than with nothing in-between (due to aiding of friction)

To investigate the structure-TMD interaction further, a time-stepping numerical model for the TMD system was devised and optimised to best represent the experimental results (section 7.4.2). The model was then extended to other slab and TMD configurations. A possible design method was proposed for the TMD system, which could be applied to many slab configurations (see section 7.6.1). The model was also seen to be very effective in reducing annoying slab vibrations due to intermittent loading, such as jumping and walking. A full worked example was illustrated for a typical slab (see appendix F).

10.3.7 Effect of human-structure interaction

Tests with a stationary standing man and his equivalent weight on the slab, led to the following findings:

- The fundamental frequency of the model slab decreased with the addition of a stationary standing man, and also with the addition of his equivalent mass.

- A stationary man significantly increased the model slab damping ratio by as much as 250%, as compared to 32% when considering the man as a mass (see table 8.1, page 170).
- Two stationary people had an approximately similar effect on slab vibration reduction as one stationary person (section 8.3.2). Hence, one person is adequate in laboratory experiments of this nature, when considering floors with few occupants.
- The energy absorption capacity of the body was confined within a fixed frequency range and was lost at higher frequencies (section 8.3.2). This is the range of natural frequencies of the component parts of the body.

Two analytical models were derived (section 8.4). The first model was an undamped 2DOF representation of the slab and the man, used to derive the body fundamental frequency (section 8.4.1). The second model represented the body as a SDOF system, with inherent stiffness and damping, on top of the damped SDOF model for the slab (section 8.4.2). The conclusions obtained from the models were:

- By considering the generalised slab mass and stiffness, and the generalised mass of the standing man, the frequency of the human body was derived as 10.43Hz, with a stiffness of 1.07×10^5N/m (section 8.4.1).
- The models show that the addition of occupants on a structure leads to changes in its fundamental frequency, depending on the mass ratio and the original fundamental frequency of the structure. If the structure frequency is lower than the body frequency, the presence of occupants will lead to a reduction in the fundamental frequency of the structure, with a new higher mode appearing to represent the motion of the occupants. For high frequency structures, the opposite is the case and the presence of occupants will increase the fundamental frequency with a new lower mode appearing for the occupants (see figure 8.9, page 176). In all cases, the individual structure and body frequencies lie inbetween the two frequencies of the human-structure system.
- With the addition of people on a structure, the new mode representing the vibration of the body can be calculated. However, it was not possible to observe this mode from the measurements of response on the structure.
- The overall damping of the human body was found to be in the range 45-55% critical.
- At resonance, the human body may experience accelerations up to 50% higher than the measured floor accelerations. This is implicitly accounted for in the perceptibility criteria of section 2.2.2 (by subjective ratings), but not explicitly noted in any of the guidelines.

- The current design codes, which assume the occupants as live load, should be altered to take account of the significant vibration reduction attributable to the human body, and also of the changes to the fundamental frequency of a structure, which may be caused by the occupants.

10.3.8 Field testing

A vibration test is reported in chapter 9 on a full scale office floor. Modal analysis techniques of chapter 4 were used to derive the dynamic characteristics of the floor in terms of its natural frequencies, damping, and stiffness parameters. The types of loading were hammer, heeldrop, shaker, and walking tests. During the tests, the observations of section 10.2.1 were confirmed in that a much better coherence and control of the test could be achieved with the use of the shaker, as opposed to the hammer. With the floor being fully furnished, its damping was higher than that of the model slab, but within the recommended ranges given in section 2.6.4.

Tests were also carried out with three men standing on the slab near the accelerometer, and the results confirmed the human-interaction model of chapter 8 (see section 9.4.2). Walking tests were conducted on the floor with various paces and types of walk to resonate the required natural frequencies (section 9.5). The highest responses were observed as a result of jumping on the floor.

10.3.9 Summary

Table 10.1 shows a simple summary of the effects of the various non-structural components on the vibration characteristics of the model experimental slab. It also shows the effects due to the addition of the TMD system and stationary occupant.

10.4 Scope for further research

The results obtained in these tests have given scope for further research into the field of concrete slab vibration behaviour. Possibilities for investigations into the effects of individual aspects are discussed below.

Prestressing force: Following these tests on a one-way spanning slab, the effects of prestressing on the dynamic behaviour of two-way slabs can be investigated. The prestressing force in each of the two orthogonal directions can be altered, changing aspect ratios, and the subsequent effects can be studied in terms of the ratios of prestress force in the two directions. Using

Table 10.1: Summary of the effects of various additions on the model slab
(↑ = increased, ↓ = decreased, ↔ = no change)

Alteration to slab	**Effect on slab dynamic behaviour**			
	fund. freq.	**damping**	**vert. accel.**	**mode shape**
increase of prestress force	↑	↓	↑	↔
inclusion of false flooring	↓	↑	↓	↔
inclusion of full-height partitions	↑	↑	↓	shows added stiffness
inclusion of cantilever partitions	↓	↑	↓	↔
inclusion of screed layers	↑	↑	↓	↔
addition of TMD system	↔	↑	↓	↔
with stationary standing man	↓	↑	↓	↔

this data, and the effects on natural frequency, can give rise to the derivation of a method for predicting the fundamental frequency of two-way spanning post-tensioned floors. Present methods do not give accurate predictions. The Concrete Society (1994) method, specifically designed for two-way slabs, considers each orthogonal direction separately, leading to poor estimates of frequency [Williams and Waldron (1994)]. In addition, more detailed research can be conducted to investigate the amount of cracking in a concrete section, and its relationship with damping. This may prove to be difficult and could need sophisticated equipment to quantify the amount of cracking.

False flooring: The conclusions derived from these laboratory experiments can be tested on real floors, where the type and manner of installation can be thoroughly investigated in relation to slab damping. At present, merely the existence of false floors is seen as evidence of additional damping. The experimental results have shown this assumption to be somewhat incorrect, hence more evidence is needed to confirm the results.

Full-height partitions: The analytical model of these partitions can be implemented on site and the accuracy of the prediction of constrained frequency can be gauged. To make the suggested design guideline applicable to types of partition other than plasterboard, a database of different partition stiffnesses can be developed. Furthermore, the model could be extended to more than one partition, and also to assess the effects on two-way spanning slabs.

Cantilever partitions: The sway characteristics of these partitions need to be investigated further with regards to their energy dissipation. Although the positioning of cantilever partitions is mainly an architectural decision, the results have shown that their direction and placement, in respect to the slab span, affects their useful contribution to the floor dynamic behaviour.

There is therefore scope for more research, particularly with other partition types, such as mobile partitions.

Viscoelastic screed layers: Constrained viscoelastic materials have been used extensively in vehicle and aeronautical industries. The use of such materials on composite floors, applied at the flanges, has also given satisfactory results [Farah et al. (1977)]. Although using the viscoelastic admixture as a free (unconstrained) layer on the main slab gave only a very small increase in damping, its usefulness has been shown by an analytical model and also recorded experimentally by others [Moiseev (1991)]. More research is possible in this field to find the most suitable concentration of material and best layer of screed, to increase damping of a given slab. Also, its effectiveness can be linked analytically to a reduction in slab response, by a suitable model. The use of constrained layers is also possible in concrete floors, where a layer of a suitable material (e.g. rubber) can be sandwiched between two thin screed layers. Bending of the system will cause the composite layer to undergo shear, dissipating energy in the rubber. The advantage of such a system is that properly designed constrained layers can usually provide more damping with less added weight than free layers. However, this brings the added complication of frequency-dependent effects as explained by Ungar (1963).

Plywood vibration absorbers: Having proposed a design guideline for the application of plywood TMDs, tests need to be conducted in the field for its validation. The TMDs can be improved with further investigation on the damping capacity of the plywood layers and on the possibility of using viscous dampers between the sheets, with known values of energy absorption. This also raises the potential of using other more uniform and permanent materials in place of the plywood sheets. The downside with any TMD system is that it is only applicable to a given frequency. However, recent research has shown successful results in the use of multiple liquid dampers for buildings [Fujino and Sun (1993)]. Hence, the use of multiple plywood TMDs can be investigated, where a row of absorbers could be installed on a floor, each tuned to a different frequency. These would coincide with any possible annoying frequency and also with second and third natural frequencies of the slab, where applicable.

Structure-human interaction: Some of the research needs in this field are: (i) the precise difference in energy absorption between a stationary and a non-stationary man, (ii) effect of the number of occupants as a function of vibration perceptibility and annoyance, (iii) more accurate measurements of the damping of the human body for a range of conditions, (iv) full evaluation of the modal mass of the human body [Ji (1995)], (v) consideration of body vibrations other than vertical (e.g. sway), (iv) possibility of calculation of the human-structure

interaction for a given activity and structure, hence modification of existing design codes to incorporate the number of occupants.

Field test results: At present, most vibration tests on full scale floors concentrate on measurements of natural frequency, damping, and heeldrop peak acceleration. Less data is available on the acceleration responses induced by normal human activities on a given floor, particularly walking. Hence, a database of floor types and their respective acceleration responses is needed, from which a better judgement can be made on the merits of various design guidelines.

Appendix A

Full experimental results

This appendix presents the detailed results of all experiments. First, the natural frequency and damping values are given from frequency and time domain analyses. The derived acceleration responses, following single sine wave loading tests, are then presented.

Frequency domain natural frequencies

Table A.1: Effect of prestress on Natural frequency (frequency-domain analysis)

Slab configuration	no. of tests	**Natural Frequencies (Hz)**					**Average values**		
		fund.		2nd		3rd	fund.	2nd	3rd
		Frequency resolution (Hz)							
		0.12	*0.06*	*0.12*	*0.06*	*0.12*			
reinforced without post-tension (weekly tests)	39*	7.60	-	30.76	-	65.38	7.54	30.38	64.58
	39*	7.54	-	30.68	-	65.33			
	39*	7.51	-	30.38	-	64.94			
	39*	7.51	-	29.69	-	62.65			
100kN post-tension force	39	7.50	7.61	29.38	29.72	63.96	7.63	29.72	64.19
	39*	7.76	-	30.07	-	64.42			
175kN post-tension force (design force)	39	8.00	8.05	30.29	30.14	65.75	8.01	31.03	65.95
	39	8.00	7.99	31.47	31.54	66.00			
	39*	7.98	-	31.72	-	66.09			
detensioned before demolishing (with screed layers)	21	9.16	9.17	36.65	36.53	71.26	9.16	36.59	71.26

[* = Instrumented hammer tests]

Table A.2: Effect of dead load on Natural frequency (frequency-domain analysis)

Slab configuration	no. of tests	**Natural Frequencies (Hz)**					**Average values**		
		fund.		2nd		3rd	fund.	2nd	3rd
		Frequency resolution (Hz)							
		0.12	*0.06*	*0.12*	*0.06*	*0.12*			
100kN post-tensioning force with dead load of $0.25kN/m^2$	39	7.25	7.20	28.71	28.31	61.53	7.22	28.51	61.53
175kN post-tensioning force with dead load of $0.25kN/m^2$	39	7.71	7.69	29.13	29.16	63.75	7.70	29.15	63.75

Table A.3: Effect of false flooring on Natural frequency (frequency-domain analysis)

Slab configuration	no. of tests	**Natural Frequencies (Hz)**					**Average values**		
		fund.		2nd		3rd	fund.	2nd	3rd
		Frequency resolution (Hz)							
		0.12	*0.06*	*0.12*	*0.06*	*0.12*			
floor layout1 (see fig. 3.15) (measured on slab level)	39	7.88	7.87	30.96	30.98	64.58	7.87	30.97	64.58
floor layout1 (measured on false floor level)	10	7.88	7.87	31.13	31.13	64.63	7.87	31.13	64.63
floor layout2 (see fig. 3.16) (measured on slab level)	39	7.61	7.63	28.12	27.91	noisy	7.62	28.02	-
floor layout2 (measured on false floor level)	15	7.56	7.61	28.17	28.17	noisy	7.59	28.17	-

Table A.4: Effect of partitions (see figure 3.12 for layout) on Natural frequency (frequency-domain analysis)

Slab configuration	no. of tests	**Natural Frequencies (Hz)**					**Average values**		
		fund.		2nd		3rd	fund.	2nd	3rd
		Frequency resolution (Hz)							
		0.12	*0.06*	*0.12*	*0.06*	*0.12*			
five cantilever partitions perpendicular to slab span (nos. (1)-(5) in fig. 3.12)	39	7.77	7.75	29.41	29.88	64.47	7.76	29.65	64.47
three cantilever partitions perpendicular to slab span (nos. (2)-(4) in fig. 3.12)	39	7.87	7.87	31.34	31.29	64.79	7.87	31.32	64.79
five perpendicular and three transverse to slab span (nos. (1)-(8) in fig. 3.12)	39	7.80	7.82	31.16	31.19	63.86	7.81	31.18	63.86
three parallel to slab span (nos. (6)-(8) in fig. 3.12)	39	-	8.00	-	31.17	-	8.00	31.17	-
three full-height partitions perpendicular to slab span	39	20.49	20.83	28.84	28.48	34.19	20.66	28.66	34.19
one full-height partition perpendicular to slab span	39	20.37	20.31	23.91 24.64	24.55 29.12	31.24 34.20	20.34	23.91 24.60 29.12	31.24 34.20
five cantilever and one full-height partitions	39	20.35	20.27	28.73 29.23	28.86 29.17	30.78	20.31	28.80 29.20	30.78

Table A.5: Effect of stationary man on Natural frequency (frequency-domain analysis)

Slab configuration	no. of tests	**Natural Frequencies (Hz)**					**Average values**		
		fund.		2nd		3rd	fund.	2nd	3rd
		Frequency resolution (Hz)							
		0.12	*0.06*	*0.12*	*0.06*	*0.12*			
one man standing near slab centre	39	7.93	7.91	31.49	31.45	66.05	7.92	31.47	66.05
equivalent mass of man near slab centre	39	7.67	7.70	31.28	31.40	64.25	7.69	31.34	64.25

Table A.6: Effect of visco-elastic resin screeds on Natural frequency (frequency-domain analysis)

Slab configuration	no. of tests	**Natural Frequencies (Hz)**					**Average values**		
		fund.		2nd		3rd	fund.	2nd	3rd
		Frequency resolution (Hz)							
		0.12	*0.06*	*0.12*	*0.06*	*0.12*			
25mm thick screed of low Concredamp concentration (see section 3.6.7)	39 39 39	8.75 - -	8.79 8.84 8.90	34.47 - -	34.72 34.73 35.09	68.15 - -	8.82	34.75	68.15
additional 25mm thick screed of high Concredamp concentration	39 8	10.09 -	10.17 10.18	38.87 -	39.50 39.42	75.24 -	10.14	39.26	75.24

Table A.7: Effect of combinations over slab on Natural frequency (frequency-domain analysis)

Slab configuration	no. of tests	**Natural Frequencies (Hz)**					**Average values**		
		fund.		2nd		3rd	fund.	2nd	3rd
		Frequency resolution (Hz)							
		0.12	*0.06*	*0.12*	*0.06*	*0.12*			
false floor layout2 and standing man (on slab level)	39	-	7.64	-	noisy	-	7.64	-	-
false floor layout2 and standing man (on floor level)	15	-	7.69	-	noisy	-	7.69	-	-
five cantilever partitions and dead load at $0.25kN/m^2$	39	7.63	7.66	28.94	28.88	63.76	7.65	28.91	63.76

Table A.8: Effect of combinations over the first screed layer on Natural frequency (frequency-domain analysis)

Slab configuration	no. of tests	**Natural Frequencies (Hz)**					**Average values**		
		fund.		2nd		3rd	fund.	2nd	3rd
		Frequency resolution (Hz)							
		0.12	*0.06*	*0.12*	*0.06*	*0.12*			
five cantilever partitions	33	-	8.75	-	34.57	-	8.75	34.57	-
one standing man	21	-	8.85	-	34.94	-	8.85	34.94	-
five cantilever partitions and standing man	12	-	8.72	-	34.46	-	8.72	34.46	-

Table A.9: Effect of combinations over second screed layer on Natural frequency (frequency-domain analysis)

Slab configuration	no. of tests	**Natural Frequencies (Hz)**					**Average values**		
		fund.		2nd		3rd	fund.	2nd	3rd
		Frequency resolution (Hz)							
		0.12	*0.06*	*0.12*	*0.06*	*0.12*			
one standing man	21	-	10.02	-	39.62	-	10.02	39.62	-
two standing men	21	-	10.00	-	39.48	-	10.00	39.48	-
equiv. mass of one standing man	21	-	9.98	-	39.62	-	9.98	39.62	-
equiv. mass of two standing men	24	-	9.87	-	38.13	-	9.87	38.13	-
five cantilever partitions	27	-	10.04	-	39.00	-	10.04	39.00	-
five cantilever partitions and dead load at $0.25kN/m^2$	9	-	9.77	-	38.31	-	9.77	38.31	-
five cantilever partitions and one standing man	21	-	9.97	-	38.88	-	9.97	38.88	-
false floor layout1	21	-	10.09	-	38.96	-	10.09	38.96	-
false floor layout1 and one standing man	12	-	10.07	-	38.91	-	10.07	38.91	-
false floor layout1 and equiv. mass of one standing man	12	-	9.80	-	39.25	-	9.80	39.25	-
false floor layout2	21	-	9.89	-	37.86	-	9.89	37.86	-
false floor layout2 and one standing man	11	-	9.91	-	noisy	-	9.91	-	-

Time-domain natural frequencies

Table A.10: Effect of prestress on Natural frequency (time-domain analysis)

Slab configuration	no. of tests	Natural Frequencies (Hz)						Average values		
		fund.			2nd		3rd	fund.	2nd	3rd
		Loading amplitude (N)								
		±5	*±10*	*±20*	*±20*	*±30*	*±30*			
100kN post-tension force	39	-	-	7.62	-	29.59	64.00	7.62	29.59	64.00
175kN post-tension force	39	8.04	8.00	8.07	30.27	-	66.06	8.03	30.27	66.06
detensioned before demolishing (with screed)	8	-	8.96	9.01	-	-	-	8.98	-	-

Table A.11: Effect of dead load on Natural frequency (time-domain analysis)

Slab configuration	no. of tests	Natural Frequencies (Hz)							Average values		
		fund.			2nd		3rd		fund.	2nd	3rd
		Loading amplitude (N)									
		±3	*±6*	*±20*	*±20*	*±50*	*±30*	*±50*			
100kN prestress force with load of $0.25kN/m^2$	39	-	-	7.13	-	28.33	-	61.26	7.13	28.33	61.26
175kN prestress force with load of $0.25kN/m^2$	39	7.69	7.73	-	28.98	-	63.89	-	7.71	28.98	63.89

Table A.12: Effect of false flooring on Natural frequency (time-domain analysis)

Slab configuration	no. of tests	Natural Frequencies (Hz)							Average vals		
		fund.					2nd	3rd	fund.	2nd	3rd
		Loading amplitude (N)									
		±10	*±15*	*±20*	*±25*	*±30*	*±25*	*±30*			
floor layout1 (see figure 3.15) (on slab level)	39	7.89	-	7.91	-	7.90	30.88	64.13	7.90	30.88	64.13
floor layout1 (on false floor level)	9	7.90	-	7.90	-	7.89	31.08	64.15	7.89	31.08	64.15
floor layout2 (see figure 3.16) (on slab level)	39	-	7.49	7.50	7.60	-	27.87	-	7.53	27.87	-
floor layout2 (on false floor level)	15	-	7.49	7.50	7.60	-	27.91	-	7.53	27.91	-

Table A.13: Effect of partitions (see figure 3.12 for layout) on Natural frequency (time-domain analysis)

Slab configuration	no. of tests	Natural Frequencies (Hz)					Average vals		
		fund.			2nd	3rd	fund.	2nd	3rd
		Loading amplitude (N)							
		±15	*±20*	*±25*	*±25*	*±30*			
five cantilever partitions perpendicular to slab span (nos. (1)-(5) in fig. 3.12)	39	7.66	7.69	7.73	29.43	63.56	7.69	29.43	63.56
three cantilever partitions perpendicular to slab span (nos. (2)-(4) in fig. 3.12)	39	7.77	7.83	7.82	31.41	64.58	7.81	31.41	64.58
five perpendicular and three transverse to slab span (nos. (1)-(8) in fig. 3.12)	39	7.70	7.75	7.87	31.14	63.40	7.77	31.14	63.40

Table A.14: Effect of stationary man on Natural frequency (time-domain analysis)

Slab configuration	no. of tests	Natural Frequencies (Hz)						Average values		
		fund.				2nd	3rd	fund.	2nd	3rd
		Loading amplitude (N)								
		±10	*±15*	*±20*	*±30*	*±20*	*±30*			
one man near slab centre	39	7.81	-	7.57	7.57	31.51	65.63	7.65	31.51	65.63
equivalent mass of man near slab centre	39	7.58	7.65	7.74	-	31.41	64.10	7.66	31.41	64.10

Table A.15: Effect of visco-elastic resin screeds on Natural frequency (time-domain analysis)

Slab configuration	no. of tests	Natural Frequencies (Hz)					Average values		
		fund.			2nd	3rd	fund.	2nd	3rd
		Loading amplitude (N)							
		±10	*±15*	*±20*	*±10*	*±20*			
25mm thick screed of low Concredamp concentration (see section 3.6.7)	21	8.71	8.73	-	34.91	noisy	8.72	34.91	noisy
additional 25mm thick screed of high Concredamp conc.	27	-	10.17	10.14	39.02	noisy	10.15	39.02	noisy

Table A.16: Effect of combinations over first screed layer on Natural frequency (time-domain analysis)

Slab configuration	no. of tests	Natural Frequencies (Hz)				Average values		
		fund.		2nd	3rd	fund.	2nd	3rd
		Loading amplitude (N)						
		±15	*±20*	-	-			
five cantilever partitions	21	8.64	8.65	-	-	8.64	-	-
one standing man	12	8.75	8.71	-	-	8.73	-	-
five cantilever partitions and standing man	21	8.63	8.64	-	-	8.63	-	-

Table A.17: Effect of combinations over second screed layer on Natural frequency (time-domain analysis)

Slab configuration	no. of tests	Natural Frequencies (Hz)				Average values		
		fund.		2nd	3rd	fund.	2nd	3rd
		Loading amplitude (N)						
		±15	*±20*	*±15*	-			
one standing man	12	9.94	9.93	-	-	9.93	-	-
two standing men	12	9.90	9.95	-	-	9.93	-	-
equiv. mass of one man	12	9.86	9.88	-	-	9.87	-	-
equiv. mass of two men	12	9.75	9.74	-	-	9.75	-	-
five cantilever partitions	12	9.93	9.95	37.84	-	9.94	37.84	-
five cantilever partitions and dead load at $0.25kN/m^2$	9	9.74	9.74	-	-	9.74	-	-
five cantilever partitions and one standing man	9	9.88	9.91	-	-	9.90	-	-
false floor layout1	18	9.97	9.98	-	-	9.97	-	-
false floor layout1 and one standing man	8	9.97	9.95	-	-	9.96	-	-
false floor layout1 and equiv. mass of one man	8	9.69	9.69	-	-	9.69	-	-
false floor layout2	10	9.78	9.79	-	-	9.79	-	-
false floor layout2 and one standing man	8	9.82	9.80	-	-	9.81	-	-

Frequency domain damping ratios

Table A.18: Effect of prestress on Damping (half-power method)

Slab configuration	no. of tests	Damping (% critical)					Average values		
		fund.		2nd		3rd	fund.	2nd	3rd
		Frequency resolution (Hz)							
		0.12	*0.06*	*0.12*	*0.06*	*0.12*			
reinforced without post-tension	39*	2.30	-	2.47	-	1.19	1.90	2.42	1.48
	39*	2.05	-	2.22	-	1.16			
	39*	1.65	-	2.40	-	1.51			
	39*	1.60	-	2.57	-	2.07			
100kN post-tension force	39	1.83	1.63	1.74	1.60	1.48	1.73	1.80	1.73
	39*	1.73	-	2.05	-	1.98			
175kN post-tension force	39	1.05	1.13	2.03	1.76	1.51	1.09	1.59	1.50
(design force)	39	1.29	1.05	1.44	1.21	1.37			
	39*	1.09	-	1.49	-	1.62			
detensioned before demolishing	21	1.78	1.91	2.08	1.32	2.56	1.84	1.70	2.56

[* = Instrumented hammer tests]

Table A.19: Effect of dead load on Damping (half-power method)

Slab configuration	no. of tests	Damping (% critical)					Average values		
		fund.		2nd		3rd	fund.	2nd	3rd
		Frequency resolution (Hz)							
		0.12	*0.06*	*0.12*	*0.06*	*0.12*			
100kN post-tensioning force with dead load of $0.25kN/m^2$	39	1.91	1.99	1.58	1.81	1.70	1.95	1.70	1.70
175kN post-tensioning force with dead load of $0.25kN/m^2$	39	1.44	1.11	1.79	2.42	2.12	1.27	2.11	2.12

Table A.20: Effect of false flooring on Damping (half-power method)

Slab configuration	no. of tests	Damping (% critical)					Average values		
		fund.		2nd		3rd	fund.	2nd	3rd
		Frequency resolution (Hz)							
		0.12	*0.06*	*0.12*	*0.06*	*0.12*			
floor layout1 (see fig. 3.15) (measured on slab level)	39	1.24	1.08	1.10	1.08	1.56	1.16	1.09	1.56
floor layout1 (measured on false floor level)	10	-	1.05	-	1.49	-	1.05	1.49	-
floor layout2 (see fig. 3.16) (measured on slab level)	39	1.69	1.69	1.41	1.37	noisy	1.69	1.39	-
floor layout2 (measured on false floor level)	15	1.93	1.93	1.39	noisy	noisy	1.93	1.39	-

Table A.21: Effect of partitions (see figure 3.12 for layout) on Damping (half-power method)

Slab configuration	no. of tests	**Damping (% critical)**					**Average values**		
		fund.		2nd		3rd	fund.	2nd	3rd
		Frequency resolution (Hz)							
		0.12	*0.06*	*0.12*	*0.06*	*0.12*			
five cantilever partitions perpendicular to slab span (nos. (1)-(5) in fig. 3.12)	39	1.44	1.19	2.91	3.52	1.45	1.31	3.22	1.45
three cantilever partitions perpendicular to slab span (nos. (2)-(4) in fig. 3.12)	39	1.51	1.22	1.55	1.24	1.42	1.37	1.40	1.42
five perpendicular and three transverse to slab span (nos. (1)-(8) in fig. 3.12)	39	1.82	1.48	1.63	1.17	1.17	1.65	1.40	1.17
three parallel to slab span (nos. (6)-(8) in fig. 3.12)	39	-	1.10	-	0.81	-	1.10	0.81	-
three full-height partitions perpendicular to slab span	39	1.55	1.94	3.10	2.71	2.17	1.75	2.91	2.17
one full-height partition perpendicular to slab span	39	2.04	1.86	3.93 3.71	2.15 2.56	1.09 2.02	1.95	3.04 3.14	1.09 2.02
five cantilever and one full-height partitions	39	2.03	1.88	3.00 2.49	3.31 2.66	1.69	1.96	3.16 2.58	1.69

Table A.22: Effect of stationary man on Damping (half-power method)

Slab configuration	no. of tests	**Damping (% critical)**					**Average values**		
		fund.		2nd		3rd	fund.	2nd	3rd
		Frequency resolution (Hz)							
		0.12	*0.06*	*0.12*	*0.06*	*0.12*			
one man standing near slab centre	39	4.59	3.00	1.42	1.23	1.31	3.80	1.33	1.31
equivalent mass of man near slab centre	39	1.68	1.15	1.31	1.16	1.19	1.41	1.24	1.19

Table A.23: Effect of visco-elastic resin screeds on Damping (half-power method)

Slab configuration	no. of tests	**Damping (% critical)**					**Average values**		
		fund.		2nd		3rd	fund.	2nd	3rd
		Frequency resolution (Hz)							
		0.12	*0.06*	*0.12*	*0.06*	*0.12*			
25mm thick screed of low Concredamp concentration (see section 3.6.7)	39 39 39	1.12 - -	1.05 1.25 1.13	2.27 - -	2.14 1.99 2.20	2.31 - -	1.14	2.15	2.31
additional 25mm thick screed of high Concredamp conc.	39 8	1.33 -	1.08 1.12	2.67 -	2.59 1.99	3.34 -	1.17	2.42	3.34

Table A.24: Effect of combinations over bare slab on Damping (half-power method)

Slab configuration	no. of tests	**Damping (% critical)**					**Average values**		
		fund.		2nd		3rd	fund.	2nd	3rd
		Frequency resolution (Hz)							
		0.12	*0.06*	*0.12*	*0.06*	*0.12*			
false floor layout2 and standing man (on slab level)	39	-	4.46	-	noisy	-	4.46	-	-
false floor layout2 and standing man (on floor level)	15	-	5.43	-	noisy	-	5.43	-	-
five cantilever partitions and dead load at $0.25kN/m^2$	39	1.35	1.59	2.24	1.36	1.51	1.47	1.80	1.51

Table A.25: Effect of combinations over first screed layer on Damping (half-power method)

Slab configuration	no. of tests	Damping (% critical)					Average values		
		fund.		2nd		3rd			
		Frequency resolution (Hz)					fund.	2nd	3rd
		0.12	*0.06*	*0.12*	*0.06*	*0.12*			
five cantilever partitions	33	-	1.22	-	2.65	-	1.22	2.65	-
one standing man	21	-	4.02	-	2.37	-	4.02	2.37	-
five cantilever partitions and standing man	12	-	4.57	-	2.27	-	4.57	2.27	-

Table A.26: Effect of combinations over second screed layer on Damping (half-power method)

Slab configuration	no. of tests	Damping (% critical)					Average values		
		fund.		2nd		3rd			
		Frequency resolution (Hz)					fund.	2nd	3rd
		0.12	*0.06*	*0.12*	*0.06*	*0.12*			
one standing man	21	-	3.09	-	3.17	-	3.09	3.17	-
two standing men	21	-	3.42	-	2.93	-	3.42	2.93	-
equiv. mass of one standing man	21	-	1.09	-	3.19	-	1.09	3.19	-
equiv. mass of two standing men	24	-	1.12	-	2.24	-	1.12	2.24	-
five cantilever partitions	27	-	1.16	-	2.54	-	1.16	2.54	-
five cantilever partitions and dead load at $25kN/m^2$	9	-	1.10	-	2.09	-	1.10	2.09	-
five cantilever partitions and one standing man	21	-	2.90	-	3.60	-	2.90	3.60	-
false floor layout1	21	-	1.19	-	2.92	-	1.19	2.92	-
false floor layout1 and one standing man	12	-	2.81	-	2.86	-	2.81	2.86	-
false floor layout1 and equiv. mass of one standing man	12	-	1.07	-	2.96	-	1.07	2.96	-
false floor layout2	21	-	1.06	-	2.47	-	1.06	2.47	-
false floor layout2 and one standing man	11	-	2.64	-	noisy	-	2.64	-	-

Time-domain damping ratios

Table A.27: Effect of prestress on Damping (logarithmic decrement method)

Slab configuration	no. of tests	Damping (% critical)						Average values		
		fund.			2nd		3rd	fund.	2nd	3rd
		Loading amplitude (N)								
		±5	*±10*	*±20*	*±20*	*±30*	*±30*			
100kN post-tension force	39	-	-	1.70	-	1.95	1.67	1.70	1.95	1.67
175kN post-tension force	39	1.16	1.05	-	1.82	-	1.59	1.11	1.82	1.59
detensioned before demolishing	8	-	1.39	2.25	-	-	-	1.82	-	-

Table A.28: Effect of dead load on Damping (logarithmic decrement method)

Slab configuration	no. of tests	Damping (% critical)							Average values		
		fund.			2nd		3rd		fund.	2nd	3rd
		Loading amplitude (N)									
		±3	*±6*	*±20*	*±20*	*±50*	*±30*	*±50*			
100kN post-tensioning force with dead load of $0.25kN/m^2$	39	-	-	2.10	-	1.61	-	1.98	2.10	1.61	1.98
175kN post-tensioning force with dead load of $0.25kN/m^2$	39	0.90	1.51	-	2.29	-	2.29	-	1.21	2.29	2.29

Table A.29: Effect of false flooring on Damping (logarithmic decrement method)

Slab configuration	no. of tests	Damping (% critical)					Average values		
		fund.			2nd	3rd	fund.	2nd	3rd
		Loading amplitude (N)							
		±20	*±25*	*±30*	*±25*	*±50*			
floor layout1 (see fig. 3.15) (on slab level)	39	1.28	-	1.19	1.11	1.58	1.24	1.11	1.58
floor layout1 (on false floor level)	9	1.21	-	1.19	1.57	1.59	1.20	1.57	1.59
floor layout2 (see fig. 3.16) (on slab level)	39	1.32	1.98	-	1.43	-	1.65	1.43	-
floor layout2 (on false floor level)	15	-	2.04	-	1.49	-	2.04	1.49	-

Table A.30: Effect of partitions (see figure 3.12 for layout) on Damping (logarithmic decrement method)

Slab configuration	no. of tests	Damping (% critical)					Average vals		
		fund.			2nd	3rd	fund.	2nd	3rd
		Loading amplitude (N)							
		±15	*±20*	*±25*	*±25*	*±30*			
five cantilever partitions perpendicular to slab span (nos. (1)-(5) in fig. 3.12)	39	-	1.13	1.50	2.42	1.42	1.31	2.42	1.42
three cantilever partitions perpendicular to slab span (nos. (2)-(4) in fig. 3.12)	39	1.24	1.49	1.59	1.65	1.42	1.44	1.65	1.42
five perpendicular and three transverse to slab span (nos. (1)-(8) in fig. 3.12)	39	1.25	1.71	2.19	1.47	1.27	1.72	1.47	1.27

Table A.31: Effect of standing man on Damping (logarithmic decrement method)

Slab configuration	no. of tests	Damping (% critical) fund. Loading amplitude (N) ±10	±15	±20	±30	2nd ±20	3rd ±30	Average values fund.	2nd	3rd
one man near slab centre	39	2.69	-	4.01	4.95	1.43	1.61	3.88	1.43	1.61
equivalent mass of man near slab centre	39	0.58	1.88	1.99	-	1.23	1.46	1.49	1.23	1.46

Table A.32: Effect of visco-elastic resin screeds on Damping (logarithmic decrement method)

Slab configuration	no. of tests	Damping (% critical) fund. Loading amplitude (N) ±10	±15	±20	2nd ±10	3rd ±20	Average values fund.	2nd	3rd
25mm thick screed of low Concredamp concentration (see section 3.6.7)	21	1.07	1.23	-	2.35	noisy	1.15	2.39	noisy
additional 25mm thick screed of high Concredamp conc.	27	-	1.34	1.33	2.23	noisy	1.33	2.52	noisy

Table A.33: Effect of combinations over first screed layer on Damping (logarithmic decrement method)

Slab configuration	no. of tests	Damping (% critical) fund. Loading amplitude (N) ±15	±20	2nd -	3rd -	Average values fund.	2nd	3rd
five cantilever partitions	21	1.31	1.44	-	-	1.38	-	-
one standing man	12	3.36	4.25	-	-	3.81	-	-
five cantilever partitions and standing man	21	3.62	3.90	-	-	3.76	-	-

Table A.34: Effect of combinations on second screed layer on Damping (logarithmic decrement method)

Slab configuration	no. of tests	Damping (% critical) fund. Loading amplitude (N) ±15	±20	2nd ±15	3rd -	Average values fund.	2nd	3rd
one standing man	12	3.02	3.21	-	-	3.12	-	-
two standing men	12	3.34	3.66	-	-	3.50	-	-
equiv. mass of one man	12	1.42	1.50	-	-	1.46	-	-
equiv. mass of two men	12	1.40	1.46	-	-	1.43	-	-
five cantilever partitions	12	1.50	1.52	2.89	-	1.51	2.89	-
five cantilever partitions and dead load at $0.25kN/m^2$	9	1.54	1.43	-	-	1.49	-	-
five cantilever partitions and one standing man	9	3.06	3.11	-	-	3.08	-	-
false floor layout1	18	1.52	1.56	-	-	1.54	-	-
false floor layout1 and one standing man	8	3.00	2.92	-	-	2.96	-	-
false floor layout1 and equiv. mass of one man	8	1.51	1.53	-	-	1.52	-	-
false floor layout2	10	1.54	1.51	-	-	1.53	-	-
false floor layout2 and one standing man	8	2.87	3.25	-	-	3.06	-	-

Steady-state acceleration responses

Table A.35: RMS steady-state accelerations at slab fundamental frequency

Slab configuration	Load amp. (N)	RMS accel. (m/s^2)	$\left(\frac{m/s^2}{N}\right)$	Slab configuration	Load amp. (N)	RMS accel. (m/s^2)	$\left(\frac{m/s^2}{N}\right)$
100kN post-tension force	±20	0.25	0.013	5 cant. & one full-height partitions	±30	0.05	0.0017
175kN post-tension force	±5 ±10	0.31 0.64	0.062 0.064	first screed layer (screed 1)	±10 ±15	0.30 0.54	0.03 0.036
detensioned for demolishing	±10 ±20	0.18 0.32	0.018 0.016	second screed layer (screed 2)	±10 ±15	0.30 0.45	0.03 0.03
100kN force with dead load	±20	0.79	0.04	screed 1 + man	±15 ±20	0.11 0.17	0.0073 0.0085
175kN force with dead load	±6	0.35	0.058	screed 1 + 5 cant. partitions	±15 ±20	0.30 0.46	0.02 0.023
false floor layout1	±10 ±20	0.41 0.82	0.041 0.041	screed 1 + man + 5 cant. parts.	±15 ±20	0.13 0.18	0.0087 0.009
false floor layout2	±15 ±20	0.24 0.36	0.016 0.018	screed 2 + man	±15 ±20	0.16 0.22	0.011 0.011
one man near slab centre	±10 ±20	0.05 0.13	0.005 0.0065	screed 2 + equiv. mass of man	±15 ±20	0.39 0.51	0.026 0.026
equiv. mass of man	±10 ±15	0.31 0.44	0.031 0.029	screed 2 + 5 cant. parts.	±15 ±20	0.41 0.55	0.027 0.0275
five cantilever partitions	±15 ±20	0.54 0.65	0.036 0.0325	screed 2+man + 5 cant. parts.	±15 ±20	0.17 0.24	0.011 0.012
5 perp. & 3 trans. partitions	±15 ±20	0.34 0.49	0.023 0.0245	screed 2 + floor layout 1	±15 ±20	0.35 0.47	0.023 0.0235
one full-height partition	±30	0.07	0.0023				

Table A.36: RMS steady-state accelerations at slab second natural frequency

Slab configuration	Load amp. (N)	RMS accel. (m/s^2)	$\left(\frac{m/s^2}{N}\right)$	Slab configuration	Load amp. (N)	RMS accel. (m/s^2)	$\left(\frac{m/s^2}{N}\right)$
100kN post-tension force	±30	0.22	0.0073	one man near slab centre	±20	0.21	0.0105
175kN post-tension force	±20	0.11	0.0055	equiv. mass of man	±20	0.22	0.011
100kN force with dead load	±50	0.40	0.008	five cantilever partitions	±25	0.16	0.0064
175kN force with dead load	±20	0.16	0.008	5 perp. & 3 trans. partitions	±25	0.22	0.0088
false floor layout1	±25	0.22	0.0088	first screed layer	±10	0.05	0.005
false floor layout2	±25	0.16	0.0064	second screed layer	±10	0.04	0.004

Table A.37: RMS steady-state accelerations at slab third natural frequency

Slab configuration	Load amp. (N)	RMS accel. (m/s^2)	$\left(\frac{m/s^2}{N}\right)$	Slab configuration	Load amp. (N)	RMS accel. (m/s^2)	$\left(\frac{m/s^2}{N}\right)$
100kN post-tension force	±30	0.34	0.011	equiv. mass of man	±30	0.32	0.011
175kN post-tension force	±30	0.38	0.0127	five cantilever partitions	±30	0.36	0.012
100kN force with dead load	±50	0.56	0.0112	5 perp. & 3 trans. partitions	±30	0.32	0.011
175kN force with dead load	±30	0.31	0.010	first screed layer	±20	0.03	0.0015
false floor layout1	±30	0.35	0.012	second screed layer	±20	0.04	0.002
one man near slab center	±30	0.37	0.0123				

Appendix B

Model slab dimensions and properties

This appendix lists the model slab dimensions and concrete properties used throughout the dissertation. The values of slab generalised mass, M_1^*, and stiffness, K_1^*, are also calculated in the fundamental mode.

L	=	5.1m	ρ	=	2340kg/m^3
b	=	1.0m	E_c	=	25.6×10^9 N/m^2
h	=	135mm	E_s	=	200×10^9 N/m^2
d	=	115mm	A_s	=	6.28×10^{-4} m^2 (8×T10 rebar)

Generalised mass

Taking a simply supported slab with mode shape, $\Phi(x) = \sin\frac{\pi x}{L}$, the generalised mass is:

$$M_1^* = \int_0^L \rho bh\Phi^2 dx = \rho bh \int_0^L \sin^2\frac{\pi x}{L} dx = \rho bh\frac{L}{2} = 806\text{kg} \tag{B.1}$$

Generalised stiffness

Taking the same $\Phi(x)$, the generalised stiffness is:

$$K_1^* = \int_0^L EI\Phi''^2 dx = EI\int_0^L -\frac{\pi^2}{L^2}\sin^2\frac{\pi x}{L} dx = \frac{EI\pi^4}{2L^3} = 2.02\times10^6\text{N/m} \tag{B.2}$$

Appendix C

Effect of cracking on concrete section

In this appendix, typical calculations for the derivation of effective second moment of area, I_e, for uncracked, cracked, and partially cracked sections are presented. These calculations apply to the model post-tensioned slab in its bare state with full prestress, no prestress, and partial prestress. Slab dimensions and concrete properties are given in appendix B.

General formula

For a cracked section, the effective second moment of area is given by: (as in section 6.2)

$$I_e = \left(\frac{M_{cr}}{M_a}\right)^3 I_u + \left[1 - \left(\frac{M_{cr}}{M_a}\right)^3\right] I_{cr} \tag{C.1}$$

This formula applies if I_e is smaller than I_u (the uncracked second moment of area). Here, M_{cr} is the bending moment at the onset of cracking and I_{cr} is the cracked second moment of area at the most heavily loaded section. The maximum possible bending moment, M_a, is:

$$M_a = \frac{\rho bhgL^2}{8} \qquad = 10.08kNm \tag{C.2}$$

Fully prestressed section

First, lets consider the slab in its uncracked state. Here, the effective concrete section is bh, and the equivalent section is as shown in figure C.1. Taking moments about the neutral axis gives:

$$bh\left(x - \frac{h}{2}\right) = \alpha(d - x) \qquad \Longrightarrow \qquad x{=}69\text{mm} \tag{C.3}$$

The second moment of area of the uncracked equivalent section, I_u, is:

$$I_u = \frac{bh^3}{12} + bh\left(x - \frac{h}{2}\right)^2 + \alpha(d - x)^2 \qquad = 2.15 \times 10^{-4}\text{m}^4 \tag{C.4}$$

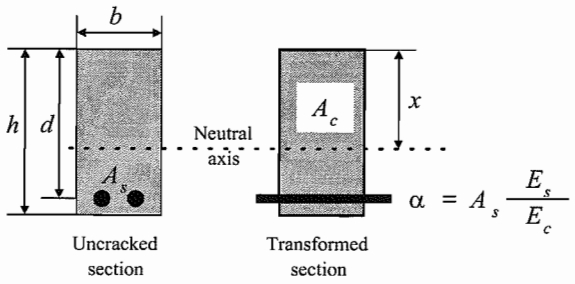


Figure C.1: Actual uncracked and its transformed (equivalent) section

With the concrete tensile strength, σ_t, derived as 3.0N/mm^2 (from cylinder splitting tests), equation 6.15 (page 107) can be used to find M_{cr}. Here, the third term in equation 6.15 is ignored, as the tendon eccentricity for the model slab was very small and difficult to achieve accurately for such a shallow slab.

$$\sigma_t = \frac{M_{cr} y_t}{I_u} - \frac{P_t}{bh} \qquad \Longrightarrow \qquad M_{cr} = 26.02\text{kNm} \tag{C.5}$$

where $P_t = 700\text{kN}$ corresponding to 175kN on each tendon. Hence, the moment required to initiate cracking is 26.02kNm, whereas the maximum possible moment in the slab is 10.08kNm (see equation C.2). Therefore, the slab remains uncracked, equation C.1 does not apply for this case and $I_e = I_u$.

Reinforced section

Now consider the slab in its reinforced state, with no post-tensioning, (see figure 6.3). Here, the concrete is assumed to be cracked up to the neutral axis and no tensile strength exists in the concrete below it. The transformed section is drawn as before assuming that the neutral axis of the cracked section passes through the centroid of the transformed section, (see figure C.2), [Kong and Evans (1989)].

Taking bending moments of the transformed section about the neutral axis gives:

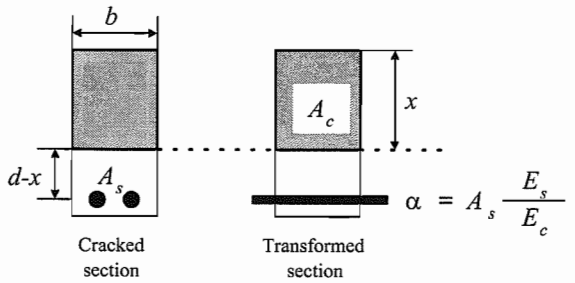


Figure C.2: Actual cracked and its transformed (equivalent) section

$$bx\left(\frac{x}{2}\right) = \alpha(d-x) \qquad \Longrightarrow \qquad x = 29\text{mm} \tag{C.6}$$

The second moment of area of the cracked section is:

$$I_{cr} = \frac{bx^3}{3} + \alpha(d-x)^2 \qquad = 4.44 \times 10^{-5}\text{m}^4 \tag{C.7}$$

Assuming that the cracked section is reinforced only, the bending moment at the onset of cracking is given by equation 6.14 (page 107), where:

$$\sigma_t = \frac{M_{cr} y_t}{I_u} \qquad \Longrightarrow \qquad M_{cr} = 9.54\text{kNm} \tag{C.8}$$

With $M_a = 10.08$kNm, (equation C.2), this means that the bending moment necessary for formation of cracks is less than the maximum possible value. Therefore equation C.1 applies where:

$$I_e = \left(\frac{9.54}{10.08}\right)^3 \times 2.15 \times 10^{-4} + \left[1 - \left(\frac{9.54}{10.08}\right)^3\right] \times 4.44 \times 10^{-5} \quad = 1.89 \times 10^{-4}\text{m}^4 \tag{C.9}$$

Partially prestressed section

In this case, some prestressing force is present and application of equation 6.15 gives:

$$\sigma_t = \frac{M_{cr} y_t}{I_u} - \frac{P_t}{bh} \qquad \Longrightarrow M_{cr} = 18.95\text{kNm} \tag{C.10}$$

where $P_t = 400$kN corresponding to 100kN on each tendon. For this case, M_{cr} lies between the values for cracked and uncracked sections. However, it is still higher than the maximum possible moment, M_a, (equation C.2). Therefore, the slab must remain uncracked, equation C.1 does not apply and $I_e = I_u$.

Appendix D

Estimations of fundamental frequency

This appendix presents typical fundamental frequency calculations for the model slab by the EBM, Static Deflection, and Concrete Society methods given in section 2.5.3. The slab is assumed to be uncracked, hence its second moment of area is taken as I_u. For consideration of cracked sections, this can be replaced by the effective value, I_e, as calculated in appendix C. The slab dimensions and concrete properties used below are as given in appendix B.

Equivalent beam method (EBM)

Taking a strip of beam one meter wide with $I_u = 2.15 \times 10^{-4}\text{m}^4$ (equation C.4), the fundamental natural frequency of the slab, when simply supported, is: (see equation 2.14)

$$f_0 = \frac{\pi}{2}\sqrt{\frac{E_c I_u}{\rho b h L^4}} \qquad = 7.96\text{Hz} \tag{D.1}$$

Static deflection method

The static deflection of the uncracked equivalent beam, simply supported, is:

$$\Delta_s = \frac{5\rho b h g L^4}{384 E_c I_u} \qquad = 4.96\text{mm} \tag{D.2}$$

Hence, the beam fundamental frequency is given as:

$$f_0 = 0.18\sqrt{\frac{g}{\Delta_s}} \qquad = 8.01\text{Hz} \tag{D.3}$$

The factor 0.18 can be calculated or derived from the conversion factor λ taken as 1.3 for a simple supported beam (see equation 2.15, page 27). Hence, expressing equation 2.5, for a lumped mass-spring system, and incorporating λ gives:

$$f_0 = \frac{1}{2\pi}\sqrt{\frac{1.3g}{\Delta_s}} = 8.07\text{Hz} \tag{D.4}$$

The small difference is due to arithmatical rounding errors.

Concrete Society method

This method is basically an extension of the EBM for two-way slabs. For the model slab, which is one-way spanning, the method is expected to give a similar result as in the EBM. The following calculations are in the long span, y, direction with l_x=1m, l_y=5.1m, n_x=1 and n_y=1. Also, I_x and I_y are taken over a one metre length strip and hence are equal where I_x=I_y=I_u=$2.15\times10^{-4}\text{m}^4$.

Hence, with reference to equations 2.16-2.20 on page 28,

$$\lambda_y = \frac{n_y l_y}{l_x}\left(\frac{E_c I_x}{E_c I_y}\right)^{\frac{1}{4}} = 5.1 \qquad k_y = 1 + \frac{1}{\lambda_y^2} = 1.04 \tag{D.5}$$

By taking the model floor in the category of slabs without perimeter beams,

$$f_y' = \frac{k_y \pi}{2}\sqrt{\frac{E_c I_x}{\rho b h l_x^4}} = 215 \tag{D.6}$$

$$f_b = \frac{\frac{\pi}{2}\sqrt{\frac{E_c I_x}{\rho b h l_x^4}}}{\sqrt{1 + \frac{E_c I_x}{E_c I_y}\frac{l_y^4}{l_x^4}}} = 7.95\text{Hz} \tag{D.7}$$

$$f_y = f_y' - \left(f_y' - f_b\right)\left[\frac{1}{2n_y} + \frac{1}{2n_x}\right] = 7.95\text{Hz} \tag{D.8}$$

And hence the fundamental natural frequency is given as:

$$\Longrightarrow \qquad f_0 = 7.95\text{Hz} \tag{D.9}$$

This result is similar to the EBM as expected.

Appendix E

Derivation of gypsum partition stiffness

The gypsum plasterboard used to simulate full-height partitions were seen to undergo lateral bowing under the vertical load imposed by the slab during vibration (see figures 6.6 and 6.7, page 112). Hence, to impose similar conditions to those of the model slab tests, the axial stiffness of the gypsum partitions, with bowing action, was found experimentally by vertical compression tests on sample specimens. During these tests, an initial lateral deflection was given to the sample specimen at its midspan and the axial and lateral deflections were measured due to axial load increments. The lateral deflections were measured at the sample midspan by dial gauges and the axial displacements were recorded at the top and bottom edges of the specimen. The samples tested were 200mm in length and were loaded under simply supported conditions. Each test was conducted in the elastic region of the load-deflection curve where on unloading, the sample returned to its original shape without permanent lateral deflections.

From figure E.1 it can be seen that the stiffness obtained from a 200mm long partition, under simply supported conditions, is comparable to the stiffness of a 400mm long partition under fixed conditions (as used in the model slab tests). This can be shown by simple beam deflection formulae.

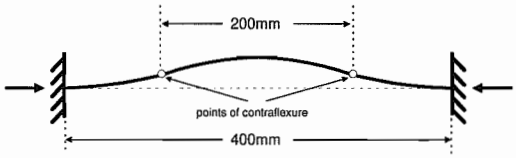


Figure E.1: Representation of a 400mm long partition, under fixed-fixed conditions, as a 200mm partition under simply supported conditions

During the axial compression tests, non-linearities were observed in the results at approximately the first three loading-unloading cycles. This was attributed to the sample 'bedding' itself into the compression chamber and also to the compression of the plaster at the micro-level. After the initial

non-linearities, the load-deflection curves for each sample were in good agreement between the tests. Figure E.2 shows these curves for six tests on a given sample. Similar results were obtained with the other specimens.

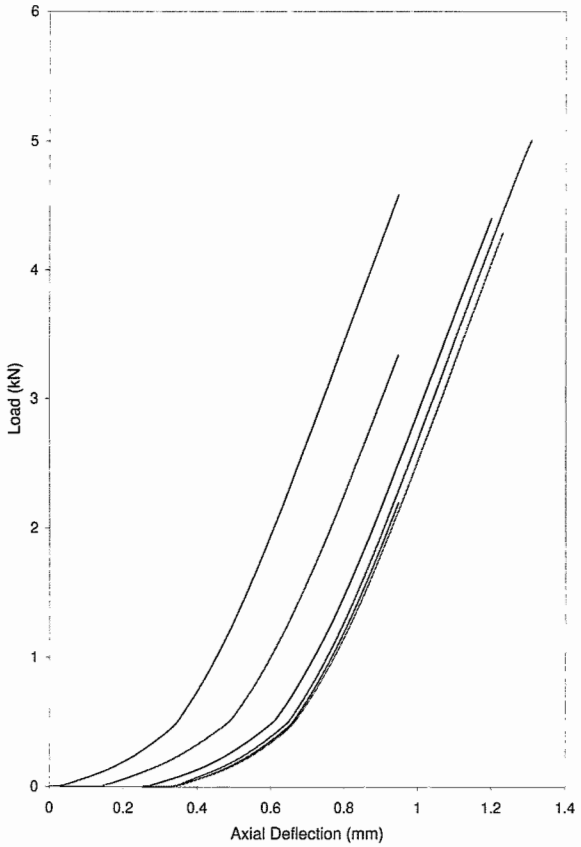


Figure E.2: Gypsum partition axial compression test results

The gradient of each curve in figure E.2 represents the stiffness of the sample for the particular test. For these tests, the gradient was calculated at the linear portion of the graph. The average stiffness obtained from all the tests was 7.52×10^6 N/m with an error range of $\pm5\%$. With the initial non-linearities, the stiffness was 7.30×10^6N/m with an error of $\pm12\%$. To substantiate these results, samples of different lengths were tested under identical conditions and the derived stiffnesses, when transformed to a 200mm sample, were within 15% of the above average value.

Hence, all calculations in this thesis take 7.52×10^6N/m as the axial stiffness (with bowing) of the 400mm long, 9mm thick, gypsum partition under fixed-fixed conditions. However, note must be made of the relatively large error range, which is mainly due to the non-uniform nature of plasterboard. Assuming a linear relationship between the axial stiffness and partition dimensions, the obtained value would increase with an increase in partition thickness and width, and would decrease with an increase in partition height.

Appendix F

Example of plywood TMD design

In chapter 7, a guideline for the design of plywood TMDs was proposed. Here, an example is given of a problematic floor, for which a plywood TMD is designed and its effectiveness evaluated. The steps given are in accordance with those listed in section 7.6.1. The description of the problem is as follows:

> *An open-plan office floor consists of a one-way spanning post-tensioned flat concrete slab supported on each side by edge-beams. A typical panel has dimensions of 9.5×8m with a slab thickness of 250mm. While in use, the occupants of the office sometimes complain of vibration annoyance during times of intense activity on the floor, namely during walking or running in the office. Instrumented hammer tests on the slab have concluded that the slab fundamental frequency is 6.2Hz, with average damping of the first mode of around 2% critical. Assess the viability of utilising a plywood TMD system to alleviate the serviceability vibration annoyance of the given floor. Assume the concrete properties to be the same as given in appendix B.*

SOLUTION

step 1 The model has to be adapted such that it is tuned to the natural frequency of the given slab. Assuming simple supports and using *the principle of generalised coordinates* to predict fundamental frequency, the above dimensions give a natural frequency of around 4.1Hz, which is an underestimate of the measured value. This would be expected as the boundary conditions are not fully simply supported and some restraints exist at the supports. By trial and error, a value of 7.7m was taken as the *equivalent simply supported span* for the slab, which gives a fundamental frequency of 6.17Hz.

step 2 Since the floor is used as an office environment, it is necessary to adopt a fairly low value of acceptable amplitude limit. Bachmann et al. (1995) suggest a limiting amplitude for offices of

$2\%g$. As explained in section 7.4.4, the walking simulations adopted in the model are based on successive heeldrops which are more severe than normal walking, hence in this example a limiting value of $4\%g$ is adopted to account for this severity. Figure F.1 shows the response of the slab (as simulated by the model) to a single heeldrop. It shows that the initial amplitudes are at the limit of acceptance chosen, hence a single heeldrop is not expected to be annoying to the occupants. However, the problem arises by people walking on the slab. With an equivalent span of 7.7m, taking each walking stride to be approximately 0.7m, it can be assumed that the maximum imposed load at the centre of the slab would be caused due to around six consecutive steps. As this is an office environment, the frequency of walking is expected to be fairly low at around 2.3Hz. However, the problem also mentions incidents of annoyance due to running or fast walking, which would be expected to be at a frequency of around 3Hz. With the slab natural frequency being 6.2Hz, resonance with the second harmonic of fast walking at this frequency may be the cause of excessive vibrations. Figure F.2 shows the slab response to six consecutive steps at 2.3Hz and 3Hz, giving a maximum peak amplitude of $16\%g$ at 3Hz, which is far above the chosen acceptance limit of 4%g.

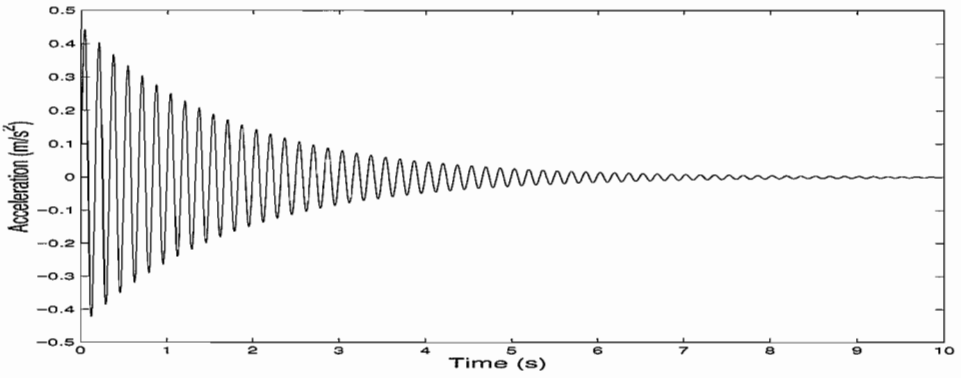


Figure F.1: Simulation of heeldrop on example slab

step 3 Having decided that a plywood TMD system is to be utilised, assume initial values for TMD damping and mass ratio. Since the case of 3Hz resonance causes the highest response, the proceeding analysis will only consider this form of loading. Keeping the TMD damping constant at 3% critical, figure F.3 shows the slab response at a range of mass ratios. From this figure, a suitable value of μ for the slab would be around 0.02. Higher values can also be considered but may prove to be impractical due to a high TMD mass.

step 4 Keeping the mass ratio constant at 0.02, figure F.4 shows the slab response at a range of damping ratios. It can be seen that initially the lower values of ζ_2 are actually more effective, but after the completion of walking, the higher damping values lead to faster decay

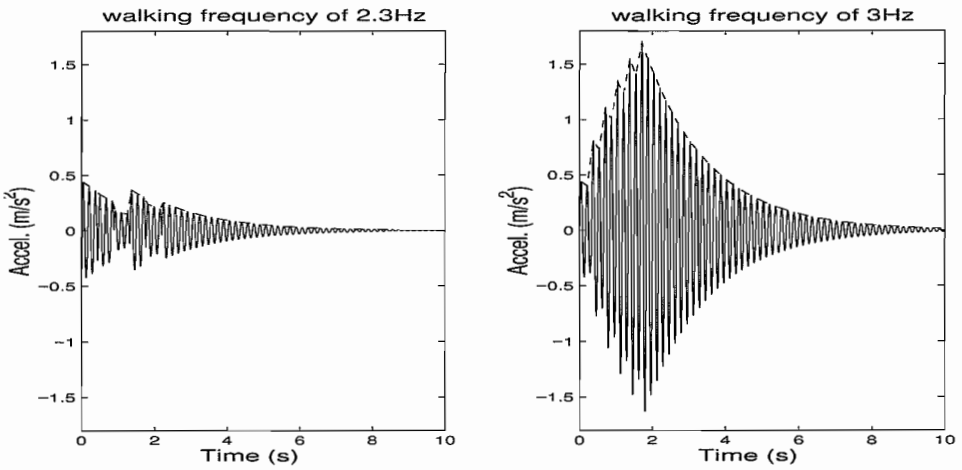


Figure F.2: Walking simulation of six steps on example slab

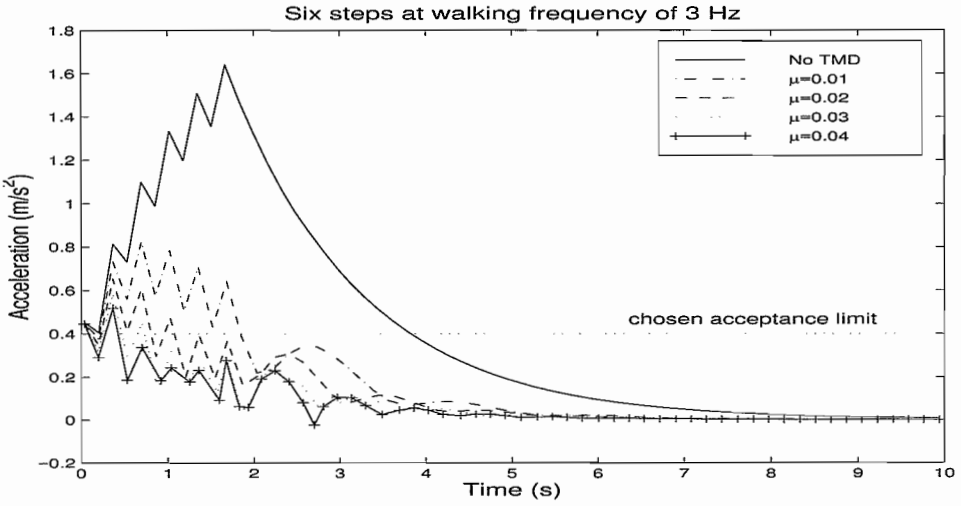


Figure F.3: Walking simulation of six steps with a range of TMD mass ratios

of vibrations. By taking practical considerations into account, table 7.2 (page 157) shows that the maximum derived value of ζ_2 for the half-scale model test was 4.3% critical. Hence, although it may prove to be a conservative assumption, it would be wise not to assume a value higher than 5% critical for this case. It must be mentioned that some purposely designed TMD systems can achieve damping capacities of over 60% critical. Here, a value of 4% is selected for the plywood system.

step 5 Having arrived at optimum values for ζ_2 and μ, figure F.5 shows the optimum slab response, with the designed TMD installed, due to worst case loading of 3Hz. The amplitudes of vibration are seen to have decreased significantly with the utilisation of the TMD system. Note that these responses are very conservative and in real cases the TMD damping would be expected to be much higher than 4% critical, leading to increased reduction of vibration response, and hence better performance of the TMD than illustrated in figure F.5.

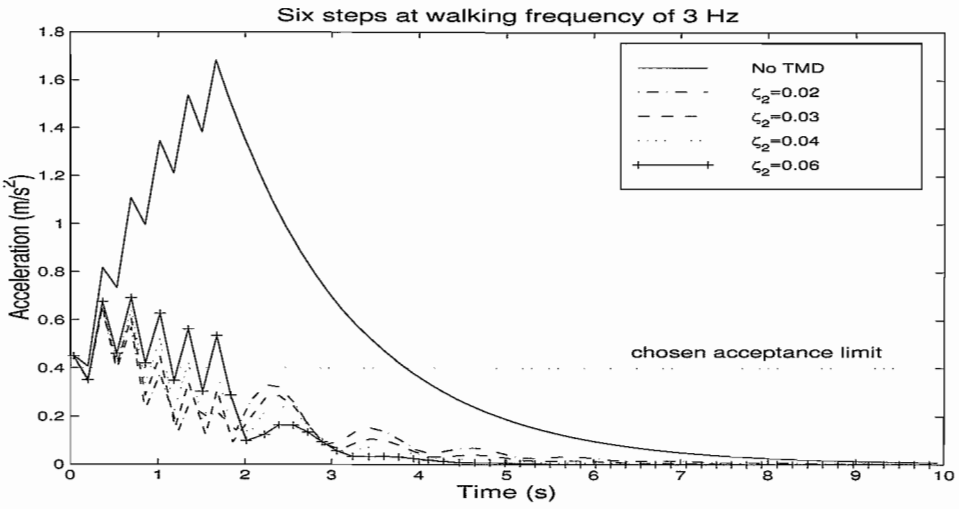


Figure F.4: Walking simulation of six steps witha range of TMD damping values

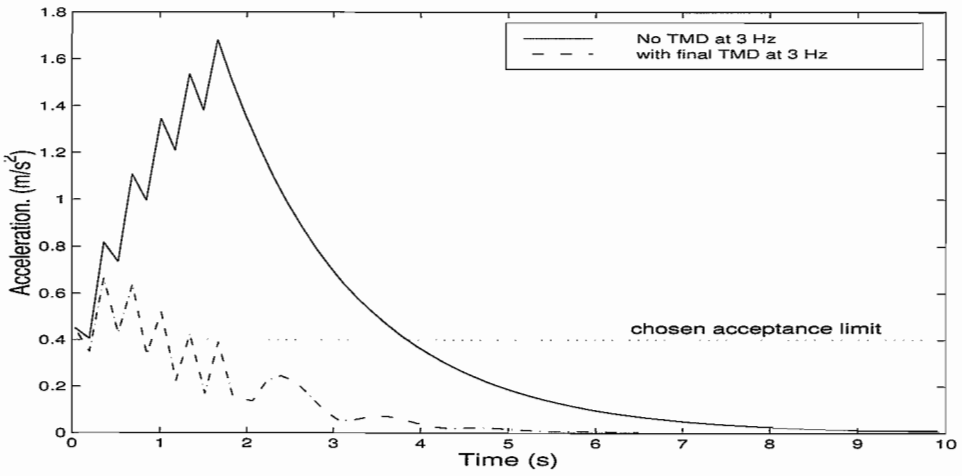


Figure F.5: Walking simulation of six steps on example slab with optimised plywood TMD system

step 6 The mass ratio to be used is 0.02, which with the generalised mass of the slab being 18.4 tonnes, gives a generalised TMD mass of 368kg. The largest sheets of plywood in market today are of the size 2.44m×1.22m×24mm, with a mass of approximately 55kg. Having decided on TMD damping of 4% critical, table 7.2 (page 157) shows that the best TMD configuration would be two layers of plywood with polythene inbetween. However, the mass of the TMD is too large to be supported by two layers of plywood, hence four layers can be supplied. This gives a value for the mass needed to tune the TMD of 258kg, uniformly distributed along the centreline of the plywood system. Although this is rather large, calculations showed that it can safely be supported by the combined 96mm thick plywood sheets. Note that by supplying four layers of plywood, it is expected that the TMD damping will be higher than the case of two layers, due to the increased number of friction surfaces.

References

ACI (1995). Building code requirements for reinforced concrete. ACI 318-95, American Concrete Institute, Detroit, Michigan, USA.

ACI-ASCE (1974). Tentative recommendations for prestressed concrete flat plates. *ACI Journal*, **71**(2), 61–71.

Advantest Corp. (1989). R9211B/C FFT servo analyser, instruction manual. Tokyo, Japan.

AISC (1997). Floor vibrations due to human activity. AISC publication D811(10M797), American Institute of Steel Construction, Chicago, Illinois. Authors: Murray T.M, Allen D.E. and Ungar E.E.

Allen, D. E. (1990a). Building vibrations from human activities. *Concrete International*, **12**(6), 66–73.

Allen, D. E. (1990b). Floor vibrations from aerobics. *Canadian Journal of Civil Engineering*, **17**(5), 771–779.

Allen, D. E. and Murray, T. M. (1993). Design criterion for vibrations due to walking. *AISC Engineering Journal*, **30**(4), 117–129.

Allen, D. E. and Pernica, G. (1984). A simple absorber for walking vibrations. *Canadian Journal of Civil Engineering*, **11**(4), 112–117.

Allen, D. E. and Rainer, J. H. (1976). Vibration criteria for long-span floors. *Canadian Journal of Civil Engineering*, **3**(2), 165–173.

Allen, D. E., Rainer, J. H., and Pernica, G. (1979). Vibration criteria for long-span concrete floors. In *Vibrations of Concrete Structures*, pp. 67–78. ACI publication SP-60. ACI, Detroit, Michigan.

Allen, D. E., Rainer, J. H., and Pernica, G. (1985). Vibration criteria for assembly occupancies. *Canadian Journal of Civil Engineering*, **12**(3), 617–623.

Allen, D. L. (1974). Vibrational behaviour of long-span slabs. *Canadian Journal of Civil Engineering*, **1**(1), 108–115.

ANSI S3.29 (1983). *Guide to the evaluation of human exposure to vibrations in buildings.* American National Standards Institute, New York, USA.

ASCE (1986). Structural Serviceability: a critical appraisal and research needs. *ASCE Journal of Structural Engineering*, **112**(12), 2646–2664. By the Ad Hoc Committee on Serviceability Research.

Bachmann, H. (1992a). Case studies of structures with man-induced vibrations. *ASCE Journal of the Structural Division*, **118**(3), 631–647.

Bachmann, H. (1992b). Vibration upgrading of gymnasia, dance halls and footbridges. *Journal of the International Assoc. for Bridge and Structural Engineering*, **12**(2), 118–124.

Bachmann, H. and Ammann, W. (1987). *Vibrations in structures induced by man and machines.* International Assoc. for Bridge and Structural Engineering, Zürich, Switzerland.

Bachmann, H. et al. (1995). *Vibration problems in structures: practical guidelines.* Birkhäuser Verlag, Basel, Switzerland.

BCA (1992). An introduction to prestressed concrete. Publication 47.022, British Cement Association, Crowthorne, UK.

Becker, R. (1980). Simplified investigation of floors under foot traffic. *ASCE Journal of the Structural Division*, **106**(11), 2221–2234.

Bert, C. W. (1973). Material damping: an introductory review of mathematical models, measures and experimental techniques. *Journal of Sound and Vibration*, **29**(2), 129–153.

Bolton, A. (1978). Natural frequencies of structures for designers. *The Structural Engineer*, **56A**(9), 245–253.

BRE 426 (1997). *The response of structures to dynamic crowd loads.* Building Research Establishment, Watford, UK.

Brüel&Kjær (1982). Measuring vibration. Nærum, Denmark.

BS5400 (1978). *Steel, concrete and composite bridges: Part2 - Specification for loads.* British Standards Institution, London, UK.

BS6399 (1996). *Loading for buildings: Part1 - Code of practice for dead and imposed loads.* British Standards Institution, London, UK.

BS6472 (1984). *Guide to the evaluation of human exposure to vibration in buildings (1Hz to 80Hz).* British Standards Institution, London, UK.

BS8110 (1985). *Structural use of concrete: Part1 - Code of practice for design and construction, and Part2 - Code of practice for special circumstances.* British Standards Institution, London, UK.

Burkhardt, L. R. (1961). Vibration analysis for structural floor systems. *ASCE Journal of the Structural Division*, **87**(7), 97–106.

Carlton, D. (1993). Application of the finite element method to structural engineering problems. *The Structural Engineer*, **71**(4), 55–59.

Caverson, R. G. (1992). Vibration characteristics of suspended concrete slabs. Master's thesis, University of Bristol, Bristol, UK.

Caverson, R. G., Waldron, P., and Williams, M. S. (1994). Review of vibration guidelines for suspended concrete slabs. *Canadian Journal of Civil Engineering*, **21**, 931–938.

Chang, F. K. (1973). Human response to motions in tall buildings. *ASCE Journal of the Structural Division*, **99**(6), 1259–1271.

Chen, P. W. and Robertson, L. E. (1972). Human perception thresholds of horizontal motion. *ASCE Journal of the Structural Division*, **98**(8), 1681–1695.

Clough, R. W. and Penzien, J. (1993). *Dynamics of structures.* McGraw-Hill, 2nd edition.

Cole, D. G. and Spooner, D. C. (1968). The damping capacity of concrete. In *The structure of concrete*, pp. 217–225, UK. Cement and Concrete Association.

Coles, B. C. and Hamilton, W. A. (1969). Repetitive dynamic loading on pre-tensioned prestressed beams. *ACI Structural Journal*, **66**(9), 745–747.

Concredamp Inc. (1993). Concredamp additive - an inter-gel pour for reducing shock, noise and vibrations in concrete. A division of Durasol Corporation. Amesbury, MA, USA.

Concrete Society (1994). Post-tensioned floors - design handbook. Technical Report TR43, The Concrete Society, Wexham Springs, UK.

Craig, R. R. (1981). *Structural dynamics: an introduction to computer methods.* Wiley, New York.

CSA (1989). Steel structures for buildings - limit state design, appendix G: guide for floor vibrations. CSA-S16.1-M89, Canadian Standards Association, Ontario, Canada.

Dall'Asta, A. and Dezi, L. (1996). Prestress force effect on vibration frequency of concrete bridges. Discussion note in *ASCE Journal of Structural Engineering*. p.458.

Deák, G. (1996). Prestress force effect on vibration frequency of concrete bridges. Discussion note in *ASCE Journal of Structural Engineering*. p.458.

Dieckmann, D. (1958). A study of the influence of vibration on man. *Ergonomics*, **1**(4), 347–355.

DIN4150/2 (1975). *Vibrations in Civil Engineering: Part2 - Effects on people in buildings.* German Institute for Standards, Berlin, Germany.

DTA (1993). *Modal testing.* Dynamic Testing Agency, London, UK.

Dytran Instruments Inc. (1993). Operating guide, model 5803a instrumented impulse hammer, twelve pound sledge.

Ebrahimpour, A. and Fitts, L. L. (1996). Measuring coherency of human-induced rhythmic loads using force plates. *ASCE Journal of Structural Engineering*, **122**(7), 829–831.

Ebrahimpour, A., Hamam, A., Sack, R. L., and Patten, W. N. (1996). Measuring and modelling dynamic loads imposed by moving crowds. *ASCE Journal of Structural Engineering*, **122**(12), 1468–1474.

Ellingwood, B. and Tallin, A. (1984). Structural Serviceability. *ASCE Journal of the Structural Division*, **110**(2), 401–418.

Ellis, B. R. (1980). An assessment of the accuracy of predicting the fundamental natural frequencies of buildings and the implications concerning the dynamic analysis of structures. *Proceedings of ICE, Design and Construction*, **69**, 763–776.

Ellis, B. R. and Ji, T. (1994). Floor vibration induced by dance type loads: Verification. *The Structural Engineer*, **72**(3), 45–50.

Ellis, B. R. and Ji, T. (1996). Dynamic testing and numerical modelling of the cardington steel framed building from construction to completion. *The Structural Engineer*, **74**(11), 186–192.

Ellis, B. R. and Ji, T. (1997). Human-structure interaction in vertical vibrations. *Proceedings of ICE, Structures and Buildings*, **122**(1), 1–9.

Ellis, B. R., Ji, T., and Littler, J. D. (1994). Crowd actions and grandstands. In *Places of assembly and long-span building structures.* Proceedings of IABSE Symposium. Birmingham, UK.

Ewins, D. J. (1984). *Modal testing: theory and practice.* Research Studies Press, Taunton, UK.

Fairley, T. E. and Griffin, M. J. (1989). The apparent mass of the seated human body: vertical vibration. *Journal of Biomechanics*, **22**(2), 81–94.

Falati, S. (1996). A study of floor vibration testing mechanisms. First year report, University of Oxford, Department of Engineering Science, Oxford, UK.

Falati, S. and Williams, M. S. (1998). Vibration tests on a model post-tensioned concrete floor. Interim report, University of Oxford, Department of Engineering Science, Oxford, UK. Report No. OUEL2155/98.

Falati, S. and Williams, M. S. (1999). Vibration testing of a model post-tensioned concrete floor slab. *Submitted to the Canadian Journal of Civil Engineering.*

Farah, A., Ibrahim, I. M., and Green, R. (1977). Damping of floor vibrations by constrained viscoelastic layers. *Canadian Journal of Civil Engineering*, **4**(4), 405–411.

FIP (1980). *Recommendations for the design of flat slabs in post-tensioned concrete using unbonded and bonded tendons.* Fédération Internationale de la Précontrainte, Slough, UK. As reported by Caverson(1992).

Flint, A. R. (1966). Current practice in design against man-made vibrations in structures. In *Proceedings of Symposium on Vibration in Civil Engineering*, pp. 207–219. British Section IAEE. Butterworth, UK.

Folz, B. and Foschi, R. O. (1991). Coupled vibrational response of floor systems with occupants. *ASCE Journal of Engineering Mechanics*, **117**(4), 870–891.

Foschi, R. O. and Gupta, A. (1987). Reliability of floors under impact vibration. *Canadian Journal of Civil Engineering*, **14**(5), 683–689.

Foschi, R. O., Neumann, G. A., Yao, F., and Folz, B. (1995). Floor vibration due to occupants and reliability based design guidelines. *Canadian Journal of Civil Engineering*, **22**(3), 471–479.

Fowler, T. J. and Karabinis, A. H. (1979). Vibration performance of industrial structures. In *Vibrations of Concrete Structures*, pp. 265–284. ACI publication SP-60. ACI, Detroit, Michigan.

Freyssinet (1994). *Post-Tensioned Slabs.* Freyssinet International, Boulogne, France. As reported by Caverson(1992).

Fujino, Y. and Sun, L. M. (1993). Vibration control by multiple tuned liquid dampers (MTLDs). *ASCE Journal of Structural Engineering*, **119**(12), 3482–3502.

Greimann, L. F. and Klaiber, F. W. (1978). Dynamic forces induced by spectators. *ASCE Journal of the Structural Division*, **104**(2), 348–351.

Grether, W. F. (1971). Vibration and human performance. *Human Factors*, **13**(3), 203–216.

Guignard, J. C. (1971). Human sensitivity to vibration. *Journal of Sound and Vibration*, **15**(1), 11–16.

Hanagan, L. M. and Murray, T. M. (1997). Active control approach for reducing floor vibrations. *ASCE Journal of Structural Engineering*, **123**(11), 1497–1505.

Hatfield, F. J. (1992). Design chart for vibration of office and residential floors. *AISC Engineering Journal*, **29**(4), 141–144.

Herterich, J. and Schnauber, H. (1992). The effects of vertical mechanical vibration on standing man. *Journal of Low Frequency Noise and Vibration*, **11**(2), 52–60.

Hudson, D. E. (1964). Resonance testing of full-scale structures. *ASCE Journal of the Engineering Mechancis Division*, **90**(3), 1–19.

Hughes, G. and Beeby, A. W. (1982). Investigation of the effect of impact loading on concrete beams. *The Structural Engineer*, **60B**(3), 45–52.

Ibrahim, I. M. and Farah, A. (1978). Enhancing the damping of slabs by viscoelastic layers. *ASCE Journal of the Structural Division*, **104**(ST5), 817–827.

Irwin, A. W. (1978). Human response to dynamic motion of structures. *The Structural Engineer*, **56**(9), 237–244.

ISO10137 (1992). *Bases for design of structures - Serviceability of buildings against vibration.* International Organisation for Standardisation, Geneva, Switzerland.

ISO2631/1 (1985). *Evaluation of human exposure to whole-body vibration: Part1 - General requirements.* International Organisation for Standardisation, Geneva, Switzerland.

ISO2631/2 (1989). *Evaluation of human exposure to whole-body vibration: Part2 - Human exposure to continuous and shock-induced vibrations in buildings (1-80Hz).* International Organisation for Standardisation, Geneva, Switzerland.

ISO7626/5 (1994). *Vibration and shock - experimental determination of mechanical mobility: Part5 - measurements using impact excitation with an exciter which is not attached to the structure.* International Organisation for Standardisation, Geneva, Switzerland.

Jain, S. K. and Goel, S. C. (1996). Prestress force effect on vibration frequency of concrete bridges. Discussion note in *ASCE Journal of Structural Engineering*. p.459.

James, M. L., Lutes, L. D., and Smith, G. M. (1964). Dynamic properties of reinforced and prestressed concrete structural components. *ACI Structural Journal*, **61**(11), 1359–1381.

Jerath, S. and Shibani, M. M. (1985). Dynamic stiffness and vibration of reinforced concrete beams. *ACI Journal*, **82**(2), 196–202.

Ji, T. (1995). A continuous model for the vertical vibration of the body in a standing position. In *Proceedings of the UK group meeting on Human Response to Vibration.* Silsoe, UK.

Ji, T. and Ellis, B. R. (1993). Evaluation of dynamic crowd effects for dance loads. In *Proceedings of International Colloquium on Structural Serviceability of Buildings*, pp. 165–172. Göteborg, Sweden.

Ji, T. and Ellis, B. R. (1994a). Floor vibration induced by dance type loads: Theory. *The Structural Engineer*, **72**(3), 37–44.

Ji, T. and Ellis, B. R. (1994b). People - a passive vibration control mechanism? In *Proceedings of first World Conference on Structural Control.* Los Anegeles, USA.

Ji, T. and Ellis, B. R. (1995). Finite element modelling in structural dynamics at BRE. Building Research Establishment. Report No. PD218/95.

Ji, T. and Ellis, B. R. (1997). Effective bracing systems for temporary grandstands. *The Structural Engineer*, **75**(6), 95–100.

Kerwin, E. M. (1959). Damping of flexural waves by a constrained viscoelastic layer. *The Journal of the Acoustical Society of America*, **31**(7), 952–962.

Khan, S. and Williams, M. S. (1995). *Post-tensioned concrete floors*. Butterworth-Heinemann, Oxford, UK.

Kong, F. K. and Evans, R. H. (1989). *Reinforced and prestressed concrete*. Van Nostrand Reinhold, London, UK, 3rd edition.

Lee-Glauser, G. J., Ahmadi, G., and Horta, L. G. (1997). Integrated passive-active vibration absorber for multistorey buildings. *ASCE Journal of Structural Engineering*, **123**(4), 499–504.

Lenzen, K. (1966). Vibration of steel joist-concrete slab floor systems. *AISC Engineering Journal*, **3**(3), 133–136.

Ling Dynamic Systems Ltd. (1972). Instruction manual, vibrator model 400. Royston, Herts. UK.

Lynn, P. A. (1992). *Digital signals, processors and noise*. MacMillan, Basingstoke, UK.

Maguire, J. R. and Severn, R. T. (1987). Assessing the dynamic properties of prototype structures by hammer testing. *Proceedings of ICE, Part 2*, **83**, 769–784.

Mahmoodi, P. (1969). Structural dampers. *ASCE Journal of the Structural Division*, **95**(8), 1661–1672.

McNamara, R. J. (1977). Tuned mass dampers for buildings. *ASCE Journal of the Structural Division*, **103**(9), 1785–1797.

Mead, D. J. and Markus, S. (1969). The forced vibration of a three-layer, damped sandwich beam with arbitrary boundary conditions. *Journal of Sound and Vibration*, **10**(2), 163–175.

Meirovitch, L. (1980). *Computational methods in structural dynamics*. Sijthoff and Noordhoff, Rockville, Maryland, USA.

Moiseev, N. (1991). Effect of a viscoelastic admixture on transient vibration in a concrete and steel floor. Cerami and Associates Inc. Long Island City, USA.

Moss, R. M. (1994). Assessment of stiffness increase due to non-strcutural screeds. *The Strcutural Engineer*, **72**(14), 221–228.

Mouring, S. E. and Ellingwood, B. R. (1994). Guidelines to minimise floor vibrations from building occupants. *ASCE Journal of the Structural Division*, **120**(2), 507–526.

Murray, T. M. (1975). Design to prevent floor vibrations. *AISC Engineering Journal*, **12**(3), 82–87.

Murray, T. M. (1981). Acceptability criterion for occupant induced floor vibrations. *AISC Engineering Journal*, **18**(1), 62–70.

Murray, T. M. (1991). Building floor vibrations. *AISC Engineering Journal*, **28**(3), 102–109.

Murray, T. M. (1999). Floor vibrations: the human tolerance side of the equation. In *Proceedings of the 17th International Modal Analysis Conference*. Orlando, Florida, USA.

Murray, T. M. and Allen, D. E. (1993). Floor vibrations: a new design approach. In *IABSE Colloquium on Structural Serviceability of Buildings*, pp. 119–124. Göteborg, Sweden.

NBCC (1985). Serviceability criteria for deflections and vibrations. Commentary A to Part 4 of the NBCC, National Building Code of Canada, Ontario, Canada. As reported by Caverson(1992).

Nelson, F. C. (1968). The use of viscoelastic material to damp vibration in buildings and large structures. *AISC Engineering Journal*, **5**(2), 72–78.

Nigam, S. P. and Malik, M. (1987). A study on a vibratory model of a human body. *Transactions of ASME Journal of Biomechanical Engineering*, **109**(2), 148–153.

Onysko, D. (1986). Serviceability criteria for residential floors based on a field study of consumer response. Technical report, Forintek Canada Corp., Ottawa, Canada.

Oppenheim, A. V., Willsky, A. S., and Young, I. T. (1983). *Signals and systems.* Prentice-Hall.

O'Rourke & Son Ltd. (1993). Concredamp - Test bed 57, Rolls Royce, Derby. A communication on the use of Concredamp.

Osborne, K. P. and Ellis, B. R. (1990). Vibration design and testing of a long-span lightweight floor. *The Structural Engineer*, **68**(10), 181–186.

Pavic, A., Reynolds, P., and Waldron, P. (1997). Modal testing of a full-scale concrete floor: test specifics and QA procedures. In *Proceedings of the Institute of Physics Conference on Modern Practice in Stress and Vibration Analysis.* Dublin, Ireland.

Pavic, A. and Waldron, P. (1996a). Guidelines on modal testing of full-scale concrete floors using instrumented hammer impact excitation. In *Proceedings of the International Seminar on Structural Assessment: the role of large and full-scale testing.* London, UK.

Pavic, A. and Waldron, P. (1996b). Parameter estimation and FE model correlation using modal testing of an experimental full-scale high strength concrete floor. In *Proceedings of International Conference on Identification in Engineering Systems.* Swansea, UK.

Pavic, A., Williams, M. S., and Waldron, P. (1994). Dynamic finite element model for post-tensioned concrete floors calibrated against field test results. In *Proceedings of International Conference on Engineering Integrity Assessment.* Glasgow, UK.

Penzien, J. (1964). Damping characteristics of prestressed concrete. *ACI Structures Journal*, **61**(9), 1125–1148.

Pernica, G. (1983). Dynamic live loads at a rock concert. *Canadian Journal of Civil Engineering*, **10**(2), 185–191.

Pernica, G. (1987). Effect of architectural components on the dynamic properties of a long-span floor system. *Canadian Journal of Civil Engineering*, **14**(4), 461–467.

Pernica, G. and Allen, D. E. (1982). Floor vibration measurements in a shopping centre. *Canadian Journal of Civil Engineering*, **9**(2), 149–155.

Pretlove, A. J. (1966). Some current methods in vibration measurement. In *Proceedings of Symposium on Vibration in Civil Engineering*, pp. 95–110. British section, IAEE. Butterworth, London.

Rade, D. A. and Steffen, V. (1999). Optimization of dynamic vibration absorbers over a frequency band. In *Proceedings of the 17th International Modal Analysis Conference.* Orlando, Florida, USA.

Raggett, J. D. (1975). Estimating damping of real structures. *ASCE Journal of the Structural Division*, **101**(9), 1823–1835.

Rainer, J. H., Pernica, G., and Allen, D. E. (1988). Dynamic loading and response of footbridges. *Canadian Journal of Civil Engineering*, **15**(1), 66–71.

Rainer, J. H. and Swallow, J. C. (1986). Dynamic behaviour of a gymnasium floor. *Canadian Journal of Civil Engineering*, **13**(3), 270–277.

Rao, D. K. (1978). Frequency and loss factors of sandwich beams under various boundary conditions. *Journal of Mechanical Engineering Science*, **20**(5), 271–282.

Rao, S. S. (1995). *Mechanical vibrations.* Addison-Wesley, 3rd edition.

Reiher, H. J. and Meister, F. J. (1931). Human sensitivity to vibration. *Forsch. auf dem Geb. des. Ing. (German)*, **2**(11), 381–386. Translation Report F-TS-616-RE, Wright Field, 1946.

Reynolds, P., Pavic, A., and Waldron, P. (1999). Dynamic FE modelling of a multi-storey car park verified by modal testing. In *Proceedings of the 17th International Modal Analysis Conference.* Orlando, Florida, USA.

Sabnis, G. M. (1979). Introduction and background: Vibrations of concrete structures. In *Vibrations of Concrete Structures*, pp. 1–12. ACI publication SP-60. ACI, Detroit, Michigan.

Saiidi, M., Douglas, B., and Feng, S. (1994). Prestress force effect on vibration frequency of concrete bridges. *ASCE Journal of Structural Engineering*, **120**(7), 2233–2241.

Saul, W. E. and Tuan, C. Y. (1986). Review of live loads due to human movements. *ASCE Journal of Structural Engineering*, **112**(5), 995–1003.

SCI (1989). Design guide on the vibration of floors. SCI publication 076, The Steel Construction Institute, Ascot, UK. Author: Wyatt, T.A.

Setareh, M. and Hanson, R. D. (1992a). Tuned mass dampers for balcony vibration control. *ASCE Journal of Structural Engineering*, **118**(3), 723–740.

Setareh, M. and Hanson, R. D. (1992b). Tuned mass dampers to control floor vibration from humans. *ASCE Journal of Structural Engineering*, **118**(3), 741–762.

Steffens, R. J. (1966). Some aspects of structural vibration. In *Proceedings of Symposium on Vibration in Civil Engineering*, pp. 1–30. British section, IAEE. Butterworth, UK.

Stewart, M. G. (1996). Serviceability reliability analysis of reinforced concrete structures. *ASCE Journal of Structural Engineering*, **122**(7), 794–802.

Szilard, R. (1974). *Theory and analysis of plates: classical and numerical methods.* Prentice-Hall.

Thomson, W. T. (1988). *Theory of vibration with applications.* Unwin Hyman, London, UK, 3rd edition.

Timoshenko, S., Young, D. H., and Weaver, W. (1974). *Vibration problems in Engineering.* John Wiley & Sons, 4th edition.

Ungar, E. E. (1963). A guide to designing highly damped structures using layers of viscoelastic material. *Machine Design*, pp. 162–168.

Vannoy, D. W. and Heins, C. P. (1979). Dynamic response of a non-composite metal deck floor system. In *Vibrations of Concrete Structures*, pp. 181–211. ACI publication SP-60. ACI, Detroit, Michigan.

Waldron, P., Caverson, R. G., Williams, M. S., and Zaman, A. (1993). Vibration criteria for unbonded prestressed concrete floors. In *Proceedings of the FIP Symposium*, pp. 877–884. Kyoto, Japan.

Warwaruk, J. (1979). Deflection requirements - history and background related to vibrations. In *Vibrations of Concrete Structures*, pp. 13–42. ACI publication SP-60. ACI, Detroit, Michigan.

Webster, A. C. and Vaicaitis, R. (1992). Application of tuned mass dampers to control vibrations of composite floor systems. *AISC Engineering Journal*, **29**(3), 116–124.

Weiss, K. (1989). Personal communication about concredamp admixure. Industrial Consulting Associates, Boston, USA.

Wheeler, J. E. (1982). Prediction and control of pedestrian induced vibration in footbridges. *ASCE Journal of the Structural Division*, **108**(9), 2045–2065.

Williams, M. S., Blakeborough, A., Houlsby, G. T., and Williams, D. M. (1998). Development of a real-time hybrid dynamic testing system. In *Proceedings of sixth SECED conference on seismic design practice into the next century*, pp. 373–379. Oxford, UK.

Williams, M. S. and Falati, S. (1998). Floor vibration tests on first level of the SCI headquarters, Silwood Park. Client report, University of Oxford, Department of Engineering Science, Oxford, UK. Report No. OUEL 2185/98.

Williams, M. S. and Falati, S. (1999). Modal testing of a post-tensioned concrete model floor slab. In *Proceedings of the 17th International Modal Analysis Conference*. Orlando, Florida, USA.

Williams, M. S. and Waldron, P. (1994). Evaluation of methods for predicting occupant induced vibrations in concrete floors. *The Structural Engineer*, **72**(20), 334–340.

Wiss, J. F. and Parmelee, R. A. (1974). Human perception of transient vibrations. *ASCE Journal of the Structural Division*, **100**(4), 773–787.

Wyatt, T. A. (1985). Floor excitation by rhythmic vertical jumping. *Engineering Structures*, **7**, 208–210.

Zaman, A. (1996). *Frequency estimation of prestressed and composite floors.* PhD thesis, City University, School of Engineering, London, UK.

Zaman, A. and Boswell, L. F. (1996). Frequency estimation of long-span floors. In *Proceedings of the second international conference on structural dynamics modelling: test, analysis and correlation*, pp. 129–139. Cumbria, UK.

Zienkiewicz, O. C. (1992). The finite element method: its genesis and future. *The Structural Engineer*, **70**(20), 355–360.